Advancing Stream-Tracer Techniques and their Mathematical Analysis

Dissertation

der Mathematisch-Naturwissenschaftlichen Fakultät
der Eberhard Karls Universität Tübingen
zur Erlangung des Grades eines Doktors
der Naturwissenschaften (Dr. rer. nat.)

vorgelegt von

Julia L.A. Knapp
aus Filderstadt

TÜBINGEN
2017

Gedruckt mit Genehmigung der Mathematisch-Naturwissenschaftlichen Fakultät der Eberhard Karls Universität Tübingen.

Tag der mündlichen Qualifikation:	24.05.2017
Dekan:	Prof. Dr. Wolfgang Rosenstiel
1. Berichterstatter:	Prof. Dr.-Ing. Olaf A. Cirpka
2. Berichterstatter:	Jun. Prof. Christiane Zarfl

ABSTRACT

Stream-tracer tests are often conducted to evaluate transport and reaction processes in streams and their adjacent hyporheic zones. But in spite of broad application, serious caveats remain, even with regards to supposedly well established approaches of stream-tracer techniques. In this thesis, I address several of these problems with regard to experiments and their mathematical analysis.

One of these common techniques are gas-tracer tests, which are used for estimating rate coefficients for reaeration across the air-water-interface. In this thesis, I illustrate how large errors are made by erroneously assuming a constant tracer input source over time, which can usually not be guaranteed in the field. I also suggest an easy-to-implement method that accounts for this temporal variability in the analysis process. Additionally, I show that neglecting dispersion in transport leads to an underestimation of reaeration rate coefficients, and that these effects carry over to the calculation of metabolic rates, such as aerobic respiration and photosynthesis from measured concentrations of dissolved oxygen.

Furthermore, conceptual models linking in-stream transport to hyporheic exchange are often stark simplifications of the processes occurring in nature. To what extent these models can nonetheless be useful in the estimation of hyporheic exchange processes I investigated by comparing in-stream and subsurface measurements of stream-tracer tests. I show that the two different observation approaches provide snapshots of very different parts of the stream-hyporheic zone system, that cannot easily be reconciled. Whereas the in-stream observations provide information on shallow hyporheic processes with effect on whole-stream chemistry, the subsurface results reveal the spatial distribution of reactivity in the stream bed that is not captured by the in-stream analysis, thereby identifying the location of a highly reactive benthic biolayer.

The shortcomings of stream-tracer techniques are also particularly evident in the context of reactive tracers, which have become a popular tool for the estimation of aerobic respiration rates and hyporheic exchange in streams. The application of the reactive tracer resazurin requires extensions of general models linking in-stream transport and hyporheic exchange with compound-specific properties. This way, models have become increasingly complex, making the reliable estimation of their associated parameters difficult. I present a nested local-in-global parameter estimation approach, that allows determining a set of transport and reaction parameters coupled with the inference of a continuous function describing the hyporheic travel-time distribution of the tracer compound in an efficient way.

This thesis thus aims at advancing stream-tracer techniques with respect to their experimental methods, the conceptual assumptions regarding transport and reaction processes as well as the estimation of parameters associated with these models.

KURZFASSUNG

Markierversuchen werden häufig durchgeführt um Transport- und Reaktionsprozessen in Flüssen und ihren angrenzenden hyporheischen Zonen zu bestimmen. Obwohl es sich hierbei um eine weit verbreitete Methode handelt, die häufig Anwendung findet, weisen verschiedenste Aspekte dieses Ansatzes grobe Defizite auf. In dieser Arbeit thematisiere ich einige dieser Defizite in Bezug auf experimentelle Methoden und ihre mathematische Auswertung.

Markierversuche mit Gasen stellen eine Gruppe dieser fehlerbehafteten Methoden dar. Diese werden häufig durchgeführt um Wiederbelüftungsraten von Flüssen zu ermitteln. In meiner Dissertation stelle ich dar, welche Fehler durch die fälschliche Annahme einer konstanten Tracergaseingabe über die Zeit gemacht werden, da dieses kontinuierliche Signal unter Feldbedingungen gewöhnlicherweise nicht gewährleistet werden kann. Ich zeige eine einfache Möglichkeit auf, den zeitlichen Trend der Gaszugabe im Auswertungsschritt zu berücksichtigen. Zudem weise ich nach, dass das Vernachlässigen von dispersivem Transport in der Auswertung zu einer Unterschätzung des Ratenkoeffizienten der Wiederbelüftung führt, die sich in der Berechnung von metabolischen Raten (aerobe Respiration und Fotosynthese) aus Konzentrationszeitreihen des gelösten Sauerstoffs fortpflanzen.

Des weiteren betrachte ich die Validität konzeptioneller Modelle, die Transport im Fluss mit hyporheischem Austausch in Verbindung setzen. Diese Modelle stellen zumeist grobe Vereinfachungen der Realität dar. In welchem Maße diese Modelle dennoch zulässige Abschätzungen hyporheischer Austauschprozesse liefern untersuche ich in dieser Arbeit anhand eines Vergleichs von Markierstoffkonzentrationen, die im Fluss selbst bzw. in der hyporheischen Zone erfasst werden. Ich zeige auf, dass diese beiden verschiedenen Betrachtungspunkte inkongruente Anteile des Gesamtsystems darstellen, die kaum in Einklang gebracht werden können. Während die Aufzeichnung im Fluss Informationen liefert über flache hyporheische Prozesse, welche die im Fluss vorherrschenden Bedingungen beeinflussen, zeigen die Beobachtungen in der hyporheischen Zone die Zonierung der Reaktivität im Flussbett auf, und ermöglichen es somit, die Lage einer reaktiven benthischen Bioschicht zu identifizieren.

Die Unzulänglichkeiten der Markierversuche in Flüssen sind besonders offensichtlich im Zusammenhang mit reaktiven Markierversuchen, die seit einigen Jahren vermehrt Einsatz finden um aerobe Respirationsraten und hyporheischen Austausch in Flüssen abzuschätzen. Für die Verwendung des reaktiven Markierstoffs Resazurin ist es notwendig, bestehende Modelle um substanzspezifische Eigenschaften des Markierstoffs zu erweitern. Dadurch nehmen die Modelle zunehmend an Komplexität zu, was die zuverlässige Abschätzung der Modellparameter erschwert. In meiner Arbeit stelle ich einen geschachtelten Algorithmus vor, der die globale Abschätzung von Transport- und Reaktionsparame-

tern mit der lokalen Inferenz einer kontinuierlichen Funktion, welche die hyporheische Fließzeitverteilung des Markierstoffs beschreibt, auf effiziente Weise verbindet.

Ziel dieser Dissertation ist es somit, bestehende Markierversuchs-Verfahren zu verbessern in Hinblick auf experimentelle Methoden, konzeptionelle Annahmen des Transport- und Reaktionsverhaltens, sowie der Abschätzung der Modellparameter.

ACKNOWLEDGMENTS

Without the help, encouragement and support of many people this thesis would not have turned out the way it is.

First and foremost I am very grateful to my advisor Olaf Cirpka for his encouragement and support throughout my studies, for giving me the freedom to pursue my own ideas and for the guidance and support he offered when I needed it.

I would also like to thank...

... Karsten Osenbrück for his help and practical input with regards to field experiments and encouragement throughout the years.

... Jud Harvey for showing me a whole new perspective and for much encouragement and support during my time at the US Geological Survey and afterward.

... Christiane Zarfl for taking interest in my research and making the time to evaluate this thesis.

... the Carl-Zeiss Stiftung for funding my PhD project, the German Academic Exchange Service (DAAD) for supporting my research stay at the USGS in Reston and the German Research Foundation (DFG) for additional funding.

... all Leverhulmees and in particular Marie Kurz and Phillip Blaen for four eventful field campaigns, for believing in me, and for wonderful memories.

... Dennis Lemke, for teaching me the ropes and introducing me to tracer work so many years ago.

... Thomas Wendel, Renate Seelig, Sara Cafisso and all the other great people at the Hydrogeochemistry lab.

... Friederike Currle, Anne-Marie Albrecht, Jens Brückmann and Lisa Emerich for their help with field work, spending many cold nights by the side of colorful streams without losing their humor.

... Wolfgang Kürner for fixing broken field equipment at short notice.

... Volker Lutz and his colleagues of the HPC BW team for their help and support with cluster-related problems.

... my fellow students and colleagues from IRTG, WESS and the Geoscience Department, for great discussions and for making work that little bit more fun on dreary days; my friends for putting up with my nerdiness, and last but not least my favorite physicist Lukas Kürten, for his unshakable belief in my abilities and for always supporting my "watered-down" science.

CONTENTS

This doctoral thesis is an accumulation of publications.

1 MOTIVATION

For many years, stream-tracer tests have been an established method to evaluate transport processes in rivers [*Knop*, 1878; *Stream Solute Workshop*, 1990; *Käss*, 2004], but their range of application is not restricted to the estimation of advective velocities and discharge. Instead, gas tracer tests can also be used to determine reaeration rates of oxygen across the air-water interface [*Wanninkhof et al.*, 1990; *Genereux and Hemond*, 1990; *Soares et al.*, 2013], and different types of natural and artificial tracers have been used more and more frequently to investigate groundwater-surface water interactions [e.g., *Bencala*, 1983; *Payn et al.*, 2009; *Harvey et al.*, 2013], a topic which has moved to a focus point of hydrology and ecology in recent years [*Sophocleous*, 2002; *Merill and Tonjes*, 2014; *Cardenas*, 2015]. In particular, the application of the reactive tracer resazurin has become a widely used method to determine hyporheic exchange processes, the reactivity of the stream bed, and respiration in the hyporheic zone [e.g., *Haggerty et al.*, 2008, 2009; *Argerich et al.*, 2011; *González-Pinzón et al.*, 2012; *Lemke et al.*, 2013a].

In spite of the broad applicability and wide utilization of stream-tracer tests, a number of serious caveats remain. This thesis therefore aims at advancing methods, the mathematical analysis, and the conceptual framework of stream-tracer techniques. In particular, I focus on reducing various sources of error associated with the different steps involved in conducting and evaluating stream-tracer tests. I chose these aspects to highlight that – in spite of their extensive application – the methods call for a number of advancements with regard to all links in the analysis chain. These include, but are not limited to a reduction of the measurement error, the conceptual error, as well as the parameter error. Whereas the conceptual (or model) error reflects inappropriate and misspecified assumptions or boundary conditions that may lead to a misinterpretation of the observed tracer test outcomes, the measurement error arises during the experimental phase of the tracer tests and propagates through to the analysis and interpretation of the experimental outcomes. The parameter error (or uncertainty), in contrast, occurs toward the end of the analysis chain, when model parameters are determined from the measured data, and different parameter sets lead to similarly good model fits [*Gupta et al.*, 2005]. This parameter uncertainty corresponds to the distribution of the best-fit parameters and thus the underlying variability of the determined parameters.

These different aspects have been a longstanding concern in environmental research in general, and in the field of stream-tracer techniques in particular. Since hyporheic exchange has become a focus of research in recent years, and stream-tracer techniques

have become a vital tool in this research area for the determination of hyporheic exchange processes and related metabolic activity, I chose to orient my thesis along aspects of stream-tracer techniques associated with hyporheic exchange:

- In order to obtain dependable information on reaeration and hyporheic exchange processes from stream-tracer tests, one needs to be sure that the recorded tracer concentrations in the stream and the parameters estimated from those measurements are as reliable as possible. This includes, but is not limited to, accurate measurement techniques for different tracer compounds, appropriate model representation of transport, hyporheic exchange and tracer properties, suitable parameter estimation algorithms and the assessment of parameter uncertainty.
- The transformation of the reactive tracer resazurin in streams is assumed to be proportional to hyporheic exchange and aerobic respiration in metabolically active storage zones in streams [*Haggerty et al.*, 2009; *Argerich et al.*, 2011]. Most of these results are based at least partly on laboratory analyses or batch experiments, especially when relating aerobic respiration rates to resazurin transformation rates [*González-Pinzón et al.*, 2012]. These method are problematic due to the small sample volume of the standardization technique compared to the larger scale of the tracer test, covering entire stream sections. Also, hydrodynamic conditions of the stream cannot be reproduced in a soil column. An independent, reliable and accurate "back-up" method to determine stream metabolism independently of the reactive tracers is needed if laboratory values are to be verified in future field studies. This "back-up" method should be as accurate as possible to ensure that even small differences in resazurin transformation between different stream sections can be attributed to actual differences in metabolism. Gas tracer tests combined with the analysis of time series of dissolved oxygen concentrations provide a potential for this.
- The majority of stream metabolism takes place in the subsurface, i.e., the hyporheic zone. Most reactive stream-tracer tests, recording tracer concentrations in the stream, are able to determine the bulk reactivity of the stream. That is, they are not able to provide information on the spatial distribution of reactivity in the hyporheic zone, as this requires tracer recordings in the subsurface. It is generally assumed that observation approaches on different scales complement each other, for which reason it is anticipated that a combined approach of in-stream and subsurface recordings allows a comparison of bulk reactivity measured in the stream to actual subsurface conditions, so that the impact of subsurface reactivity on whole-stream chemistry can be estimated. I examined, to what extent this is correct.

2 STATE OF THE ART

The hyporheic zone, the transition zone between streams and groundwater, is of major importance for the ecological functioning of streams [*Boulton et al.*, 2010]. Through filtering of particles, nutrient retention and pollutant degradation, it plays a key role with respect to the self-cleaning potential of streams [*Boulton et al.*, 1998], thus influencing water quality and ecosystem health [*Young and Huryn*, 1999]. Furthermore, conditions of pH, temperature, nutrient availability and flow velocities of water within the hyporheic zone differ greatly from those prevailing in the main channel, making it an ideal habitat for microorganisms and aquatic organisms [*Bencala et al.*, 2011]. Due to these unique, advantageous conditions, reactions can take place in the subsurface that would not be possible in the main channel. The majority of a stream's biogeochemical turnover and aerobic respiration thus takes place in the hyporheic zone [*González-Pinzón et al.*, 2012].

These geochemical and hydrological processes of hyporheic exchange have been the subject of research for several years [see overview by *Cardenas*, 2015] and stream-tracer tests on the reach-scale have become an established method to estimate exchange processes in experimental studies [e.g., *Wagner and Harvey*, 1997; *Wörman et al.*, 2002; *Payn et al.*, 2009]. The general procedure of a stream-tracer test is always the same, independent of the tracer compound, and even of the underlying scientific question. The tracer compound is injected into the stream at a chosen location and the compound's concentration is measured over time at one or more locations downstream of the injection site, yielding concentration breakthrough curves. All the tracer mass can either be injected at once (this type of injection is termed a "slug" or "instantaneous" injection) or, in case of a "continuous" injection, the tracer is introduced into the stream at a constant rate over a longer duration [*Käss*, 2004].

The obtained breakthrough curves can be analyzed in various ways described below. The goal of the analysis is usually the derivation of transport parameters, but also parameters of hyporheic exchange and reaeration rates can be determined. For this purpose, different approaches exist, ranging from a direct interpretation of plateau concentrations (in case of a continuous injection) or the temporal moments of the breakthrough curves to an inverse modeling approach, in which parameters are determined by fitting a model that simulates the processes of interest.

2.1 Conceptual models of Transport and Hyporheic Exchange

At times, it can become necessary to fit a mathematical model to measured breakthrough curves. In some cases this is done to obtain noise-free extended concentration time series which can be used for further processing. Usually, however, model fitting is done to obtain model parameters. For this, the relevant processes need to be conceptualized in an appropriate model framework. In the following, I review the most common one-dimensional advection-dispersion based models for stream flow and hyporheic exchange that are of relevance in the context of my thesis.

General Advective Dispersive Transport in Streams

One-dimensional transport in streams can be described by the advection-dispersion equation, here described with uniform and time-invariant coefficients.

$$\frac{\partial c(x,t)}{\partial t} + v\frac{\partial c(x,t)}{\partial x} - D\frac{\partial^2 c(x,t)}{\partial x^2} = 0 \tag{2.1}$$

In this, $c(x,t)$ [ML^{-3}] denotes the solute concentration in the stream dependent on location x [L] and time t [T] (for brevity, the dependence of the concentration on time and space is dropped in the following). v [LT^{-1}] denotes the advective velocity and D [$\mathrm{L}^2\mathrm{T}^{-1}$] the dispersion coefficient. Equation (2.1) thus incorporates advective mass transport as well as Fickian dispersion, leading to ideal tracer breakthrough curves.

In this case, parametric transfer functions, describing the system response to a unit pulse, can be described by inverse-Gaussian functions [*Kreft and Zuber*, 1978] and a convolution of the input signal (e.g., a tracer pulse c_{in}) with the transfer function $g(\tau)$ [T^{-1}] computes the output signal (e.g., a breakthrough curve c_{out}):

$$c_{\mathrm{out}}(t) = (c_{\mathrm{in}} * g)(t) = \int_0^\infty c_{\mathrm{in}}(t-\tau)g(\tau)d\tau \tag{2.2}$$

with the travel time τ [T]. Under Fickian transport, this output signal corresponds to the analytical solution of equation (2.1). Conversely, a deconvolution of the in- and output signals identifies the appropriate transfer function.

For a conservative tracer, the transfer function equals the travel-time distribution times the tracer recovery, with the travel-time distribution describing the time of a water parcel to reach a certain location. For a reactive tracer, additional processes alter the transfer function, e.g., the decay or production of the compound, or its degassing in case of a volatile compound.

In the real world, however, transport often deviates from Fickian behavior, leading to tracer breakthrough curves that differ from the analytical solution of equation (2.1). In this case, the calculation of a nonparametric transfer function may be more appropriate. This shape-free approach does not enforce a certain parametric shape on the transfer

function, but allows multi-modal functions or untypical late-time behavior and is thus free to adjust to the data. It is only constrained to be non-negative for all travel times τ and its smoothness may be described by a linear semi-variogram function γ_g [for details see *Cirpka et al.*, 2007; *Knapp and Cirpka*, 2017]:

$$\gamma_g(\tau_i - \tau_j) = \frac{1}{2} E\left[\left(g(\tau_i) - g(\tau_j)\right)^2\right] = \Theta\,|\tau_i - \tau_j| \tag{2.3}$$

with the expected value operator $E[\cdot]$ and the slope, Θ [T^{-3}], of the semi-variogram function. In a 1-D application, assuming a linear varigram function is identical to first-order Thikonov-regularization [*Kitanidis*, 1997].

Models for Hyporheic Exchange

The Transient Storage Model (TSM) [*Bencala*, 1983; *De Smedt et al.*, 2005] describes transport in the main channel, coupled to temporary storage of water and solutes in an adjacent storage zone. While transport in the channel is represented by the one-dimensional advection-dispersion equation, the exchange between the mobile channel water and the immobile water in the storage zone is assumed to be proportional to the concentration difference of the two compartments.

$$\begin{aligned} \frac{\partial c}{\partial t} + A_r \frac{\partial c_s}{\partial t} + v\frac{\partial c}{\partial x} - D\frac{\partial^2 c}{\partial x^2} &= 0 \\ \frac{\partial c_s}{\partial t} &= k(c - c_s) \end{aligned} \tag{2.4}$$

subject to appropriate boundary and initial conditions.

The TSM is thus an expansion of the advection dispersion equation, incorporating additionally exchange with the storage zone with concentration, c_s [ML^{-3}], while k [T^{-1}] is the rate coefficient of the linear exchange between the mobile and immobile zone. A_r [-] is the ratio between the cross-sectional areas of the storage zone and the mobile channel. In the most simple version of equation (2.4), a single, well-mixed storage zone with an exponential hyporheic residence time distribution is assumed, even though it is also possible to account for several distinct storage zones with different residence times [e.g., *Gooseff et al.*, 2005; *Kerr et al.*, 2013]. To solve equation (2.1), a transformation to the Laplace domain is convenient. This is true for all transport and exchange models discussed in the following, and details can be found in Appendix A.

Solute source or sink terms can also be described, both within the main channel or in the storage zone. For this, equation (2.4) has to be expanded as follows:

$$\begin{aligned} \frac{\partial c}{\partial t} + A_r \frac{\partial c_s}{\partial t} + v\frac{\partial c}{\partial x} - D\frac{\partial^2 c}{\partial x^2} &= S_m \\ \frac{\partial c_s}{\partial t} &= k(c - c_s) + S_s \end{aligned} \tag{2.5}$$

with the reaction term in the main channel S_m [$ML^{-3}T^{-1}$] and the reaction in the storage zone S_s [$ML^{-3}T^{-1}$]. In case of a first-order reaction, these sink terms are proportional to the respective concentration, $S_j = \lambda c_j$, with $j = m, s$ and the reaction rate constant λ [T^{-1}].

Due to its simple conceptualization and easy applicability, the TSM has become very popular and is applied quite often [e.g., *Hart*, 1995; *Marion et al.*, 2003; *Kelleher et al.*, 2013]. However, the standard transient storage model exhibits several major shortcomings in its standard conceptualization. For one, the residence time distribution of the water in the storage zone is assumed to be an exponential function [*Bencala*, 1983; *Runkel*, 1998]. Numerous studies have indicated that this exponential shape of the residence time distribution is not able to capture the late-time behavior of tracer breakthrough curves sufficiently well and several other parametric shapes have been suggested instead, including (truncated) power-law and log-normal functions [e.g., *Haggerty et al.*, 2000, 2002; *Wörman et al.*, 2002] as well as nonparametric functions [*Liao et al.*, 2013]. It can thus be advantageous to generalize equation (2.4) for any shape of transfer function:

$$\frac{\partial c}{\partial t} + v\frac{\partial c}{\partial x} - D\frac{\partial^2 c}{\partial x^2} = q_{he}\left(\int_0^t g_0(\tau)c(t-\tau)d\tau - c(t)\right) \tag{2.6}$$

subject to the initial and boundary conditions for a slug injection, e.g., where the tracer mass m [M] is injected over the cross-sectional area A [L^2] of the main channel as a Dirac pulse:

$$\begin{aligned} c(t_0, x) &= 0, \\ \left(vc - D\frac{\partial c}{\partial x}\right)\Big|_{x=0} &= \frac{m}{A}\delta(t), \\ \lim_{x\to\infty} c(t, x) &= 0 \;\forall t. \end{aligned} \tag{2.7}$$

In this, the hyporheic transfer function $g_0(\tau)$ [T^{-1}] describes the probability density of a tracer particle entering the hyporheic zone at time zero to leave it after the time period τ [T]. Equivalent to the in-stream transfer function discussed above, the hyporheic transfer function of the conservative tracer quantifies the tracer recovery multiplied by the hyporheic travel-time distribution. In the above equation, the transfer function can take any parametric or nonparametric shape desired.

Furthermore, the conceptualization of the storage zone as a well-mixed reactor is intuitively not correct. According to the TSM, the stream samples water of different hyporheic ages with the same probability. Instead, gradients of reactivity and nutrient distributions are commonly found in real streams, that cannot be represented by the transient storage model. This has already been shown to be true for catchment outlets [*Rinaldo et al.*, 2015], and one would assume that the age distribution of the hyporheic zone is also selected in a non-uniform way by the stream.

Finally, the TSM is not able to distinguish between different types of storage zones, and in-stream and subsurface storage are usually lumped together. Therefore, the TSM is not able to reliably identify hyporheic zones in its standard conceptualization. This is also reflected in the analysis of a tracer test with a single, conservative tracer compound. The observed breakthrough curve usually exhibits pronounced tailing, caused by a combination of in-stream storage (e.g., in still-water zones) and subsurface storage in the hyporheic zone. The individual contributions to the total are usually impossible to disentangle from outcomes of a single, conservative tracer test.

Incorporation of Reactive Tracers Whereas the first two shortcomings will be addressed in a different part of this thesis, *Haggerty et al.* [2008, 2009] proposed injecting the reactive "smart" tracer resazurin together with a conservative compound to tackle the last shortcoming mentioned above. Resazurin is a weakly fluorescent, phenoazine dye that is reduced to the compound resorufin in living cells, e.g., in bacteria [*O'Brien et al.*, 2000]. In fact, *O'Brien et al.* [2000] found that the reduction of resazurin to resorufin occurred in a medium by cellular activity, but not in a highly reduced medium without cellular activity. Since most microorganisms in streams are found in the hyporheic zone [*González-Pinzón et al.*, 2012, 2014], the resazurin-to-resorufin transformation can be used as proxy for microbial activity and aerobic respiration, as occurring in the hyporheic zone. If concentration breakthrough curves of the reactive and conservative tracers are jointly analyzed, exchange with metabolically active transient storage zones can be distinguished from transient storage in metabolically inactive zones like surface water dead zones [*Haggerty et al.*, 2008, 2009]. Equation (2.6) then has to be extended to account for resazurin (index 1) and resorufin (index 2):

$$\frac{\partial c_1}{\partial t} + v\frac{\partial c_1}{\partial x} - D\frac{\partial^2 c_1}{\partial x^2} = q_{he}\left(\int_0^t g_1(\tau)c_1(t-\tau)d\tau - c_1(t)\right) \tag{2.8}$$

$$\frac{\partial c_2}{\partial t} + v\frac{\partial c_2}{\partial x} - D\frac{\partial^2 c_2}{\partial x^2} = q_{he}\left(\int_0^t \left(g_{12}(\tau)c_1(t-\tau) + g_2(\tau)c_2(t-\tau)\right)d\tau - c_2(t)\right) \tag{2.9}$$

subject to

$$\begin{aligned} c(t_0, x) &= 0, \\ \left(vc_1 - D\frac{\partial c_1}{\partial x}\right)\Big|_{x=0} &= \frac{m_1}{A}\delta(t), \\ \left(vc_2 - D\frac{\partial c_2}{\partial x}\right)\Big|_{x=0} &= 0 \end{aligned} \tag{2.10}$$

Whereas equation (2.8) incorporates the hyporheic transfer function of resazurin $g_1(\tau)$, that quantifies the decay of resazurin on its passage through the subsurface, equation (2.9) contains the cross-compound transfer function $g_{12}(\tau)$ in addition to the hyporheic transfer function of resorufin, $g_2(\tau)$. This cross-compound transfer function describes resorufin leaving the hyporheic zone caused by a pulse of resazurin entering it.

Liao et al. [2013] coupled hyporheic exchange processes of resazurin and resorufin to additional compound-specific properties like equilibrium and kinetic sorption in the subsurface to obtain a better fit of the recorded concentration breakthrough curves. A nonparametric distribution was assumed for the conservative tracer, and the transfer functions of the reactive tracer and its reaction product were derived from the transfer function of the conservative tracer, $g_0(\tau)$. For the reactive tracer resazurin and its reaction product resorufin, taking into account equilibrium and kinetic sorption in the hyporheic zone, as well as transformation of the compounds, the following relationships hold:

$$R_i \frac{\partial c_{i,hz}}{\partial \tau} + K_i \frac{\partial c_i^*}{\partial \tau} + \frac{\partial c_{i,hz}}{\partial \tau^*} = r_{i,hz} \tag{2.11}$$

$$\frac{\partial c_i^*}{\partial \tau} = k_i \left(c_{i,hz} - c_i^* \right) \tag{2.12}$$

$$c_{i,hz}(\tau, 0) = b_i \delta(\tau) \tag{2.13}$$

with

$$r_{1,hz} = -\lambda_1 c_{1,hz} \tag{2.14}$$

$$r_{2,hz} = \lambda_{12} c_{1,hz} - \lambda_2 c_{2,hz} \tag{2.15}$$

with the tracer concentration of compound i ($i = 1$ for resazurin and $i = 2$ for resorufin) in the hyporheic zone, $c_{i,hz}$ [ML^{-3}], and at the kinetically sorbing sites, c_i^* [ML^{-3}]. R_i [-] quantifies retardation by linear equilibrium sorption in the hyporheic zone, whereas K_i [-] is the kinetic sorption coefficient, with the associated mass transfer rate coefficient k_i [T^{-1}]. Resazurin and resorufin decay with the decay coefficients λ_i [T^{-1}], and λ_{12} [T^{-1}] quantifies the transformation from resazurin to resorufin, with $\lambda_{12} \leq \lambda_1$. This means that the product of resazurin decay is not exclusively resorufin, but resazurin is also transformed to other, unknown compounds. Resorufin can be reversibly converted to the colorless dihydroresorufin under anaerobic conditions. Since the reoxidation to resorufin is fast under aerobic conditions (i.e., in stream water), this reaction is not included in the equations above. However, over time resorufin is also degraded to other unknown products, which is represented by the decay rate constant λ_2. The dimensionless coefficient b_i quantifies the relative amount of tracer introduced into the hyporheic zone at time $\tau = 0$.

Reactive Tracers in the Subsurface

So far, I have considered transport in a stream undergoing hyporheic exchange. In one part of my thesis, however, I take a look at the subsurface component of transport alone, i.e., conceptualized as vertical transport. This can be done by adapting equation (2.1) for sources and sinks. Furthermore, the concentration term now denotes concentration in the hyporheic zone $c_{i,hz}$ [ML^{-3}] for different compounds i instead of the open channel. If porosity is assumed to be constant over depth it does not need to be considered separately.

For a conservative tracer ($i = 0$), a reactive tracer ($i = 1$) and the reaction product ($i = 2$) the governing equations thus read as follows:

$$\frac{\partial c_{0,hz}}{\partial t} + v_z \frac{\partial c_{0,hz}}{\partial z} - D_z \frac{\partial^2 c_{0,hz}}{\partial z^2} = -q_{in} c_{0,hz} \tag{2.16}$$

$$R_1 \frac{\partial c_{1,hz}}{\partial t} + v_z \frac{\partial c_{1,hz}}{\partial z} - D_z \frac{\partial^2 c_{1,hz}}{\partial z^2} = -\lambda_1 c_{1,hz} - q_{in} c_{1,hz} \tag{2.17}$$

$$R_2 \frac{\partial c_{2,hz}}{\partial t} + v_z \frac{\partial c_{2,hz}}{\partial z} - D_z \frac{\partial^2 c_{2,hz}}{\partial z^2} = -\lambda_2 c_{2,hz} + \lambda_{12} c_{1,hz} - q_{in} c_{2,hz} \tag{2.18}$$

with the vertical spatial coordinate z [L]. The advection and dispersion parameters are apparent parameters, describing only the vertical component of transport. They are therefore denoted v_z [LT^{-1}] and D_z [L^2T^{-1}]. q_{in} [T^{-1}] is a rate coefficient accounting for mixing with (here tracer-free) groundwater and the net effect of mixing is therefore dilution acting to the same extent on all three tracer compounds. Reaction and retardation are considered as before with the coefficients λ_i and R_i.

2.2 Method of Moments

Breakthrough curves can be concisely summarized by their temporal moments and the zeroth to third moments are able to describe the accumulated mass, the mean, variance and skewness of the breakthrough curve [*Harvey and Gorelick*, 1995]. In this, the k-th temporal moment μ_k [$ML^{-3}T^{k+1}$] of a breakthrough curve at a given location x is defined as:

$$\mu_k(x) = \int_0^\infty t^k c(x,t) dt. \tag{2.19}$$

in which $c(x,t)$ is the tracer concentration measured in the stream and t is time.

The zeroth moment at any given location is the area under the breakthrough curve. Multiplied with stream discharge Q [L^3T^{-1}] it provides a measure of the tracer mass m [M] passing a particular location x:

$$\mu_0(x) \cdot Q = \int_0^\infty c(x,t) dt \cdot Q = m(x) \tag{2.20}$$

The first temporal moment normalized by the zeroth moment quantifies the mean arrival time $\mu_\tau(x)$ [T] of the tracer at the given location x:

$$\frac{\mu_1(x)}{\mu_0(x)} = \frac{\int_0^\infty c(x,t) t dt}{\int_0^\infty c(x,t) dt} = \mu_\tau(x) \tag{2.21}$$

In the case of the second temporal moment, the central moment is used more commonly than the raw moment:

$$\mu_{2c}(x) = \int_0^\infty \left(t - \frac{\mu_1(x)}{\mu_0(x)} \right)^2 c(x,t) dt \tag{2.22}$$

The variance of the travel-times $\sigma_\tau^2(x)$ can be calculated from the second central moment normalized by the zeroth moment:

$$\frac{\mu_{2c}(x)}{\mu_0(x)} = \frac{\mu_2(x)}{\mu_0(x)} - \left(\frac{\mu_1(x)}{\mu_0(x)}\right)^2 = \sigma_\tau^2(x) \tag{2.23}$$

The skewness (providing information on the tailing) and kurtosis (i.e., the "peakedness") of the breakthrough curve are described by the third and fourth temporal moments, respectively.

Moment-generating equations can be obtained by multiplying the given expression (e.g., the advection-dispersion equation) with t^k and a subsequent integration over time. In case of the general advection-dispersion equation (equation (2.1)) without any sources or sinks this leads to:

$$-k\mu_{k-1}(x) + v\frac{\partial \mu_k(x)}{\partial x} - D\frac{\partial^2 \mu_k(x)}{\partial x^2} = 0. \tag{2.24}$$

To determine the temporal moments, alternatively, the derivative of the Laplace transformed concentrations [*Kučera*, 1965; *Harvey and Gorelick*, 1995] can be analyzed by:

$$\int_0^\infty c(x,t)t^k = \mu_k(x) = (-1)^k \frac{\partial^k \tilde{c}(x,s)}{\partial s^k}\bigg|_{s\to 0} \tag{2.25}$$

This approach is illustrated exemplarily for equations (2.16) to (2.18) in Appendix B, as will be made use of in *Knapp et al.* [2017] to determine tracer recovery and residence times in the subsurface.

2.3 Oxygen Balance of Streams

Hyporheic processes influence not only nutrient availability, but also have an important influence on the amount of available dissolved oxygen in the stream water through aerobic respiration in the subsurface. The amount of dissolved oxygen available in a stream is commonly considered an important quantity of water quality and ecosystem health [*Young and Huryn*, 1999]. Its available concentration depends not only on respiration, but also on photosynthesis (or primary production) and reaeration across the air-water interface. While respiration leads to a decrease in oxygen concentrations at a relatively constant rate r_{resp} [$\text{ML}^{-3}\text{T}^{-1}$] over time, photosynthesis produces oxygen at a rate r_{photo} [$\text{ML}^{-3}\text{T}^{-1}$] proportional to the available solar radiation. Reaeration, in contrast, drives the system towards its equilibrium concentration by interchangeably introducing and removing oxygen from the water according to the saturation deficit, the difference between the saturation concentration, c_{sat} [ML^{-3}], and the actual concentration of oxygen, c_{O_2} [ML^{-3}], at any given time with the rate constant k_2 [T^{-1}]. A simplified approach, neglecting the influence of (advective and dispersive) transport, summarizes the oxygen balance as

follows [*Odum*, 1956; *Hoellein et al.*, 2013]:

$$\frac{dc_{O_2}}{dt} = r_{\text{photo}} - r_{\text{resp}} + k_2(c_{\text{sat}} - c_{O_2}) \tag{2.26}$$

The effect of these processes is illustrated in Figure 2.1.

The magnitudes of the individual processes described above cannot directly be determined from concentrations of dissolved oxygen. Instead, usually a step-wise approach is taken, quantifying one contributing process after another. Commonly, the reaeration rate constant k_2 is determined first, which then allows to quantify nighttime respiration. If this is assumed to be constant throughout the day, photosynsthesis can be calculated as the remainder.

Reaeration across the air-water-interface

Reaeration across the air-water interface drives the concentration of dissolved gases in streams towards the equilibrium concentration and may be related to a number of hydraulic and morphological properties of the stream, like the flow velocity, flow depths and slope of the stream bed. In semi-empirical approximations [e.g., *O'Connor and Dobbins*, 1956; *Tsivoglou and Neal*, 1976], information on the bedslope, discharge and advective in-stream velocity can be used to determine reaeration rate coefficients. These approximation, however, usually only hold for very defined conditions and have been found to underestimate reaeration especially in smaller streams [*Young and Huryn*, 1999; *Soares et al.*, 2013].

Determining reaeration via gas tracer tests is much more time-consuming, but also more precise [*Wanninkhof et al.*, 1990]. During these gas tracer tests, a volatile compound is continuously injected as tracer into the stream [e.g., *Wanninkhof et al.*, 1990; *Marzolf et al.*, 1994] and its concentration measured at two or more locations downstream of the injection site. Generally, a first-order loss of the gas concentration c_g [ML^{-3}] with travel-time τ [T] is assumed, which reads for a volatile compound with negligible atmospheric concentration as:

$$\frac{dc_g}{d\tau} = -k_2 c_g. \tag{2.27}$$

The rate constant k_2 can thus be determined according to the following relationship:

$$k_2 = \frac{1}{\tau} \ln \left(\frac{c_g^{\text{up}}}{c_g^{\text{down}}} \right) \tag{2.28}$$

with the concentrations of the dissolved gas at an upper and a lower measurement station in the stream, c_g^{up} and c_g^{down}, respectively.

If the determination of reaeration rates of oxygen is of interest, propane is a suitable tracer compound [e.g., *Marzolf et al.*, 1994; *Young and Huryn*, 1999]. Then, the obtained

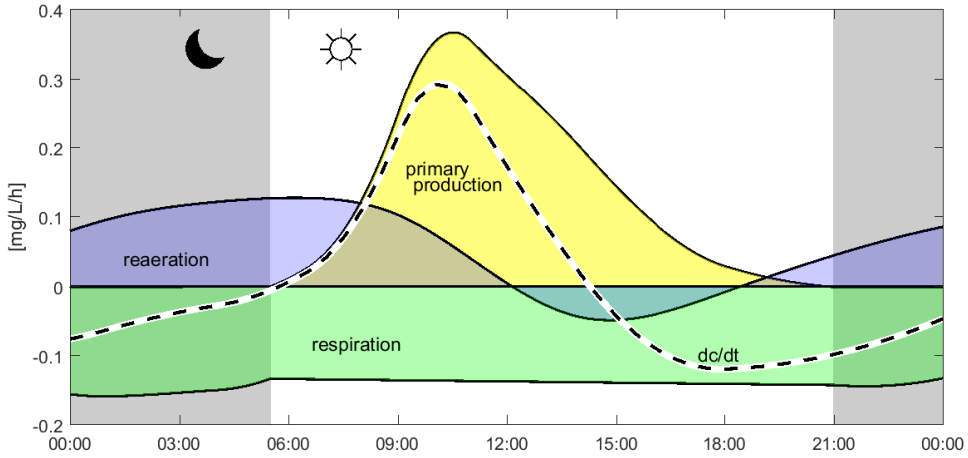

Figure 2.1: The rate of change of oxygen (dc/dt, dashed line) is the sum of reaeration (blue), respiration (green) and photosynthesis/primary production (yellow). Shaded areas indicate night time, light areas day time. Adapted from *Kurz and Knapp* [in preparation].

reaeration rate constants of the tracer compound can easily be transferred to those of oxygen through a multiplication with a constant:

$$k_{2,\text{Oxygen}} = 1.39 \cdot k_{2,\text{Propane}} \tag{2.29}$$

This is possible since the molecular diffusion coefficients and Henry constants of the two compounds are relatively similar [*Rathbun et al.*, 1978].

The Relationship between Resazurin and Aerobic Respiration

González-Pinzón et al. [2012] presented a method that allows using the transformation of resazurin to resorufin not only as an indicator for metabolism, but permits calculating rates of aerobic respiration, since a number of studies found that different types of aerobs or facultative anaerob organisms are able to reduce resazurin to resorufin, but not strict anaerobs [*Karakashev et al.*, 2003]. For this calculation, the decay rate of resazurin obtained from a reach-scale stream-tracer test is multiplied by the molar processing ratio of dissolved oxygen to resazurin, K_{DO}^{Raz} [-], quantifying the ratio of moles of dissolved oxygen processed per mole of resazurin processed. This processing ratio is obtained from batch experiments, where a sample of stream sediment is spiked with resazurin in a recirculating chamber closed to the atmosphere, and both oxygen and resazurin concentrations are recorded over time. The method allows eliminating the effect of reaeration from the oxygen balance when correlating resazurin transformation and oxygen consumption in a field setting and takes into account the sediment (and microorganism community) specific properties regarding resazurin transformation.

2.4 Model Fitting and Parameter Estimation

When statements are to be made about hyporheic exchange or oxygen-related processes, the parameters described in the various models above need to be determined. This can be obtained by fitting the respective model to measured data. For the estimation of parameters through inverse modeling, approaches of different complexity are available. In general, the goodness of fit and thus the adequacy of the parameters is determined from a comparison of the simulated and measured data, and the parameter guesses are adapted accordingly. The most simple algorithms for this are gradient-based methods like the Gauss-Newton method and its stabilized Levenberg-Marquardt modification [e.g., *Press et al.*, 1992, chapter 15]. In case of multi-modal parameter spaces, however, these are usually not able to find the global optimum of the parameter space, and instead tend to get stuck in a local optimum. The location of this optimum often depends on the initial guess of the parameters, and no information is available on how good the encountered local optimum is compared to the (unknown) global optimum. The probability of encountering the global optimum usually decreases with the complexity of the underlying model (one good example is the fit performance in the study of *Liao et al.* [2013]).

In these cases of multi-modality, global-search methods fare better as they are able to systematically search the parameter space in order to find the global optimum. Examples for global-search algorithms are different kinds of evolutionary algorithms (e.g., the genetic algorithm, for an overview see *Bäck and Schwefel* [1993]) that mimic real life evolution processes, or Monte Carlo methods where random simulations are used to find approximate solutions. These approaches differ greatly in their efficiency, but have one problem in common. Uncertainties of the estimated parameters can usually only be obtained based on a linearized uncertainty propagation, which is not trustworthy. This problem is circumvented by a number of algorithms combining evolutionary algorithms with Bayesian computation in a Markov-chain Monte Carlo approach [e.g., the DE-MC, DREAM and DREAM(ZS) algorithms by *Ter Braak*, 2005; *Vrugt et al.*, 2008, 2009]. These algorithms are able to find the globally optimal parameter set and compute the posterior distribution of the estimated parameters, thereby evaluating the uncertainty of the parameters.

When it comes to estimating the relatively high number of parameters involved in the models using reactive tracers to quantify hyporheic exchange, the Markov-chain Monte Carlo approach can be particularly advantageous and was successfully tested by *Lemke et al.* [2013a] for the estimation of hyporheic exchange parameters from a reactive stream-tracer test. In his approach, however, an exponential hyporheic travel-time distribution was assumed which can be described by a single parameter. In case of more complex parametric transfer functions, or even a nonparametric approach requiring

a continuous function to be estimated, the computational effort would likely increase dramatically.

Some studies tried to reduce the number of parameters required to be estimated by fixing decay and transformation rate coefficients of the reactive tracer and its product to laboratory-determined, sediment-specific values [e.g., *Haggerty et al.*, 2009]. Other studies [e.g., *Argerich et al.*, 2011] used the conservative tracer to determine parameters of in-stream transport from a standard TSM model, and kept these fixed when determining hyporheic exchange rates from the reactive tracers. Both approaches are not ideal. Laboratory methods are always affected by the disadvantage that ambient conditions cannot be recreated sufficiently well, and sample volumes usually represent only a limited number of sites. Using different models to estimate different parameters characterizing one integrated system (i.e., in-stream transport and hyporheic exchange) is problematic since the parameters are usually highly correlated. Fixing in-stream transport thus introduces a bias towards certain strengths of hyporheic exchange. Therefore, a different model framework is required, that can reliably and efficiently estimate parameters of models with higher complexity.

3 OBJECTIVES AND CONTRIBUTIONS

This thesis aims to advance stream-tracer techniques by overcoming shortcomings related to the experimental methods, the mathematical analysis and the parameter estimation through modeling associated with common types of stream-tracer tests. In particular, I address the following questions in this work:

1. How can different experimental stream-tracer techniques be improved?
2. How do tracer observations conform with standard conceptual and mathematical models?
3. How can the mathematical analysis of reactive stream-tracer techniques be advanced to improve determining hydraulic parameters of complex models?

With regard to the experimental set-up, this work highlights potential sources of measurement error in current standard sampling methods applied in reactive-tracer tests with resazurin and resorufin, as well as gas tracer tests (e.g., with propane). I evaluate the effectiveness of the proposed improvements and their impact on rate calculations of metabolism.

I quantify the importance of dispersive transport in streams and examine to what extent calculations of metabolic rates are influenced if additional transport processes other than advection are considered. To this end, this work compares the effect of Fickian and non-Fickian dispersion on solute transport by including full travel-time distributions rather than purely advective mean travel-times into further analysis steps of gas tracer test outcomes.

Furthermore, this work systematically analyzes common observation protocols of stream-tracer tests and contrasts the information gained from in-stream and subsurface tracer sampling. To this effect, I compare how and why outcomes from the two types of observations disagree with each other and with common conceptual models of in-stream transport and hyporheic exchange. The results illustrate the danger of a direct physical interpretation of the estimated exchange parameters.

I present a local-in-global model fitting approach that combines the nested updating of the hyporheic transfer function as a continuous function with the global estimation of a set of hydraulic parameters. The proposed procedure efficiently estimates the hyporheic

transfer function dependent on the chosen parameter set, finds the global optimum of the parameters and further provides information on the distribution of the estimated parameters. It is therefore an illustration of how an improved and therefore complex model of hyporheic exchange can be used to reliably determine a comparably large number of related parameters. This allows the application of relatively sophisticated models that incorporate more processes and thereby better represent the realities of hyporheic exchange.

4 RESULTS AND DISCUSSION

This section summarizes results presented in the peer-reviewed articles of *Knapp et al.* [2015], *Knapp et al.* [2017] and *Knapp and Cirpka* [2017], which can be found in the Appendix, amended by results not included in these articles.

4.1 How can different experimental stream-tracer techniques be improved?

Fluorescence sensitivities of the measurement devices

Lemke et al. [2013b] and others presented a detailed illustration of the methods applied to conduct and analyze reactive stream-tracer tests with the compound resazurin. They presented an online fluorometer that is able to record fluorescence signals of fluorescein (a conservative tracer), resazurin and resorufin in-situ. I used the same instrument during my field measurements, but encountered frequent violations of the mass balance between consecutive stream sections, with apparently increasing mass of the reactive tracer resazurin along the reach or negative concentrations of the reaction product resorufin. A thorough laboratory analysis revealed that the band widths of the filters of the online fluorometers are too wide to efficiently separate the tracers resazurin and resorufin. *Wratten92* and *Wratten25* filters are used for resazurin and resorufin detection [*Schnegg*, pers. comm.], respectively, which are high pass filters only filtering out wavelengths below 625 nm, respectively 580 nm. Furthermore, the wavelengths of the LEDs used as excitation light sources are somewhat lower than the wavelengths of maximum compound sensitivity. That this combination of excitation and emission wavelengths is not able to capture the fluorescence maxima of the reactive tracer compounds and furthermore integrates over a relatively large signal range is illustrated in Figure 4.1. Small variations in the fluorescence signal (during the measurement itself or between instrument calibration and measurement) make it difficult to reliably determine the contributions of the individual tracers to the mixture following the matrix approach described by *Lemke et al.* [2013b].

For this reason, it is not possible to accurately determine the concentration of the reactive tracers from the online fluorometers in spite of careful on-site calibration, even though they generally record the true shape of the concentration breakthrough curves. I have therefore amended the measurement protocol to include a small number of grab samples timed carefully over the course of the breakthrough curve, that are later analyzed on a bench-top fluorometer in the laboratory with much higher precision – a suggested approach which has now been adopted also by other studies [e.g., *Blaen et al.*,

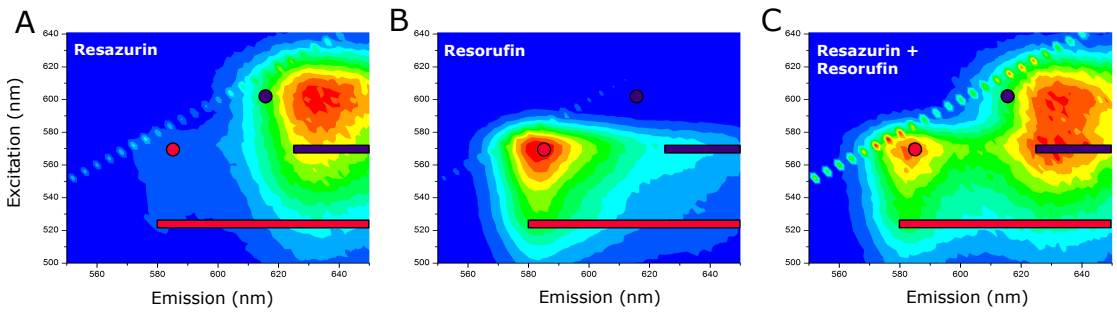

Figure 4.1: Fluorescence spectra of resazurin (A), resorufin (B) and a mix of the two compounds (C). Colors indicate fluorescence intensity, with highest intensity in red and lowest in blue - not to scale. Dots mark the suggested wavelengths of excitation and emission by *Haggerty et al.* [2008], bars the approximate wavelengths covered by the GGUN-FL 30 fluorometers. Blue symbols indicate measurements sensitive for resazurin, red ones for resorufin.

submitted]. Not only is it possible to correct the recorded breakthrough curves for actual concentrations from the concentrations determined this way, but these grab samples can also be used to estimate measurement uncertainties of the recorded breakthrough curves through repeated analysis – which was not possible from fluorometer data alone. This can be used to validate tracer-dilution effects and thus changes in discharge along the reach.

Influence of temporal variations of the gas tracer input

Even though gas tracer tests have been a standard tool for the assessment of stream metabolism and reaeration of oxygen for many years, the standard approach is based on two major simplifying assumptions. Transport is considered to be strictly advective, and the gas input into the stream is required to be steady over time. Whereas the first assumption is one that comes into play during the processing and analysis of the tracer data and will be discussed in a later section, the second is an experimental challenge that is hard to satisfy, especially since durability and cost efficiency of field equipment is usually of primary concern, so accuracy cannot always be guaranteed. I managed to stabilize the input signal as much as possible by fitting the outlet system of the propane gas cylinder with an additional pressure regulation valve and a flowmeter. However, even with this improvement it is still hardly possible to keep the input signal constant. To investigate the actual stability of the gas signal, I sampled repeatedly at the first measurement station downstream of the injection site and thus analyzed the temporal trend of the gas input. At all other measurement stations, only one set of samples (three to four individual samples were collected per set to reduce measurement uncertainty) was taken, but the propagation of the temporal trend of the input signal at these locations was determined mathematically in a recursive manner (for details see *Knapp et al.* [2015]).

To quantify this effect on analysis outcomes, I compared the calculated reaeration rates from a propane gas tracer test taking into account the unsteady signal compared

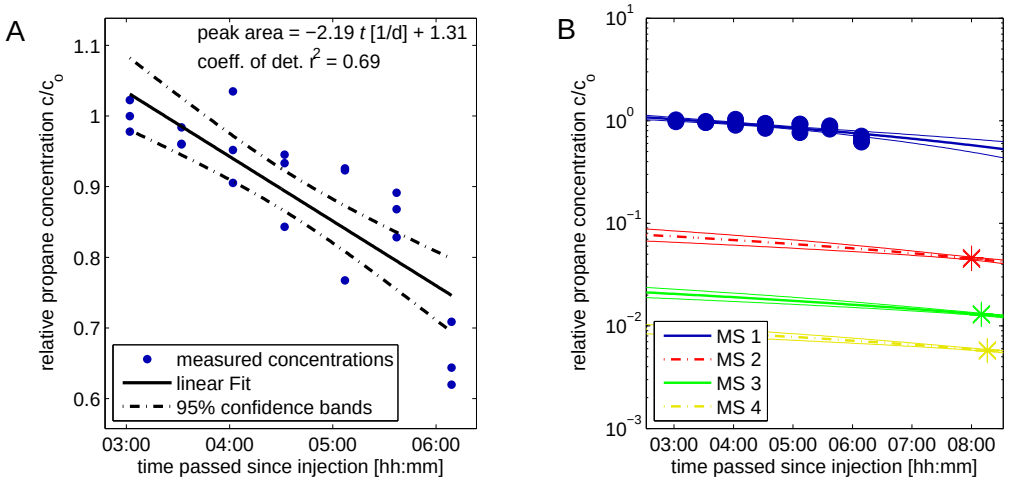

Figure 4.2: Relative propane concentrations at the first measurement station (left) and at all measurement stations (right) with a fitted linear regression line and measured concentrations (stars and filled circles). For details on the recursive calculation of the temporal variations at all measurement stations following the first measurement station (lines in right figure) see [*Knapp et al.*, 2015].

to an analysis where this unsteadiness was neglected in *Knapp et al.* [2015]. For this comparison, I used the standard analysis approach from equation (2.28) with mean travel times between measurement stations determined from the first temporal moments of a conservative tracer that was injected as a slug at the same location as the propane gas.

Figure 4.2A shows the time series of measured propane concentrations over time with fitted linear regression at the first measurement station, whereas the measured concentrations and recursively calculated concentration trends over time at all measurement stations are shown in Figure 4.2B. It is obvious from the figure that the concentrations decrease over time, which propagates along the reach and Figure 4.3 shows how this temporal trend in the input signal affects calculated reaeration rate coefficients. A comparison between the standard approach with constant signal (neglecting the unsteady input signal, left bars) and the standard approach with fluctuating signal (taking into account the temporal trend of the gas signal, bars second from left) shows that the unsteadiness of the signal has a large impact on the estimated reaeration rate coefficients in the different reach sections. The difference is significant in all cases with differences up to 10 % between the two approaches. The direction of the effect also differs between stream sections, depending on the time of sampling relative to the travel time of the sampled water parcel. Ideally, the same water parcel would be sampled both at the upstream and downstream measurement station of any given stream section, in which case both analysis approaches would lead to the same outcome (since this is achieved mathematically by incorporating the temporal trend in the signal). If erroneously assuming a constant signal, however, an

earlier water parcel may be sampled at the downstream site, in this case leading to an underestimation of the reaeration rate coefficient due to the decreasing propane signal over time. The magnitude of the under- or overestimation, however, depends on the individual tracer test (i.e., the actual temporal fluctuation of the signal) and on by how much the correct water parcel was missed.

In *Knapp et al.* [2015] I was able to show how important it is to account for the temporal trend of the signal to obtain precise and reliable measures of reaeration, since in practice it is nearly impossible to obtain a constant gas flux into the stream or sample the same water parcel at all measurement stations. This is of particularly high importance when these rates are used in climate models or for further calculations of stream metabolism, where precision is required (see Figure 7 in *Knapp et al.* [2015]).

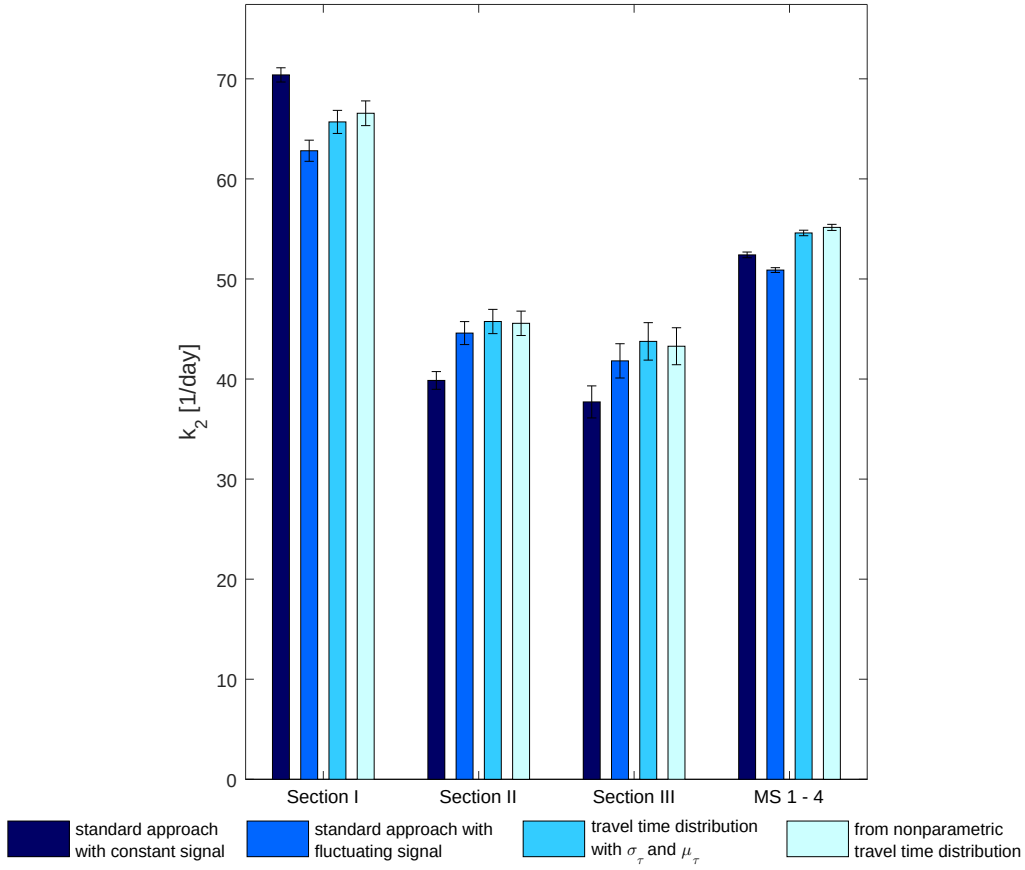

Figure 4.3: Reaeration rate coefficients k_2 of oxygen calculated from the outcomes of a propane gas tracer test for individual stream sections I to III and for the whole reach between first and last measurement station (MS1-4). The two darker shades of blue compare the effect of the temporal variability of the input signal on rate calculations for a purely advection-based approach, whereas the two lighter shades of blue incorporate transfer functions of stream flow and thus dispersive effects. Uncertainties in reaeration rate coefficients were determined from an ensemble approach. Adapted from [*Knapp et al.*, 2015]

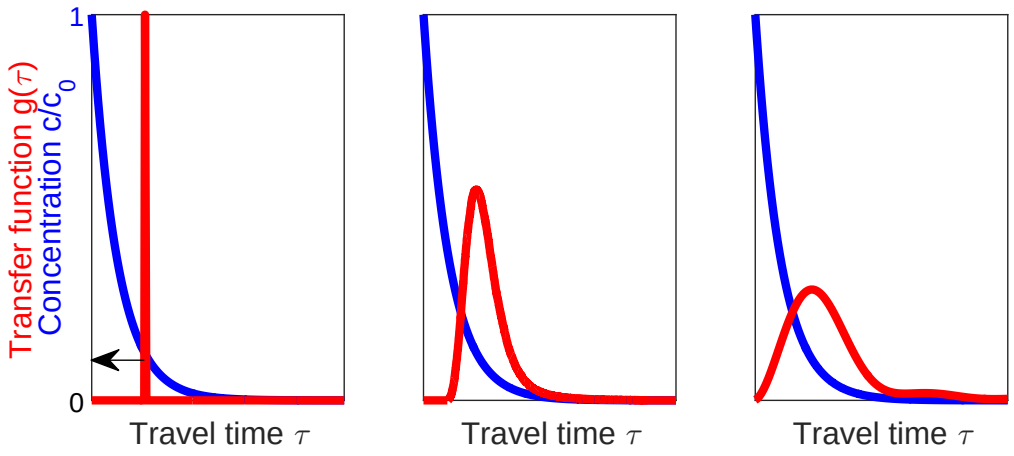

Figure 4.4: A schematic illustration of the effect of the conservative transfer function shape on rate calculations according to equation (2.2). The conservative transfer functions acts as a weighting function on the reaction term (here, the exponential decrease of concentration). In case of advection only (left), one concentration ratio is chosen as input signal. In case of Fickian dispersion (center) different parts of the concentration signal are weighed differently and low concentrations (thus higher reaeration) at late arrival times also have an influence on the calculation. In case of a transfer function with a secondary peak or extended tailing (right), this effect is increased even more, leading to higher reaeration rates.

4.2 How do tracer observations conform with standard conceptual and mathematical models?

Influence of the travel time distribution on stream reaeration

To determine whether neglecting dispersive effects on transport introduces a significant error, I compared calculated reaeration and metabolic rates from gas tracer test results based on the standard approach described in equation (2.28) with calculation outcomes that account for Fickian and non-Fickian transport. I determined section-wise shapefree transfer functions required for this purpose by nonparametric deconvolution [*Cirpka et al.*, 2007]. As input for this, I used the breakthrough curves of the conservative dye tracer test conducted simultaneously with the gas tracer test. I also calculated inverse-Gaussian distributions with identical recovery, mean and standard deviation as the nonparametric transfer functions. These describe Fickian transport as would have been observed under the assumption of transport according to the advection-dispersion equation with constant coefficients (see section 2.1).

Figure 4.3 compares calculated reaeration rate coefficients for different stream sections according to the three approaches: the standard approach (second from left), the approach including Fickian transport (second from right) and the approach including non-Fickian transport (rightmost bars, from nonparametric transfer functions). All cases

account for the signal fluctuations discussed in section 4.1, meaning that differences can be clearly attributed to the assumed transport behavior. With increasing complexity of the approach, the calculated rates increase, indicating that reaeration is underestimated more with each simplification, since the weight of longer travel-times and hence more reaeration is not accurately accounted for in simpler approaches (Figure 4.4). The importance of longer travel-times also explains why the differences between reaeration rates calculated from the Fickian and nonparametric transfer functions are not equally pronounced for all sections. If the nonparametric transfer function can be represented relatively well by an inverse-Gaussian distribution, the calculated reaeration rate coefficients also coincide. In case of secondary peaks or pronounced tailing in the nonparametric transfer functions, however, reaeration rates from the Fickian approach are less suited.

Overall, the difference between the three approaches was systematic, but not always significant. However, including the full transfer function in the calculation of the reaeration rate coefficient is neither difficult nor time consuming, and conservative tracer breakthrough curves usually have to be recorded anyway to determine (mean) travel-times between measurement stations. The experimental field work does therefore not become any more complex if transfer functions are required for the calculation. Furthermore, errors introduced in the calculation of the reaeration rate coefficient carry over to calculations of metabolic rates (aerobic respiration and primary production), and should therefore be restricted to a minimum. I therefore recommend including complete transfer functions (nonparametric or otherwise) in the calculation of reaeration rate coefficients. After all, I investigated a stream in which dispersion was not particularly pronounced (dispersion coefficient D = 0.54 m^2/s for the whole study section between the first and last measurement stations, determined from the second central moment of the nonparametric transfer function) and I would expect the differences between the various approaches to be of greater importance in case of stronger dispersion.

The Benthic Biolayer Concept

The majority of a stream's metabolic activity is restricted to its stream bed and the presence of benthic biofilms on top of the streambed has been confirmed by a number of studies [e.g., *Battin et al.*, 2003; *Hansen et al.*, 2007]. These benthic biofilms show increased reactivity and nutrient turnover and are therefore important for stream metabolism. In *Knapp et al.* [2017] I proposed that this increased reactivity is not limited to the interface between main channel and hyporheic zone, but postulate zones of different reactivity in the subsurface, thus a benthic biolayer rather than a benthic biofilm. For this, concentration breakthrough curves of a conservative and bioreactive tracer were recorded and analyzed at several depths in the subsurface. The results indicate that the potential for tracer transformation (i.e., the reaction rate coefficient) varied with depth in the hyporheic zone (see Figure 4.5A).

The highest reactivity is not necessarily found at the top of the stream bed – as would be postulated by the benthic biofilm concept. Instead, the reactive zone extends over several centimeters, which rather supports the concept of a benthic biolayer. The pattern and magnitude of the encountered reactivities differ between the sampling locations, indicating that the location of the benthic biolayer depends greatly on local conditions (e.g., hydraulic conditions, organic carbon content, etc.).

How does the reactivity in the subsurface compare to assumptions of the transient storage model?

The transient storage model and its adaptations assume a single, fully mixed storage zone with an exponential residence time distribution, from which water of different ages is sampled at equal probability. Therefore, it implicitly assumes that the vertical distributions of the conservative and reactive tracers are identical. It is obvious that this does not conform with reality, but I wanted to examine whether the transient storage model can nevertheless be used as a meaningful simplification of reality. To evaluate the importance of reactivity zonations in the hyporheic zone, I analyzed the results of a reach-scale stream-tracer test where bromide was injected as conservative tracer and resazurin as bioreactive tracer in *Knapp et al.* [2017]. Concentrations of these two tracers along with concentrations of the reaction product resorufin were sampled over the course of several hours both in the stream and within the hyporheic zone at several depths between 0-9 cm below the stream. The transformation of resazurin was used as an indicator of metabolism, and high-reactivity zones were identified from depth profiles.

Instead of basing the interpretation of the subsurface analysis on estimated parameters, I interpret metrics of reactivity and reaction time scales derived from temporal moments of the recorded breakthrough curves (see Appendix B). A comparison of the conservative and reactive tracer showed a faster disappearance of resazurin with depth than of bromide, meaning that the conservative tracer was still recovered at depths which did not show any reactive tracer (Figure 4.5C). This was due to a generally higher relative mass loss of resazurin (f_{reac}, Figure 4.5B) in the upper layers of the hyporheic zone than in deeper layers. The reactive depth of the hyporheic zone is thus much shallower than its total depth. Likewise, the calculated mean water ages in the different depths varied between the conservative and reactive tracer (Figure 4.5D).

This shows that the subsurface is in reality made up of layers with different reactivities (Figure 4.5A) and tracer residence times. Since the differences of these individual layers are often significant, the simplifications assumed by the transient storage model by lumping the subsurface into one single zone implies that it cannot represent the reality in any meaningful way.

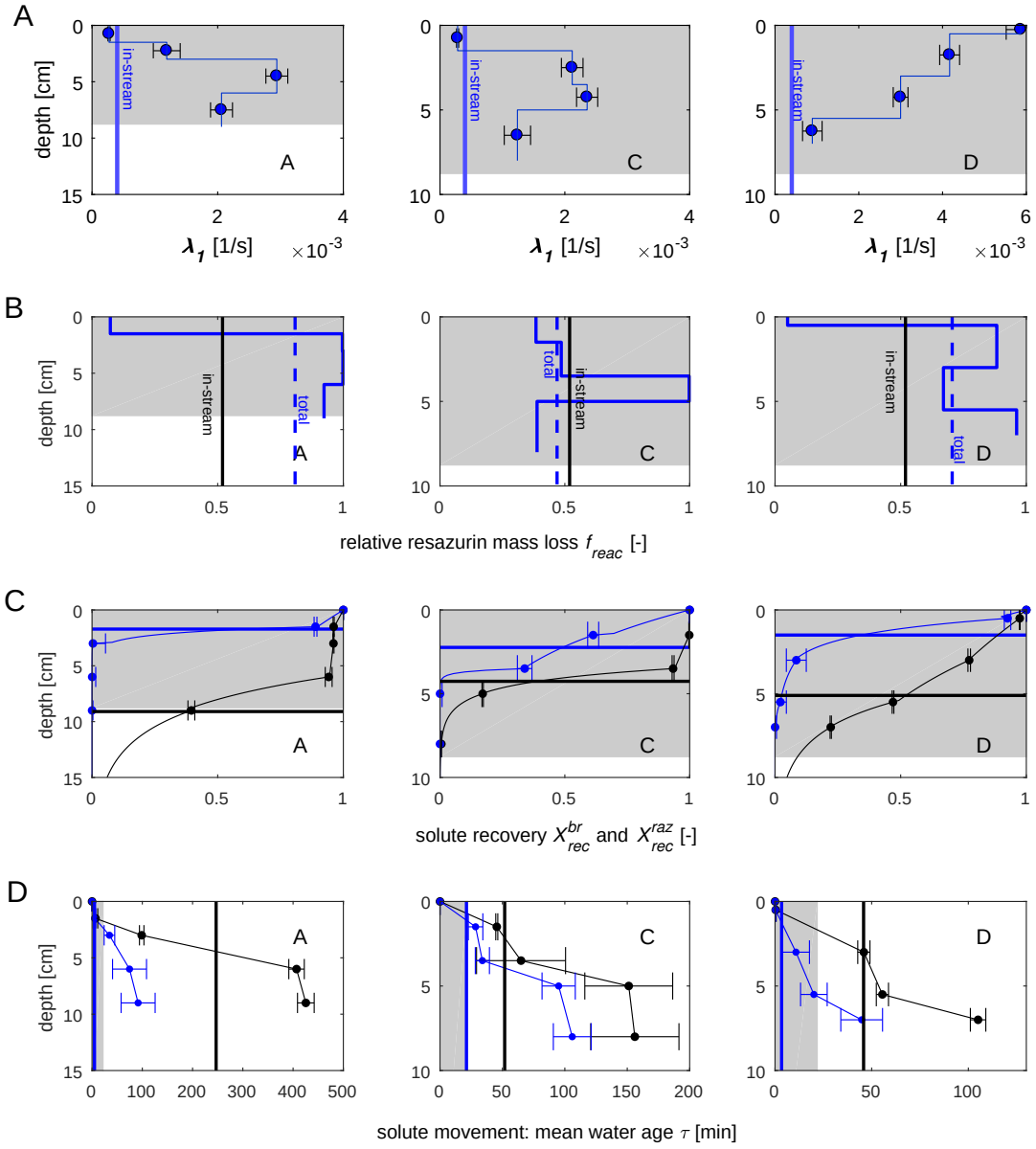

Figure 4.5: Reaction rate coefficients of resazurin, λ_1, relative resazurin mass loss, f_{reac}, solute recovery of the conservative and reactive tracer, X_{br}^{rec} and X_{raz}^{rec}, and mean hyporheic water ages, τ, obtained from in-stream and subsurface tracer recordings. The shaded areas in A-C indicate the depth of the hyporheic zone determined from the in-stream approach, and the hyporheic travel-time in D. The different columns represent results for three different subsurface samplers, A, C and D, of which A was located in the channel thalweg and C and D in two different pools. Black lines illustrate outcomes for the conservative tracer, and blue ones those of the reactive tracer resazurin. Adapted from *Knapp et al.* [2017].

The limitations of the traditional transient storage model can furthermore be revealed by a comparison between the subsurface profiles of the reactive and conservative tracer. Commonly, stream-tracer tests with sampling only in the main channel are performed to derive quantities of hyporheic exchange. But how well is this in-stream analysis really able to capture processes occurring in the subsurface? A comparison between the results of the in-stream analysis and the recorded depth profiles showed a general missmatch between the magnitudes of the calculated metrics. The reaction rate coefficient λ_1 [T^{-1}] quantifying the transformation of resazurin obtained from the in-stream approach was much lower than most of the rate coefficients calculated from the subsurface analysis (see Figure 4.5A). The observed pattern was similar for the mass loss of the reactive tracer, with a higher mass loss observed along the vertical flow paths than could be seen from the in-stream analysis (f_{reac}, Figure 4.5B). For the hyporheic exchange rate q_{he} [T^{-1}], quantifying the fraction of stream water undergoing exchange with the hyporheic zone per time, the pattern was reversed and higher exchange rates were calculated from the in-stream results than from the subsurface profiles (see Table 3 in *Knapp et al.* [2017]).

Similarly, the water ages calculated from the in-stream approach are much shorter than those revealed by the subsurface analysis (see Figure 4.5D). This is due to conceptual differences of the underlying in-stream and subsurface models. The age of the water returning to the stream (i.e., the hyporheic travel-time distribution) is determined from the in-stream approach, whereas the subsurface analysis only allows calculating the age of the water at a specific point within the hyporheic zone (i.e., the hyporheic residence time distribution). Just like the in-stream analysis is not able to tell where exactly the water went in the hyporheic zone, the subsurface analysis cannot provide information on when – if at all – the water from the subsurface will return to the main channel. Contrary to general assumptions, the information provided by the two different approaches therefore describes two different parts of the system that are not identical and cannot be combined easily.

This implies, that the in-stream approach possibly over-estimates the exchange flux, and consequently under-estimates the reactivity of the hyporheic zone. Alternatively, the findings indicate that the majority of the biochemical processing observed at the reach-scale is due to rapid exchange along flow paths through a shallow, hyporheic layer. Deeper flow paths with increased reactivity sampled by the subsurface analysis, however, are not seen by the tracer recovered by the in-stream analysis since they do not make it back to the stream at a significant enough portion to influence the in-stream results. It is therefore necessary to distinguish between the relevance of the different flow paths for different processes. Whole-stream chemistry is most likely only affected by the shallow, rapid exchange captured by the in-stream analysis and the transient storage model thus provides integrated information about the reaction zones which have the largest impact

on downstream water chemistry. Its quantification of the extent of and residence time in the hyporheic zone should however not be interpreted literally. Reactive parts of the hyporheic zone, by contrast, can only be separated from non-reactive parts by the subsurface analysis, which allows to determine the local zonation of reactivity. These local properties and processes are of special interest when evaluating restoration efforts, but individual point-measurements provide no information on general spatial distributions of reactive zones.

4.3 How can the mathematical analysis of reactive stream-tracer techniques be advanced to improve determining hydraulic parameters of complex models?

Most approaches of parameter optimization do not reliably encounter the global optimum of the parameter space. This is even more so the case when the complexity of the models is high. Furthermore, many optimization procedures are not able to provide posterior distributions of the estimated parameters and therefore do not quantify the inherent parameter uncertainty. In the final step of my thesis I therefore aimed to improve estimating of hydraulic parameters of complex models. A prime example of a complex model is the model presented by *Liao et al.* [2013], that requires the simultaneous inference of the continuous function of the hyporheic travel-time distribution together with a set of transport and reaction parameters. In the presented approach, I incorporated the parameter estimation from recorded tracer breakthrough curves into a global optimization framework that allowed finding the global optimum of the (highly multi-modal) parameter distribution. It also provided posterior distributions of parameters and thus a measure of uncertainty for the encountered parameter set. Furthermore, I combined the global-search of hydraulic and reactive parameters with a nested local search method for the inference of the shape-free hyporheic travel-time distribution, a continuous function dependent on the hydraulic parameters (see Figure 4.6). For the global-search I applied an adaptation of the DiffeRential Evolution Adaptive Metropolis (DREAM) algorithm [*Vrugt et al.*, 2008, 2009], DREAM(ZS). This is a multi-chain Markov-Chain Monte Carlo method that has successfully been applied to various hydrologic optimization problems in the past [e.g., *He et al.*, 2011; *Laloy and Vrugt*, 2012; *Joseph and Guillaume*, 2013] and is an ideal tool for finding the global optimum of a multi-modal objective function.

In the nested local search I inferred the hyporheic transfer function through an iterative updating process, which I achieved with a Gauss-Newton method. I used an extension of the model proposed by *Liao et al.* [2013] solving advective-dispersive transport in the stream coupled to hyporheic exchange, which is described by an exchange rate term and a shape-free travel-time distribution. This transfer function is a nonparametric

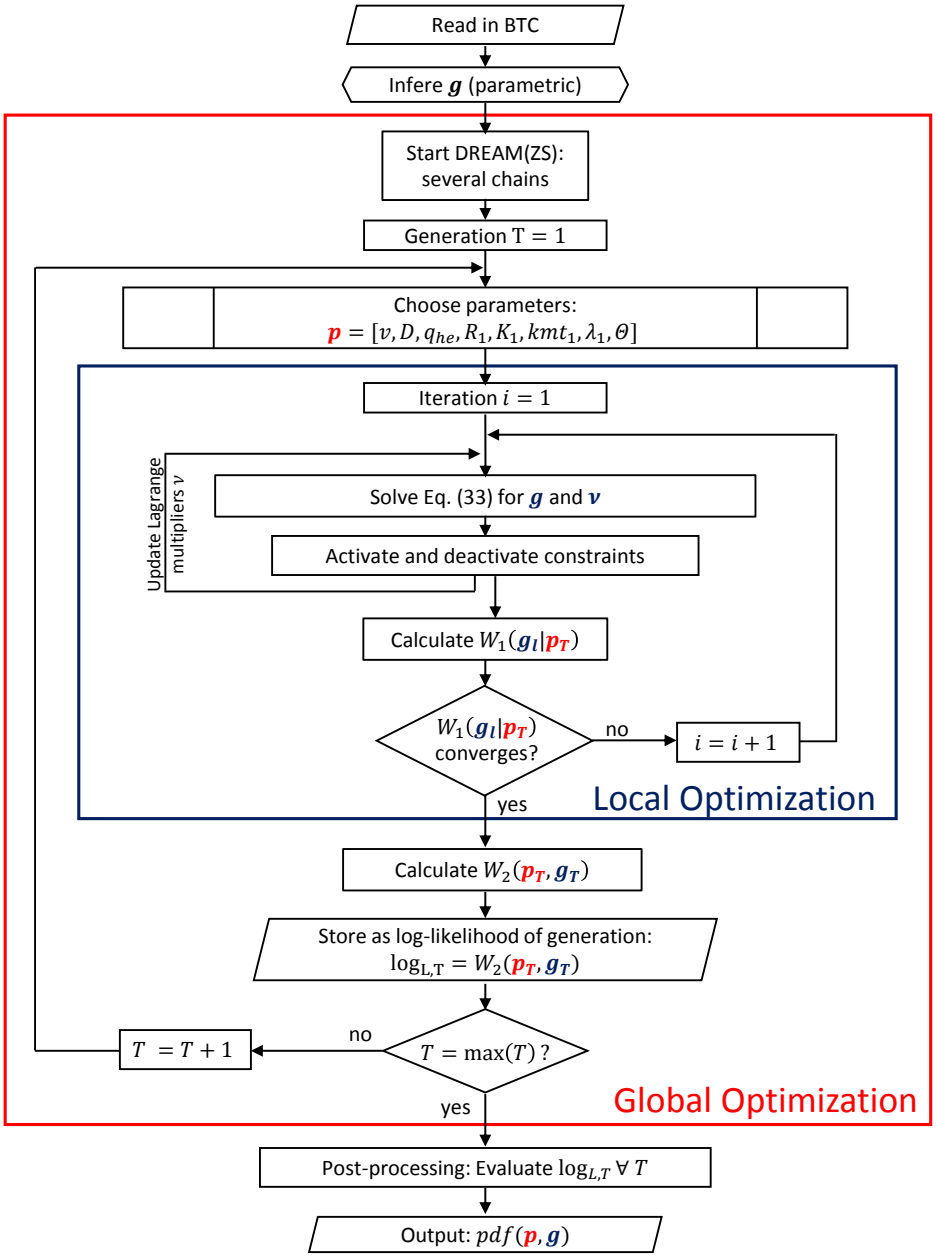

Figure 4.6: Illustration of the optimization procedure: During the global search different hydraulic parameter sets $\mathbf{p}$ are tested, and the local optimization infers the conservative hyporheic transfer function $\mathbf{g}$ based on the selected parameter set with a set of Lagrange multipliers ν ensuring non-negativity of the transfer function. The goodness of fit is evaluated with the two objective function values $W_1(\mathbf{g}_\ell|\mathbf{p})$ and $W_2(\mathbf{p}, \mathbf{g})$, *Knapp and Cirpka* [2017].

function that is only constrained to be non-negative and exhibits a certain smoothness, but does not require a parametric shape.

The objective functions for both the global- and local-search were based on Bayes' Theorem, with the one for the local search, $W_1(\mathbf{g}_\ell|\mathbf{p})$, evaluating the conditional log-likelihood of the hyporheic transfer function $\mathbf{g}_\ell$ of the conservative tracer given the selected global parameters $\mathbf{p}$, and the objective function for the global-search, $W_2(\mathbf{p}, \mathbf{g})$, describing the log-likelihood of the transfer function and the parameters given the measured tracer concentrations. Both functions penalize large residuals between measured and simulated concentrations and also large fluctuations of the transfer function. The global objective function furthermore includes a term punishing large smoothness factors Θ [for details see equations (29) and (30) in *Knapp and Cirpka*, 2017].

I applied this model to the data of a stream-tracer test with fluorescein and resazurin and assumed section-wise constant coefficients. This marks a step forward in terms of interpretability of the estimated parameters, since estimated parameters can now be linked to a specific stream section, instead of integrating over increasingly long section lengths as was done by *Liao et al.* [2013]. (The changed boundary conditions alter the equations derived for the parameter estimation and incorporated sensitivity analysis. These are given in Appendix C.) The model was able to represent the measured concentration breakthrough curves relatively well, indicating the general validity of the model. Furthermore, the global DREAM(ZS) algorithm provides not only estimations of best-fit parameters, but distributions of those parameters. These were relatively narrow, but increase in width for the reaction product resorufin, which was fitted in a separate estimation run based on fixed parameters for the conservative and reactive tracer drawn from an ensemble of the parameter distributions.

The nonparametric approach in combination with known parameter distributions permits different shapes of transfer functions arising from different combinations of parameters. I found conservative transfer functions to feature near-exponential decay if higher dispersion coefficients were paired with lower hyporheic exchange rates, whereas the opposite led to transfer functions with several later peaks, and less extreme combinations covering the range in between (see Figure 4.7). The whole continuum of transfer function shapes in combination with appropriate other parameters was able to fit the recorded concentration breakthrough curves equally well. This indicates that the shape of the transfer function cannot be determined unambiguously from the concentration breakthrough curves. Furthermore, the mean travel-times differed for the different shapes of the functions, with significantly shorter ones for those with near-exponential decay than the multi-modal distributions. Pre-selecting the parametric shape of the function may thus lead to a bias in the obtained hyporheic travel-times, which are often of particular interest, e.g., when evaluating stream restoration efforts.

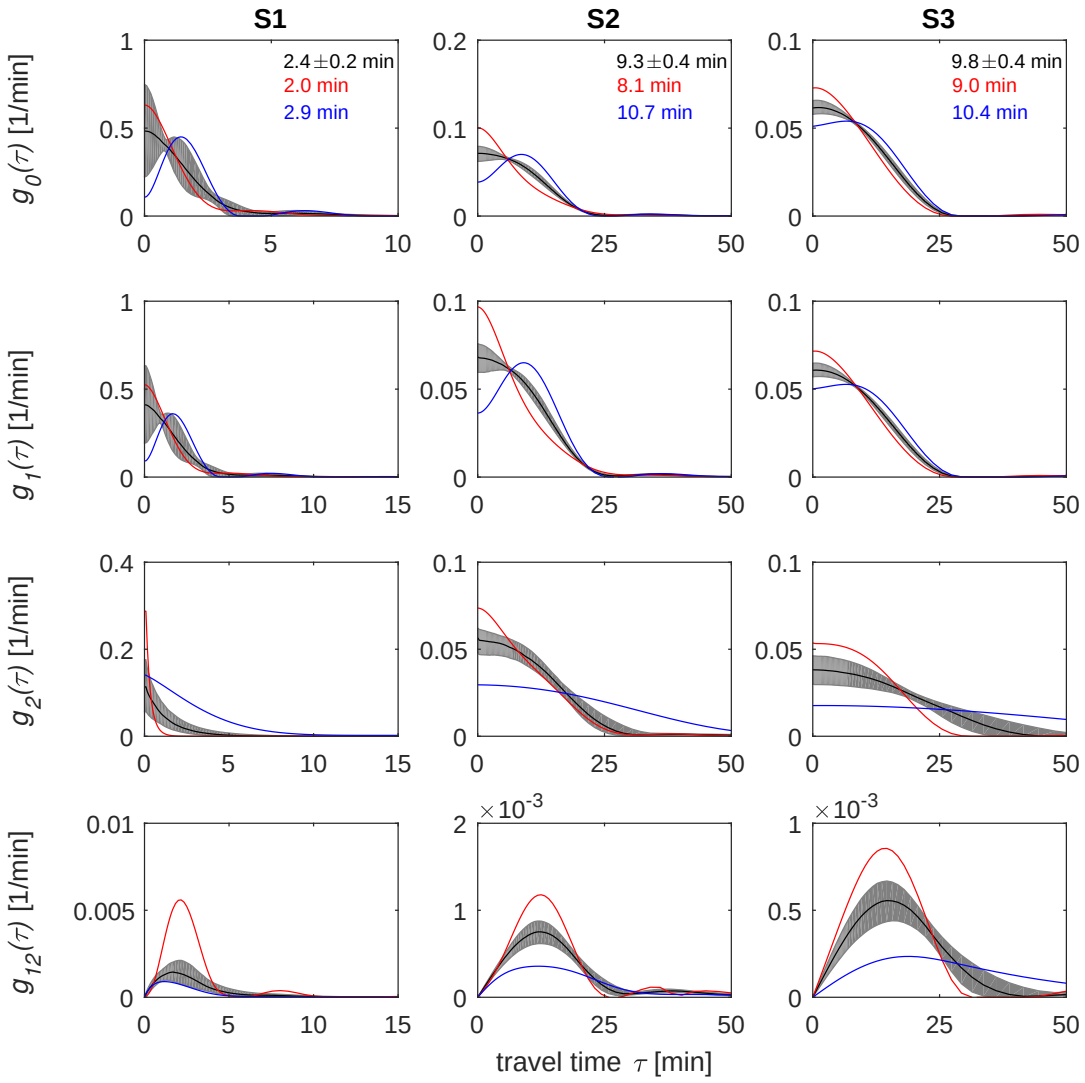

Figure 4.7: Hyporheic transfer functions of three consecutive stream sections (S1-S3) for the conservative tracer, $g_0(\tau)$, the reactive tracer resazurin, $g_1(\tau)$, and the reaction product resorufin, $g_2(\tau)$. $g_{12}(\tau)$ represents the cross-compound transfer function for the transformation of resazurin to resorufn. Solid black lines indicate median transfer functions of the ensemble, whereas the shaded areas depict the probability range between 16 % and 84 %. The blue and red lines illustrate two examples of extreme transfer functions. Panels for $g_0(\tau)$ also display mean travel-times of the ensemble (black) and of the two extreme cases of travel-time shapes displayed in the figure. *Knapp and Cirpka* [2017].

The method applied here has the advantage over the approach used by *Liao et al.* [2013] that it is not biased by the initial parameter guess. Furthermore, the smoothness parameter of the transfer function is here also fitted by the global fitting algorithm, and not predefined by the experimenter as was done by *Liao et al.* [2013]. The approach presented in my thesis can therefore be considered a reliable method for the determination of hyporheic exchange parameters and hyporheic transfer functions from recorded tracer breakthrough curves in the relatively complex framework of shape-free travel-time distributions and a high number of additional parameters. This approach, however, is not limited to the estimation of parameters from reactive tracer tests, but could likely be a suitable tool for different problems, where a continuous function is to be inferred simultaneously with a set of additional parameters. A be source-identification problems with reactive transport could be one example of such a case, with the release history of the reactant or its initial spatial distribution is described by a continuous function.

It should be noted, that the parameter estimation step is not necessarily the last step in the analysis chain – even though it was discussed last in this thesis. When interpreting parameters of conceptual models, as was done both in *Knapp et al.* [2015] and *Knapp et al.* [2017], the parameter uncertainty is an important issue. Although not discussed in this summary, parameter uncertainties were considered in both studies. The in-stream and subsurface parameters and their distributions presented in *Knapp et al.* [2017] were determined with a global-search method, and an ensemble approach was chosen for the estimation of uncertainties of calculated reaeration rate coefficients in *Knapp et al.* [2015].

5 CONCLUSIONS AND OUTLOOK

During my thesis I advanced different aspects of stream-tracer techniques, spanning from the experimental design to the conceptual model framework to implications for parameter estimation through inverse modeling.

5.1 Experimental Design

I was able to significantly improve the sampling technique for a reactive dye tracer with online fluorometers presented by *Lemke et al.* [2013b], through an additional verification of the recorded concentrations by grab samples. If necessary, this also allows to correct the recorded concentration breakthrough curves, while retaining the advantages of quasi-continuous in-situ sensing provided by the fluorometers. This advancement has significantly improved the validity of the measured concentrations and at the same time eradicated all mass balance errors and negative concentrations of the reaction product resorufin encountered previously.

The sampling of volatile compounds has been a longstanding issue as field methods are generally either unreliable, or expensive and time-consuming [*Sanford et al.*, 1996]. Furthermore, I found in previous experiments that maintaining a constant source concentration of the tracer gas is challenging. For this reason, I quantified the error made by wrongly assuming a constant source signal and suggested an easy-to-implement way of accounting for fluctuations in the input signal that is cost-effective and time-efficient in *Knapp et al.* [2015]. It merely requires taking a few extra samples at the first measurement station and allows for the recursive calculation of unsteady signals at all measurement stations.

To increase the accuracy of the gas signal itself, I took replicate samples. This has helped to reduce the variablity in the signal to a certain extent. A large uncertainty in the gas signal remains, however, as gas may escape from the sampling container during sampling, storage, transport and analysis. I therefore highly encourage the application of an in-situ analysis for the sampled gases, for example with the help of a membrane-inlet mass spectrometer [*Mächler et al.*, 2012; *Brennwald et al.*, 2016].

5.2 Conceptual Model Framework

The importance of quantifying the travel-time distribution of stream flow and its incorporation into the calculation of metabolic rates I showed in *Knapp et al.* [2015], by quantifying the influence of Fickian and non-Fickian dispersion on reaeration rates. The observed dispersion effects, however, are not only relevant in the context of gas tracer test, but play a role in all types of reactive transport analysis. This approach could therefore provide an improved method for many timely questions, e.g. in the investigation of the removal of wastewater-related contaminants in streams [*Guillet et al.*, in prep.] and other Lagrangian-based sampling techniques. Furthermore, resazurin decay occurs according to a first order rate law, and commonly [e.g., as presented by *González-Pinzón and Haggerty*, 2013] mean travel-times are used as normalization factors, similar to the standard approach for the analysis of gas tracer tests. These analysis approaches could therefore also benefit from an incorporation of dispersive effects.

More research is needed, however, when it comes to differentiating between streams where dispersion (or even non-Fickian dispersion) is of significant relevance. This requires an improved knowledge base on how much dispersion influences estimated rate coefficients in different systems, so future research can assess more easily whether the effect of dispersion is relevant in the scientific question asked (i.e., how significant are the expected effects of dispersion in comparison to other effects investigated). This knowledge is necessary, so simplifications can be better justified and potential sources of error avoided.

An adequate description of transport is not only vital in the stream itself, but also through the hyporheic zone. Specific parametric shapes are often enforced when estimating hyporheic travel-time distributions from measured concentration breakthrough curves. In *Knapp and Cirpka* [2017] I demonstrate that different shapes of hyporheic travel-time distributions are able to recreate the same breakthrough curve (together with appropriate other parameters) by using a shape-free approach which allowed the travel-time distributions to take any possible shape (without negative entries). Notably, the mean hyporheic travel-times calculated from the different approaches differed quite significantly, which highlights the danger of pre-defining the parametric shape of the distribution as is commonly done in stream-tracer analysis.

In *Knapp et al.* [2017] I illustrated that the theoretical assumptions of the transient storage model do not conform with reality regarding the make-up of the storage zone. This highlights that even though the transient storage model is legitimate as a conceptual framework, it is thoroughly unsuitable for the determination of the actual extent of the hyporheic storage zone or average reactivity therein, so one should refrain from a direct physical interpretation of its parameters. Furthermore, it cannot capture the layering

of the hyporheic zone observed in the real world, for which reason it is doubtful that the additional application of a reactive tracer is able to actually determine the size of the metabolically active transient storage zone as suggested by *Haggerty et al.* [2009]; *Argerich et al.* [2011] and others. Since the in-stream analysis captures the flow paths with the largest contribution to the hyporheic flux (i.e., the fast and shallow ones), it is, however, very well suited to quantify the bulk effect of hyporheic exchange on whole-stream chemistry. Subsurface profiles, by contrast, paint a highly localized picture by characterizing a very limited number of flow paths at a specific sampling station. This way, they capture the reaction effect of the deeper subsurface and identify the location and properties of the reactive benthic biolayer, but provide little information on the relevance of these individual flow paths for the conditions in the main channel.

This mismatch of results from different scales is not only true for the results obtained in *Knapp et al.* [2017], but holds for all field and modeling studies on hyporheic exchange. Most studies investigating hyporheic exchange either focus on the reach-scale [e.g., *Kasahara and Wondzell*, 2003; *Gooseff et al.*, 2003] or investigate small-scale effects [e.g., *Harvey and Fuller*, 1998; *O'Connor et al.*, 2012; *Briggs et al.*, 2015] in their efforts to determine the governing processes of hyporheic exchange. A scale-transferability or validity of the results on other scales is often implicitly assumed, but usually not verified. Contrary to *González-Pinzón et al.* [2015], who found co-interpretation of results across spatial scales to be useful, I come to the conclusion that a combination of investigations on different scales does not improve our understanding of the relevant processes, at least not in a quantitative manner. Potentially, this could be achieved by a consistent, coupled model, considering transformation in the hyporheic zone as function of the hyporheic residence time, thus linking in-stream transport and hyporheic exchange in a more direct manner.

5.3 Model Fitting and Parameter Estimation

The most common parameter estimation techniques suffer from two shortcomings. They are often not able to find the global optimum of the parameter space and they merely provide best fit parameters without information on their uncertainty. I applied a genetic algorithm based Markov-Chain Monte Carlo method [DREAM(ZS); *Vrugt et al.*, 2009; *Laloy and Vrugt*, 2012] to address these two issues. In this way, I was not only able to determine posterior parameter distributions for the in-stream and subsurface analysis of reactive tracers in *Knapp et al.* [2017], but I also fitted transport and reaction parameters together with a transfer function in a nested, two-step optimization approach in *Knapp and Cirpka* [2017]. This method yields more reliable results than the method presented by *Liao et al.* [2013], who applied a gradient-based search method to a similar problem, since the estimated parameters from the global-search are independent of the initial parameter

guess. The method also provides a better prediction of the uncertainty associated with the estimated parameters .

Furthermore, in addition to an improved parameter estimation approach, I also adapted the approach of *Liao et al.* [2013] to account for section-wise variations of hyporheic exchange, instead of integrating over increasingly longer reaches spanning from the injection point to any given measurement station. This is essential if different stream sections are to be compared with respect to their hyporheic exchange properties. Furthermore, this step is vital, if actual section-wise resazurin transformation rates are to be compared to aerobic respiration rates determined from gas tracer tests. Studies with a field-based validation of resazurin transformation are still lacking, even though a field based analysis of resazurin compared to lab analysis of sediment respiration with pure and mixed bacterial cultures indicates that a strong relationship between resazurin transformation and aerobic respiration exists [*González-Pinzón et al.*, 2012].

BIBLIOGRAPHY

Argerich, A., R. Haggerty, E. Martí, F. Sabater, and J. Zarnetske, Quantification of metabolically active transient storage (MATS) in two reaches with contrasting transient storage and ecosystem respiration, *Journal of Geophysical Research: Biogeosciences*, *116*(G3), 2011.

Bäck, T., and H.-P. Schwefel, An overview of evolutionary algorithms for parameter optimization, *Evolutionary computation*, *1*(1), 1–23, 1993.

Battin, T. J., L. A. Kaplan, J. D. Newbold, and C. M. Hansen, Contributions of microbial biofilms to ecosystem processes in stream mesocosms, *Nature*, *426*(6965), 439–442, 2003.

Bencala, K. E., Simulation of solute transport in a mountain pool-and-riffle stream with a kinetic mass transfer model for sorption, *Water Resources Research*, *19*(3), 732–738, 1983.

Bencala, K. E., M. N. Gooseff, and B. A. Kimball, Rethinking hyporheic flow and transient storage to advance understanding of stream-catchment connections, *Water Resources Research*, *47*(3), 2011.

Blaen, P., M. Kurz, J. Drummond, J. L. A. Knapp, and et al., Woody debris determines reach-scale hotspots of lowland stream ecosystem respiration, *Ecohydrology*, submitted.

Boulton, A. J., S. Findlay, P. Marmonier, E. H. Stanley, and H. M. Valett, The functional significance of the hyporheic zone in streams and rivers, *Annual Review of Ecology and Systematics*, *29*(1), 59–81, 1998.

Boulton, A. J., T. Datry, T. Kasahara, M. Mutz, and J. A. Stanford, Ecology and management of the hyporheic zone: stream–groundwater interactions of running waters and their floodplains, *Journal of the North American Benthological Society*, *29*(1), 26–40, 2010.

Brennwald, M. S., M. Schmidt, J. Oser, and R. Kipfer, A portable and autonomous mass spectrometric system for on-site environmental gas analysis, *Environmental Science & Technology*, *50*(24), 13,455–13,463, 2016.

Briggs, M. A., F. D. Day-Lewis, J. P. Zarnetske, and J. W. Harvey, A physical explanation for the development of redox microzones in hyporheic flow, *Geophysical Research Letters*, *42*(11), 4402–4410, 2015.

Cardenas, M. B., Hyporheic zone hydrologic science: A historical account of its emergence and a prospectus, *Water Resources Research*, *51*(5), 3601–3616, 2015.

Cirpka, O. A., M. N. Fienen, M. Hofer, E. Hoehn, A. Tessarini, R. Kipfer, and P. K. Kitanidis, Analyzing bank filtration by deconvoluting time series of electric conductivity, *Ground Water*, *45*(3), 318–328, 2007.

De Smedt, F., W. Brevis, and P. Debels, Analytical solution for solute transport resulting from instantaneous injection in streams with transient storage, *Journal of Hydrology*, *315*(1), 25–39, 2005.

Genereux, D. P., and H. F. Hemond, Naturally occurring radon 222 as a tracer for streamflow generation: Steady state methodology and field example, *Water resources research*, *26*(12), 3065–3075, 1990.

González-Pinzón, R., and R. Haggerty, An efficient method to estimate processing rates in streams, *Water Resources Research*, *49*(9), 6096–6099, 2013.

González-Pinzón, R., R. Haggerty, and D. D. Myrold, Measuring aerobic respiration in stream ecosystems using the resazurin-resorufin system, *Journal of Geophysical Research: Biogeosciences*, *117*(G3), 2012.

González-Pinzón, R., R. Haggerty, and A. Argerich, Quantifying spatial differences in metabolism in headwater streams, *Freshwater Science*, *33*(3), 798–811, 2014.

González-Pinzón, R., et al., A field comparison of multiple techniques to quantify groundwater-surface-water interactions, *Freshwater Science*, *34*(1), 139–160, 2015.

Gooseff, M. N., S. M. Wondzell, R. Haggerty, and J. Anderson, Comparing transient storage modeling and residence time distribution (RTD) analysis in geomorphically varied reaches in the Lookout Creek basin, Oregon, USA, *Advances in Water Resources*, *26*(9), 925–937, 2003.

Gooseff, M. N., J. LaNier, R. Haggerty, and K. Kokkeler, Determining in-channel (dead zone) transient storage by comparing solute transport in a bedrock channel–alluvial channel sequence, oregon, *Water Resources Research*, *41*(6), 2005.

Guillet, G., J. L. A. Knapp, S. Merel, O. A. Cirpka, P. Grathwohl, and M. Schwientek, Fate of wastewater-related contaminants in rivers: a new method to improve Lagrangian sampling accuracy, in prep.

Gupta, H. V., K. J. Beven, and T. Wagener, Model calibration and uncertainty estimation, *Encyclopedia of hydrological sciences*, 2005.

Haggerty, R., S. McKenna, L. Meigs, et al., On the late-time behavior of tracer test breakthrough curves., *Water Resources Research*, *36*(12), 3467–3479, 2000.

Haggerty, R., S. M. Wondzell, and M. A. Johnson, Power-law residence time distribution in the hyporheic zone of a 2nd-order mountain stream, *Geophysical Research Letters*, *29*(13), 2002.

Haggerty, R., A. Argerich, , and E. Martí, Development of a "smart" tracer for the assessment of microbiological activity and sediment-water interaction in natural waters: The resazurin-resorufin system, *Water Resources Research*, *44*, 2008.

Haggerty, R., E. Martí, A. Argerich, D. Von Schiller, and N. B. Grimm, Resazurin as a "smart" tracer for quantifying metabolically active transient storage in stream ecosystems, *Journal of Geophysical Research: Biogeosciences*, *114*(G3), 2009.

Hansen, S. K., P. B. Rainey, J. A. Haagensen, and S. Molin, Evolution of species interactions in a biofilm community, *Nature*, *445*(7127), 533–536, 2007.

Hart, D. R., Parameter estimation and stochastic interpretation of the transient storage model for solute transport in streams, *Water Resources Research*, *31*(2), 323–328, 1995.

Harvey, C. F., and S. M. Gorelick, Temporal moment-generating equations: Modeling transport and mass transfer in heterogeneous aquifers, *Water Resources Research*, *31*(8), 1895–1911, 1995.

Harvey, J. W., and C. C. Fuller, Effect of enhanced manganese oxidation in the hyporheic zone on basin-scale geochemical mass balance, *Water Resources Research*, *34*(4), 623–636, 1998.

Harvey, J. W., J. K. Böhlke, M. A. Voytek, D. Scott, and C. R. Tobias, Hyporheic zone denitrification: Controls on effective reaction depth and contribution to whole-stream mass balance, *Water Resources Research*, *49*(10), 6298–6316, 2013.

He, M., T. S. Hogue, K. J. Franz, S. A. Margulis, and J. A. Vrugt, Characterizing parameter sensitivity and uncertainty for a snow model across hydroclimatic regimes, *Advances in Water Resources*, *34*(1), 114–127, 2011.

Hoellein, T. J., D. A. Bruesewitz, and D. C. Richardson, Revisiting Odum (1956): A synthesis of aquatic ecosystem metabolism, *Limnology and Oceanography*, *58*(6), 2089–2100, 2013.

Hollenbeck, K., INVLAP. M: A matlab function for numerical inversion of Laplace transforms by the de Hoog algorithm, *unpublished work*, 1998.

Joseph, J., and J. H. Guillaume, Using a parallelized MCMC algorithm in R to identify appropriate likelihood functions for SWAT, *Environmental modelling & software*, *46*, 292–298, 2013.

Karakashev, D., D. Galabova, and I. Simeonov, A simple and rapid test for differentiation of aerobic from anaerobic bacteria, *World Journal of Microbiology and Biotechnology*, *19*(3), 2003.

Kasahara, T., and S. M. Wondzell, Geomorphic controls on hyporheic exchange flow in mountain streams, *Water Resources Research*, *39*(1), 2003.

Käss, W., *Lehrbuch der Hydrogeologie Band 9, Geohydrologische Markierungstechnik*, 2. ed., Gebrüder Borntraeger, Berlin, 2004.

Kelleher, C., T. Wagener, B. McGlynn, A. Ward, M. Gooseff, and R. Payn, Identifiability of transient storage model parameters along a mountain stream, *Water Resources Research*, *49*(9), 5290–5306, 2013.

Kerr, P., M. Gooseff, and D. Bolster, The significance of model structure in one-dimensional stream solute transport models with multiple transient storage zones–competing vs. nested arrangements, *Journal of Hydrology*, *497*, 133–144, 2013.

Kitanidis, P. K., The minimum structure solution to the inverse problem, *Water resources research*, *33*(10), 2263–2272, 1997.

Knapp, J. L. A., and O. A. Cirpka, Determination of hyporheic travel time distributions and other parameters from concurrent conservative and reactive tracer tests by local-in-global optimization, *Water Resources Research*, in press, 2017.

Knapp, J. L. A., K. Osenbrück, and O. A. Cirpka, Impact of non-idealities in gas-tracer tests on the estimation of reaeration, respiration, and photosynthesis rates in streams, *Water research*, *83*, 205–216, 2015.

Knapp, J. L. A., R. González-Pinzón, J. D. Drummond, L. G. Larsen, O. A. Cirpka, and J. W. Harvey, Tracer-based characterization of hyporheic exchange and benthic biolayers in streams, *Water Resources Research*, 2017.

Knop, A., Über die hydrographischen Beziehungen zwischen der Donau und der Aachquelle im badischen Oberlande, 1878.

Kreft, A., and A. Zuber, On the physical meaning of the dispersion equation and its solutions for different initial and boundary conditions, *Chemical Engineering Science*, *33*(11), 1471–1480, 1978.

Kučera, E., Contribution to the theory of chromatography: Linear non-equilibrium elution chromatography, *Journal of Chromatography A*, *19*, 237–248, 1965.

Kurz, M., and J. Knapp, Using diel element cycles to assess ecohydrological interface processing, in *Ecohydrological Interfaces*, edited by S. Krause, 1. ed., Wiley, in preparation.

Laloy, E., and J. A. Vrugt, High-dimensional posterior exploration of hydrologic models using multiple-try DREAM (ZS) and high-performance computing, *Water Resources Research*, *48*(1), 2012.

Lemke, D., Z. Liao, T. Wöhling, K. Osenbrück, and O. A. Cirpka, Concurrent conservative and reactive tracer tests in a stream undergoing hyporheic exchange, *Water Resources Research*, *49*(5), 3024–3037, 2013a.

Lemke, D., P.-A. Schnegg, M. Schwientek, K. Osenbrück, and O. A. Cirpka, On-line fluorometry of multiple reactive and conservative tracers in streams, *Environmental earth sciences*, *69*(2), 349–358, 2013b.

Liao, Z., and O. A. Cirpka, Shape-free inference of hyporheic traveltime distributions from synthetic conservative and "smart" tracer tests in streams, *Water Resources Research*, *47*(7), 2011.

Liao, Z., D. Lemke, K. Osenbrück, and O. A. Cirpka, Modeling and inverting reactive stream tracers undergoing two-site sorption and decay in the hyporheic zone, *Water Resources Research*, *49*(6), 3406–3422, 2013.

Mächler, L., M. S. Brennwald, and R. Kipfer, Membrane inlet mass spectrometer for the quasi-continuous on-site analysis of dissolved gases in groundwater, *Environmental science & technology*, *46*(15), 8288–8296, 2012.

Marion, A., M. Zaramella, and A. I. Packman, Parameter estimation of the transient storage model for stream–subsurface exchange, *Journal of Environmental Engineering*, *129*(5), 456–463, 2003.

Marzolf, E. R., P. J. Mulholland, and A. D. Steinman, Improvements to the diurnal upstream–downstream dissolved oxygen change technique for determining whole-stream metabolism in small streams, *Canadian Journal of Fisheries and Aquatic Sciences*, *51*(7), 1591–1599, 1994.

Merill, L., and D. J. Tonjes, A review of the hyporheic zone, stream restoration, and means to enhance denitrification, *Critical Reviews in Environmental Science and Technology*, *44*(21), 2337–2379, 2014.

O'Brien, J., I. Wilson, T. Orton, and F. Pognan, Investigation of the Alamar Blue (resazurin) fluorescent dye for the assessment of mammalian cell cytotoxicity, *European Journal of Biochemistry*, *267*(17), 5421–5426, 2000.

O'Connor, B. L., J. W. Harvey, and L. E. McPhillips, Thresholds of flow-induced bed disturbances and their effects on stream metabolism in an agricultural river, *Water Resources Research*, *48*(8), 2012.

O'Connor, D., and W. Dobbins, Mechanisms of reareation in natural streams, *Trans.Am.Soc.Civ.Eng*, 1956.

Odum, H. T., Primary production in flowing waters, *Limnology and oceanography*, *1*(2), 102–117, 1956.

Payn, R., M. Gooseff, B. McGlynn, K. Bencala, and S. Wondzell, Channel water balance and exchange with subsurface flow along a mountain headwater stream in Montana, United States, *Water Resources Research*, *45*(11), 2009.

Press, W. H., S. A. Teukolsky, W. T. Vetterling, and B. P. Flannery, *Numerical Recipes in FORTRAN 77: The Art of Scientific Computation*, 2nd ed., Cambridge University Press, New York, 1992.

Rathbun, R. E., D. Tai, D. J. Shultz, and D. Stephens, Laboratory studies of gas tracers for reaeration, *Journal of the Environmental Engineering Division*, *104*(2), 215–229, 1978.

Rinaldo, A., P. Benettin, C. J. Harman, M. Hrachowitz, K. J. McGuire, Y. Van Der Velde, E. Bertuzzo, and G. Botter, Storage selection functions: A coherent framework for quantifying how catchments store and release water and solutes, *Water Resources Research*, *51*(6), 4840–4847, 2015.

Runkel, R. L., One-dimensional transport with inflow and storage (OTIS): A solute transport model for streams and rivers, 1998.

Sanford, W. E., R. G. Shropshire, and D. K. Solomon, Dissolved gas tracers in groundwater: Simplified injection, sampling, and analysis, *Water Resources Research*, *32*(6), 1635–1642, 1996.

Schnegg, P.-A., personal communication.

Soares, P. A., G. Faht, A. Pinheiro, M. R. Silva, and E. Zucco, Determination of reaeration-rate coefficient by modified tracer gas technique, *Hydrological Processes*, *27*(19), 2710–2720, 2013.

Sophocleous, M., Interactions between groundwater and surface water: the state of the science, *Hydrogeology journal*, *10*(1), 52–67, 2002.

Stream Solute Workshop, Concepts and methods for assessing solute dynamics in stream ecosystems, *Journal of the North American Benthological Society*, *9*(2), 95–119, 1990.

Ter Braak, C. J., Genetic algorithms and Markov Chain Monte Carlo: Differential Evolution Markov Chain makes Bayesian computing easy (revised), *Tech. rep.*, Wageningen UR, Biometris, 2005.

Tsivoglou, E., and L. Neal, Tracer measurement of reaeration: Iii. predicting the reaeration capacity of inland streams, *Journal (Water Pollution Control Federation)*, pp. 2669–2689, 1976.

Vrugt, J. A., C. J. Ter Braak, M. P. Clark, J. M. Hyman, and B. A. Robinson, Treatment of input uncertainty in hydrologic modeling: Doing hydrology backward with Markov chain Monte Carlo simulation, *Water Resources Research*, *44*(12), 2008.

Vrugt, J. A., C. Ter Braak, C. Diks, B. A. Robinson, J. M. Hyman, and D. Higdon, Accelerating Markov chain Monte Carlo simulation by differential evolution with self-adaptive randomized subspace sampling, *International Journal of Nonlinear Sciences and Numerical Simulation*, *10*(3), 273–290, 2009.

Wagner, B. J., and J. W. Harvey, Experimental design for estimating parameters of rate-limited mass transfer: Analysis of stream tracer studies, *Water Resources Research*, *33*(7), 1731–1741, 1997.

Wanninkhof, R., P. Mulholland, and J. Elwood, Gas exchange rates for a first-order stream determined with deliberate and natural tracers, *Water Resources Research*, *26*(7), 1621–1630, 1990.

Wörman, A., A. I. Packman, H. Johansson, and K. Jonsson, Effect of flow-induced exchange in hyporheic zones on longitudinal transport of solutes in streams and rivers, *Water Resources Research*, *38*(1), 2002.

Young, R., and A. Huryn, Effects of land use on stream metabolism and organic matter turnover, *Ecological Applications*, *9*(4), 1359–1376, 1999.

LIST OF SYMBOLS

indices i:	1	conservative tracer compound
	2	reactive tracer resazurin
	3	reaction product resorufin
A_r	[-]	ratio between hyporheic and in-stream cross-sectional area
c_i	[ML^{-3}]	concentration of compound i
c_g^{up} / c_g^{down}	[ML^{-3}]	gas concentration at the up- / downstream measurement station
c_{in} / c_{out}	[ML^{-3}]	concentration of the input / output signal
c_s	[ML^{-3}]	concentration in the storage zone
$c_{i,hz}$	[ML^{-3}]	concentration of compound i in the hyporheic zone
c_i^*	[ML^{-3}]	concentration of compound i at kinetically sorbed sites
c_{O_2}	[ML^{-3}]	concentration of dissolved oxygen
c_{sat}	[ML^{-3}]	saturation concentration (here: of oxygen)
D	[L^{2}T^{-1}]	longitudinal dispersion coefficient
$\delta()$		Dirac delta function
$E[\cdot]$		expected value operator
f_{reac}	[-]	relative resazurin mass loss
$g_i(\tau)$	[T^{-1}]	transfer function of compound i
$g_{12}(\tau)$	[T^{-1}]	cross-compound transfer function from resazurin to resorufin
γ_g	[T^{-2}]	linear semi-variogram function of the transfer function
k	[T^{-1}]	first order mass transfer rate coefficient
k_2	[T^{-1}]	reaeration rate coefficient
K_i	[-]	kinetic sorption coefficient of compound i
λ_i	[T^{-1}]	reaction rate coefficient of compound i
m_i	[M]	injected tracer mass of compound i
μ_k		k-th temporal moment
q_{he}	[T^{-1}]	hyporheic exchange rate
q_{in}	[T^{-1}]	rate coefficient accounting for mixing with groundwater
R_i	[-]	linear equilibrium sorption coefficient of compound i
r_{resp}	[ML^{-3}T^{-1}]	respiration rate
r_{photo}	[ML^{-3}T^{-1}]	photosynthesis rate
$r_{i,hz}$	[ML^{-3}T^{-1}]	reaction term in the hyporheic zone of compound i
S_m / S_s	[ML^{-3}T^{-1}]	reaction term in the main channel / storage zone
t	[T]	time
τ	[T]	travel-time
Θ	[T^{-3}]	smoothness factor / slope of linear semi-variogram
v	[LT^{-1}]	advective velocity
x	[L]	location
X_{rec}^{br} / X_{rec}^{raz}	[-]	solute recovery of the conservative tracer / of resazurin

LIST OF FIGURES

APPENDICES

A The Laplace Transform

B Method of Moments

C Section-wise Analysis of Reactive Tracer Tests

Publications:

Knapp, J.L.A., K. Osenbrück, and O. A. Cirpka, Impact of non-idealities in gas-tracer tests on the estimation of reaeration, respiration, and photosynthesis rates in streams, *Water research*, 83, 205–216, 2015. DOI: 10.1016/j.watres.2015.06.032

Knapp, J.L.A., R. González-Pinzón, J. D. Drummond, L. G. Larsen, O. A. Cirpka, and J. W. Harvey, Tracer-based characterization of hyporheic exchange and benthic biolayers in streams, *Water Resources Research*, 2017. DOI: 10.1002/2016WR019393

Knapp, J.L.A., and O. A. Cirpka, Determination of hyporheic travel-time distributions and other parameters from concurrent conservative and reactive tracer tests by local-inglobal optimization, *Water Resources Research*, 2017, in press. DOI: 10.1002/2017WR020734

THE LAPLACE TRANSFORM

A

The Laplace transform converts a function $f(t)$ dependent on the time t [T] to a function $\tilde{f}(s)$ with the complex Laplace frequency s [T^{-1}].

$$\mathcal{L}\{f(t)\} = \int_0^\infty e^{-st} f(t) dt = \tilde{f}(s) \tag{A.1}$$

For a time derivative $\frac{\partial f}{\partial t}$ the Laplace transform yields:

$$\begin{aligned} \frac{\partial \tilde{f}}{\partial t} &= \int_0^\infty \frac{\partial f}{\partial t}\, e^{-st} dt = s\tilde{f} - f_0 \\ &= s\tilde{f} \qquad \text{for} \quad f_0 = 0 \end{aligned} \tag{A.2}$$

The application of the Laplace transform is convenient in the case of the equations presented in this thesis because the time-derivative of the concentration drops out in the Laplace domain, turning the equation into a second-order ordinary differential equation. For example, Laplace transform of equation (2.4) yields:

$$s\tilde{c}(x,s) + A_r s\tilde{c}_s(x,s) + v\frac{d\tilde{c}(x,s)}{dx} - D\frac{d^2\tilde{c}(x,s)}{dx^2} = 0 \tag{A.3}$$

$$s\tilde{c}_s(x,s) = k\left(\tilde{c}(x,s) - \tilde{c}_s(x,s)\right) \tag{A.4}$$

(Please note that the subscript s identifies concentrations found in the storage zone and is different from the complex Laplace frequency s.)

Furthermore, with the Laplace transform, the convolution of the transfer function $g(\tau)$ with the concentration signal $c(x,s)$ becomes a simple multiplication. The Laplace transform of equation (2.6) thus becomes:

$$\left(s + q_{he} - q_{he}\tilde{g}_0\right)\tilde{c}(x,s) + v\frac{d\tilde{c}(x,s)}{dx} - D\frac{d^2\tilde{c}(x,s)}{dx^2} = 0 \tag{A.5}$$

subject to the boundary conditions:

$$v\tilde{c}(x,s) - D\frac{d\tilde{c}(x,s)}{dx}\bigg|_{x=0} = \frac{m}{A} \tag{A.6}$$

$$\lim \tilde{c}(x,s)_{x\to\infty} = 0 \;\forall s \tag{A.7}$$

The above equations can easily be solved for $\tilde{c}(x,s)$ in the Laplace domain. Back-transformation to the time-dimension is achieved numerically in all cases presented in this thesis, using the MATLAB code `invlap.m` [*Hollenbeck*, 1998].

METHOD OF MOMENTS

B

The application of the relationship given in equation (2.25) is illustrated here exemplarily for the transport equation in the hyporheic zone. This is being made use of in *Knapp et al.* [2017] to determine tracer recovery and residence times in the subsurface. Please not that in *Knapp et al.* [2017], resorufin breakthrough curves (i = 2) were not analyzed, because concentrations were to small to yield meaningful results. The derivations are given here nonetheless.
Equations (2.16) to (2.18) in the Laplace domain become (the subscripts z of v and D and hz of $\tilde{c}$ are dropped here for readability):

$$\tilde{c}_0(z,s)f_0 + v\frac{d\tilde{c}_0(z,s)}{dz} - D\frac{d^2\tilde{c}_0(z,s)}{dz^2} = 0 \tag{B.1}$$

$$\tilde{c}_1(z,s)f_1 + v\frac{d\tilde{c}_1(z,s)}{dz} - D\frac{d^2\tilde{c}_1(z,s)}{dz^2} = 0 \tag{B.2}$$

$$\tilde{c}_2(z,s)f_2 + \tilde{c}_1(z,s)f_{12} + v\frac{d\tilde{c}_2(z,s)}{dz} - D\frac{d^2\tilde{c}_2(z,s)}{dz^2} = 0 \tag{B.3}$$

here subject to:

$$\lim_{z\to\infty} \tilde{c}_i(z,s) = 0 \; \forall i \tag{B.4}$$

with

$$f_0 = s + q_{in} \tag{B.5}$$

$$f_1 = sR_1 + \lambda_1 + q_{in} \tag{B.6}$$

$$f_2 = sR_2 + \lambda_2 + q_{in} \tag{B.7}$$

$$f_{12} = -\lambda_{12} \tag{B.8}$$

Assuming an idealized Dirac delta-pulse in the stream as input to the subsurface (at $z = z_0$):

$$c_i(z_0,t) = \delta(t) \Rightarrow \tilde{c}_i(z_0,s) = 1 \; \forall s. \tag{B.9}$$

The ODEs (equations B.1 to B.3), subject to the boundary conditions (equations B.4 and B.9) are solved by:

$$\tilde{c}_i(z,s) = \exp\left(-\int_0^z \frac{\sqrt{v^2+4Df_i(s)}-v}{2D}d\zeta\right) \text{ for } i = 0,1 \tag{B.10}$$

$$\tilde{c}_2(z,s) = \exp\left(-\int_0^z \frac{\sqrt{v^2+4Df_2(s)}-v}{2D}d\zeta\right) + k_{12}\exp\left(-\int_0^z \frac{\sqrt{v^2+4Df_1(s)}-v}{2D}d\zeta\right) \tag{B.11}$$

with

$$k_{12} = \frac{f_{12}}{f_1 - f_2} = \frac{\lambda_{12}}{\lambda_2 + R_2 s - \lambda_1 - R_1 s} \tag{B.12}$$

For simplicity, we define the celerity v_{i*} as follows:

$$v_{i*} = \sqrt{v^2 + 4Df_i(s=0)} \tag{B.13}$$

The disappearance (or, in case of resorufin, emergence and dissappearance) of tracer with depth can then be calculated as the recovery of compound i with:

$$X^i_{\text{rec}}(z) = \frac{\mu_0(z)}{\mu_0(0)} = \frac{\tilde{c}_i(z,0)}{\tilde{c}_i(0,0)} \tag{B.14}$$

With equation B.9 this yields for the three different tracer compounds:

$$X^0_{\text{rec}}(z) = \exp\left(-\int_0^z \frac{-v+v_{0*}}{2D}d\zeta\right) \tag{B.15}$$

$$X^1_{\text{rec}}(z) = \exp\left(-\int_0^z \frac{-v+v_{1*}}{2D}d\zeta\right) \tag{B.16}$$

$$X^2_{\text{rec}}(z) = \exp\left(-\int_0^z \frac{-v+v_{2*}}{2D}d\zeta\right) + \frac{\lambda_{12}}{\lambda_2-\lambda_1}\exp\left(-\int_0^z \frac{-v+v_{1*}}{2D}d\zeta\right) \tag{B.17}$$

Similarly, the mean residence time in the hyporheic zone can be calculated from the first moment:

$$\tau_{hz,i}(z) = \frac{\mu_1(z,0)}{\mu_0(z,0)} = \frac{-\left.\frac{\partial\tilde{c}_i(z,s)}{\partial s}\right|_{s=0}}{\tilde{c}_i(z,0)} \tag{B.18}$$

This yields for the three different tracer compounds:

$$\tau_{hz,0}(z) = \int_0^\infty \frac{1}{v_{0*}}d\zeta \tag{B.19}$$

$$\tau_{hz,1}(z) = \int_0^\infty \frac{R_1}{v_{1*}}d\zeta \tag{B.20}$$

$$\begin{aligned}\tau_{hz,2}(z) = {} & \frac{\int_0^\infty \frac{R_2}{v_{2*}}d\zeta}{1+\frac{\lambda_{12}}{\lambda_2-\lambda_1}\exp\left(\int_0^z \frac{v_{2*}-v_{1*}}{2D}d\zeta\right)} \\ & + \left(\frac{\lambda_{12}}{\lambda_2-\lambda_1}\right)\frac{\int_0^\infty \frac{R_1}{v_{1*}}d\zeta + \frac{R_2-R_1}{\lambda_2-\lambda_1}}{\frac{\lambda_2-\lambda_1}{\lambda_{12}}\exp\left(\int_0^z \frac{v_{1*}-v_{2*}}{2D}d\zeta\right)+1}\end{aligned} \tag{B.21}$$

The variance of the residence times can then be determined from the second central moment:

$$\sigma^2_{hz,i}(z) = \frac{\mu_2(z,0)}{\mu_0(z,0)} - \frac{\mu_1^2(z,0)}{\mu_0^2(z,0)} = \frac{\left.\frac{\partial^2\tilde{c}_i(z,s)}{\partial s^2}\right|_{s=0}}{\tilde{c}_i(z,0)} - \tau^2_{hz,i}(z) \tag{B.22}$$

This yields for the three different tracer compounds:

$$\sigma^2_{hz,0}(z) = \int_0^\infty \frac{2D}{v_{0*}^3}d\zeta \tag{B.23}$$

$$\sigma^2_{hz,1}(z) = \int_0^\infty \frac{2DR_1^2}{v_{1*}^3}d\zeta \tag{B.24}$$

$$\begin{aligned}\sigma^2_{hz,2}(z) = {} & \frac{\left(\int_0^\infty \frac{R_1}{v_{1*}}d\zeta\right)^2 + \int_0^\infty \frac{2DR_1^2}{v_{1*}^3}d\zeta + 2\int_0^z \frac{-R_1}{v_{1*}}d\zeta\frac{R_1-R_2}{\lambda_2-\lambda_1} + 2\left(\frac{R_2-R_1}{\lambda_2-\lambda_1}\right)^2}{\frac{\lambda_2-\lambda_1}{\lambda_{12}}\exp\left(\int_0^z \frac{v_{1*}-v_{2*}}{2D}d\zeta\right)+1} \\ & + \frac{\left(\int_0^\infty \frac{R_2}{v_{2*}}d\zeta\right)^2 + \int_0^\infty \frac{2DR_2^2}{v_{2*}^3}d\zeta}{1+\frac{\lambda_{12}}{\lambda_2-\lambda_1}\exp\left(\int_0^z \frac{v_{2*}-v_{1*}}{2D}d\zeta\right)} - \tau^2_{hz,2}(z)\end{aligned} \tag{B.25}$$

SECTION-WISE ANALYSIS OF REACTIVE TRACER TESTS

C

Subdividing the study reach into consecutive sub-sections requires adapting the boundary conditions for all but the first section (reaching from the injection to the first measurement station) compared to *Liao et al.* [2013]. The solution of the forward problem and the incorporated sensitivity analysis are given below.

C.1 Solution of the forward problem

The first index of the parameters used below identifies the tracer compound ($i = 0$ for fluorescein, $i = 1$ for resazurin, $i = 2$ for resorufin), whereas the second index identifies the stream section ($k = 1$ for the stream section between injection and first measurement station, $k = 2$ between measurement station 1 and 2 etc.). As the variables x, v, D, q_{he} are identical for all tracers, their only subscript refers to the stream section. The injected tracer mass m, on the other hand, only depends on the tracer, which is therefore represented by its only subscript. Equations (2.8) to (2.9), subject to Dirichlet boundary conditions, become in the Laplace domain:

$$\underbrace{(s + q_{he} - q_{he}\tilde{g}_0)}_{=f_{0,k}}\tilde{c}_0(s,x) + v\frac{d\tilde{c}_0(s,x)}{dx} - D\frac{d^2\tilde{c}_0(s,x)}{dx^2} = 0 \tag{C.1}$$

$$\underbrace{(s + q_{he} - q_{he}\tilde{g}_1)}_{=f_{1,k}}\tilde{c}_1(s,x) + v\frac{d\tilde{c}_1(s,x)}{dx} - D\frac{d^2\tilde{c}_1(s,x)}{dx^2} = 0 \tag{C.2}$$

$$\underbrace{(s + q_{he} - q_{he}\tilde{g}_2)}_{=f_{2,k}}\tilde{c}_2(s,x)\underbrace{-q_{he}\tilde{g}_{12}}_{=f_{12,k}}\tilde{c}_1(s,x) + v\frac{d\tilde{c}_2(s,x)}{dx} - D\frac{d^2\tilde{c}_2(s,x)}{dx^2} = 0 \tag{C.3}$$

Dirichlet boundary conditions imply that $\tilde{c}_0(s,x)$, $\tilde{c}_1(s,x)$ and $\tilde{c}_2(s,x)$ at the upstream location are known (which is a breakthrough curve, not a Dirac pulse, except for $k = 1$). Due to the section-wise calculation, the section length will be denoted $L_k = x_{k+1} - x_k$. L_k and the variable x will be used interchangeably. The attentive reader will note that it is not possible to derive with respect to a constant. However, I will use it in the following as shorthand meaning $|_{x=L_k}$. Likewise, x_k and x_{k+1} are used for $|_{x=x_k}$ and $|_{x=x_{k+1}}$.

Solving the above equations for concentrations at the downstream location x_{k+1} yields the following solutions:

$$\tilde{c}_0(s,x_{k+1}) = \tilde{c}_0(s,x_k)\exp(-\alpha_{0,k}L_k) \tag{C.4}$$

$$\tilde{c}_1(s,x_{k+1}) = \tilde{c}_1(s,x_k)\exp(-\alpha_{1,k}L_k) \tag{C.5}$$

$$\tilde{c}_2(s,x_{k+1}) = a_{2,k}\exp(-\alpha_{2,k}L_k) + a_{12,k}\exp(-\alpha_{1,k}L_k) \tag{C.6}$$

The concentrations have to be calculated successively, starting from the injection site (where the input is a Dirac pulse) to the first measurement station, and then extending for

all further sections. With

$$\tilde{c}_i(s, x_1) = \frac{m_i}{A} \frac{1}{v_1 + \alpha_{i,1} D_1} \tag{C.7}$$

at the injection site, this yields for the downstream locations of stream section n:

$$\tilde{c}_i(s, x_{n+1}) = \frac{m_i}{A} \frac{1}{v_1 + \alpha_{i,1} D_1} \prod_{k=1}^{n+1} \exp(-\alpha_{i,k} L_k) \tag{C.8}$$

The compound-dependent coefficient α_i for $i = 0, 1$ is obtained by inserting the appropriate solution (equations C.4 and C.5) into the transport equations in the Laplace domain (equations C.1 and C.2):

$$\alpha_{0,k} = \frac{-v_k + \sqrt{v_k^2 + 4 D_k f_{0,k}}}{2 D_k} \tag{C.9}$$

$$\alpha_{1,k} = \frac{-v_k + \sqrt{v_k^2 + 4 D_k f_{1,k}}}{2 D_k} \tag{C.10}$$

Substituting equations C.6 and C.5 into equation C.3 yields:

$$f_{2,k} - \alpha_{2,k} v_k - \alpha_{2,k}^2 D_k = 0$$

$$\alpha_{2,k} = \frac{-v_k + \sqrt{v_k^2 + 4 D_k f_{2,k}}}{2 D_k} \tag{C.11}$$

$$a_{12,k} = \frac{f_{12,k}}{f_{1,k} - f_{2,k}} \tilde{c}_1(s, x_k) \tag{C.12}$$

$a_{2,k}$ can only be determined from the boundary condition of $\tilde{c}_2$, which is here a Dirichlet boundary condition. Equation C.6 thus leads to:

$$a_{2,k} = \tilde{c}_2(s, x_k) - \frac{f_{12,k}}{f_{1,k} - f_{2,k}} \tilde{c}_1(s, x_k) \tag{C.13}$$

With this, all coefficients of the solutions in the Laplace domain (equations C.4 to C.6) are known. Back-transformation to the time-domain is achieved numerically (Appendix A).

C.2 Sensitivity Analysis

To compute sensitivities of the concentrations with respect to the transfer function a small perturbation analysis of equations (2.8) to (2.9) is performed (for details, see Appendix C of *Liao and Cirpka* [2011]). The sensitivities are required for the calculation of the Jacobian.

$$\frac{\partial c_0'}{\partial t} + v \frac{\partial c_0'}{\partial x} - D \frac{\partial^2 c_0'}{\partial x^2} = q_{he} \left(\int_0^t g_0(\tau) c_0'(t-\tau) d\tau - c_0' + \int_0^t g_0'(\tau) \bar{c}_0(t-\tau) d\tau \right) \tag{C.14}$$

$$\frac{\partial c_1'}{\partial t} + v \frac{\partial c_1'}{\partial x} - D \frac{\partial^2 c_1'}{\partial x^2} = q_{he} \left(\int_0^t g_1(\tau) c_1'(t-\tau) d\tau - c_1' + \int_0^t g_1'(\tau) \bar{c}_1(t-\tau) d\tau \right) \tag{C.15}$$

$$\begin{aligned} \frac{\partial c_2'}{\partial t} + v \frac{\partial c_2'}{\partial x} - D \frac{\partial^2 c_2'}{\partial x^2} = q_{he} \Bigg(& \int_0^t g_{12}(\tau) c_1'(t-\tau) d\tau + \int_0^t g_2(\tau) c_2'(t-\tau) d\tau - c_2' \\ & + \int_0^t g_{12}'(\tau) \bar{c}_1(t-\tau) d\tau + \int_0^t g_2'(\tau) \bar{c}_2(t-\tau) d\tau \Bigg) \end{aligned} \tag{C.16}$$

Dirichlet boundary conditions apply (because concentrations at the upstream measurement station are known exactly):

$$c_i'(t, x_k) = 0 \; \forall i \tag{C.17}$$

Parameters with an overbar indicate mean values, those with a prime perturbed parameters.
In the Laplace domain this becomes:

$$f_0\tilde{c}_0' + v\frac{d\tilde{c}_0'}{dx} - D\frac{d^2\tilde{c}_0'}{dx^2} = q_{he}\tilde{g}_0'\widetilde{\bar{c}}_0 = q_{he}\tilde{g}_0'\widetilde{\bar{c}}_0(s, x_k)\exp\left(-\alpha_0 L_k\right) \tag{C.18}$$

$$f_1\tilde{c}_1' + v\frac{d\tilde{c}_1'}{dx} - D\frac{d^2\tilde{c}_1'}{dx^2} = q_{he}\tilde{g}_1'\widetilde{\bar{c}}_1 = q_{he}\tilde{g}_1'\widetilde{\bar{c}}_1(s, x_k)\exp\left(-\alpha_1 L_k\right) \tag{C.19}$$

$$f_2\tilde{c}_2' + v\frac{d\tilde{c}_2'}{dx} - D\frac{d^2\tilde{c}_2'}{dx^2} = q_{he}\tilde{g}_{12}\tilde{c}_1' + q_{he}\tilde{g}_{12}'\widetilde{\bar{c}}_1 + q_{he}\tilde{g}_2'\widetilde{\bar{c}}_2 \tag{C.20}$$

Subject to Dirichlet boundary conditions:

$$\tilde{c}_i'(s, x_k) = 0 \; \forall i \tag{C.21}$$

The homogenous solution for all tracers is analogous to the forward solutions:

$$\tilde{c}_{i,h}'(s, x_{k+1}) = \tilde{c}_i'(s, x_k)\exp(-\alpha_{i,k}L_k) \text{ for } i = 0, 1, 2 \tag{C.22}$$

This part, however, is of no interest, as $\tilde{c}_i'(s, x_k) = 0$ (see boundary condition).
The ansatz for the special solution (and thus the full solution) for fluorescein and resazurin ($i = 0, 1$) is:

$$\tilde{c}_{i,s}'(s, x_{k+1}) = k_{i,k}x_k\exp(-\alpha_{i,k}L_k) \tag{C.23}$$

Substitution into equations C.18 & C.19 lead to:

$$k_{i,k} = \frac{q_{he,k}\tilde{g}_i'\widetilde{\bar{c}}_i(s, x_k)}{v_k + 2D_k\alpha_{i,k}} \tag{C.24}$$

Again, $\widetilde{\bar{c}}_i(s, x_k)$ is the Laplace transformed concentration at any upstream location (same as for equations C.4 to C.6), which is calculated according to equation C.8; but only as far as x_n as the upstream concentration is required here. With

$$\widetilde{\bar{c}}_i(s, x_1) = \frac{m_i}{A}\frac{1}{v_1 + \alpha_i L_1} \tag{C.25}$$

as a starting point for the section reaching from the injection point to the first measurement station, we get for $k_{i,n}$:

$$\begin{aligned} k_{i,n} &= \frac{q_{he}\tilde{g}_i'}{v_n + 2D_n\alpha_{i,n}}\widetilde{\bar{c}}_i(s, x_{n-1}) \\ &= \frac{q_{he}\tilde{g}_i'}{v_n + 2D_n\alpha_{i,n}}\left(\frac{m_i}{A}\frac{1}{v_1 + \alpha_{i,1}L_1}\prod_{j=1}^{n}\exp(-\alpha_{i,j}L_j)\right) \end{aligned} \tag{C.26}$$

The full solution for $\tilde{c}_i', i = 0, 1$ is thus the special solution:

$$\tilde{c}_i'(s, x_{k+1}) = k_{i,k}L_k\exp(-\alpha_{i,k}L_k) \tag{C.27}$$

For resorufin, we substitute the forward solutions of resazurin and resorufin (equations C.5 & C.6, here denoted as $\widetilde{\widetilde{c}}_1$ and $\widetilde{\widetilde{c}}_2$) and the full solution for $\tilde{c}'_1$ (equation C.27) into equation C.20 (the subscript k is dropped in the following for readability):

$$\begin{aligned} f_2\tilde{c}'_2 + v\frac{d\tilde{c}'_2}{dx} - D\frac{d^2\tilde{c}'_2}{dx^2} \\ = & q_{he}\tilde{g}_{12}k_1 L\exp(-\alpha_1 L) + q_{he}\tilde{g}'_{12}\widetilde{\widetilde{c}}_1(s,x)\exp(-\alpha_1 L) \\ & + q_{he}\tilde{g}'_2\widetilde{\widetilde{c}}_2(s,x)\exp(-\alpha_2 L) + q_{he}\tilde{g}'_2 a_{12}\exp(-\alpha_1 L) \end{aligned} \tag{C.28}$$

The ansatz for the special solution of resorufin and its derivatives are as follows:

$$\tilde{c}'_{2,s} = (b_{12}L + d_{12})\exp(-\alpha_1 L) + b_2 L\exp(-\alpha_2 L) \tag{C.29}$$

$$\frac{d\tilde{c}'_{2,s}}{dx} = (b_{12}(1 - L\alpha_1) - \alpha_1 d_{12})\exp(-\alpha_1 L) + b_2(1 - \alpha_2 L)\exp(-\alpha_2 L) \tag{C.30}$$

$$\frac{d^2\tilde{c}'_{2,s}}{dx^2} = (d_{12}\alpha_1^2 - 2b_{12}\alpha_1 + Lb_{12}\alpha_1^2)\exp(-\alpha_1 L) + b_2(L\alpha_2^2 - 2\alpha_2)\exp(-\alpha_2 L) \tag{C.31}$$

Insertion into equation C.28 yields:

$$\begin{aligned} & \exp(-\alpha_1 L)\left[f_2 d_{12} + vb_{12} - v\alpha_1 d_{12} - Dd_{12}\alpha_1^2 + 2Db_{12}\alpha_1 - q_{he}\tilde{g}'_{12}\widetilde{\widetilde{c}}_1(s,x) - q_{he}\tilde{g}'_2 a_{12}\right] \\ & + L\exp(-\alpha_1 L)\left[f_2 b_{12} - vb_{12}\alpha_1 - Db_{12}\alpha_1^2 - q_{he}\tilde{g}_{12}k_1\right] \\ & + \exp(-\alpha_2 L)\left[vb_2 + 2Db_2\alpha_2 - q_{he}\tilde{g}'_2\widetilde{\widetilde{c}}_2(s,x)\right] + Lb_2\exp(-\alpha_2 L)\left[-v\alpha_2 - D\alpha_2^2 + f_2\right] = 0 \end{aligned} \tag{C.32}$$

From this, the coefficients of the special solution $\tilde{c}'_{2,s}$ can be calculated:

$$\begin{aligned} vb_2 + 2Db_2\alpha_2 - q_{he}\tilde{g}'_2\widetilde{\widetilde{c}}_2(s,x) = 0 \\ b_2 = \frac{q_{he}\tilde{g}'_2\widetilde{\widetilde{c}}_2(s,x)}{v + 2D\alpha_2} \end{aligned} \tag{C.33}$$

$$\begin{aligned} f_2 b_{12} - vb_{12}\alpha_1 - Db_{12}\alpha_1^2 - q_{he}\tilde{g}_{12}k_1 = 0 \\ b_{12} = \frac{q_{he}\tilde{g}_{12}k_1}{f_2 - v\alpha_1 - D\alpha_1^2} \end{aligned} \tag{C.34}$$

$$\begin{aligned} f_2 d_{12} + vb_{12} - v\alpha_1 d_{12} - Dd_{12}\alpha_1^2 + 2Db_{12}\alpha_1 - q_{he}\tilde{g}'_{12}\widetilde{\widetilde{c}}_1(s,x) - q_{he}\tilde{g}'_2 a_{12} = 0 \\ d_{12} = \frac{-b_{12}(v + 2D\alpha_1) + q_{he}\tilde{g}'_{12}\widetilde{\widetilde{c}}_1(s,x) + q_{he}\tilde{g}'_2 a_{12}}{f_2 - v\alpha_1 - D\alpha_1^2} \end{aligned} \tag{C.35}$$

Due to the homogeneous solution of resorufin being zero, the special solution of resorufin becomes its full solution:

$$\tilde{c}'_2 = (b_{12}L + d_{12})\exp(-\alpha_1 L) + b_2 L\exp(-\alpha_2 L) \tag{C.36}$$

Water Research 83 (2015) 205–216

Contents lists available at ScienceDirect

Water Research

journal homepage: www.elsevier.com/locate/watres

Impact of non-idealities in gas-tracer tests on the estimation of reaeration, respiration, and photosynthesis rates in streams

Julia L.A. Knapp [a], Karsten Osenbrück [b], Olaf A. Cirpka [a, *]

[a] University of Tübingen, Center for Applied Geoscience, Hölderlinstr. 12, 72074 Tübingen, Germany
[b] Water and Earth System Science (WESS) Competence Cluster, c/o University of Tübingen, Hölderlinstr. 12, 72074 Tübingen, Germany

ARTICLE INFO

Article history:
Received 10 March 2015
Received in revised form
13 June 2015
Accepted 19 June 2015
Available online 21 June 2015

Keywords:
Reaeration
Gas-tracer tests
Whole-stream metabolism
Dispersion
Oxygen balance of streams

ABSTRACT

Estimating respiration and photosynthesis rates in streams usually requires good knowledge of reaeration at the given locations. For this purpose, gas-tracer tests can be conducted, and reaeration rate coefficients are determined from the decrease in gas concentration along the river stretch. The typical procedure for analysis of such tests is based on simplifying assumptions, as it neglects dispersion altogether and does not consider possible fluctuations and trends in the input signal. We mathematically derive the influence of these non-idealities on estimated reaeration rates and how they are propagated onto the evaluation of aerobic respiration and photosynthesis rates from oxygen monitoring. We apply the approach to field data obtained from a gas-tracer test using propane in a second-order stream in Southwest Germany. We calculate the reaeration rate coefficients accounting for dispersion as well as trends and uncertainty in the input signals and compare them to the standard approach. We show that neglecting dispersion significantly underestimates reaeration, and results between sections cannot be compared if trends in the input signal of the gas tracer are disregarded. Using time series of dissolved oxygen and the various estimates of reaeration, we infer respiration and photosynthesis rates for the same stream section, demonstrating that the bias and uncertainty of reaeration using the different approaches significantly affects the calculation of metabolic rates.

© 2015 Elsevier Ltd. All rights reserved.

1. Introduction

The variation of dissolved oxygen (DO) in streams is caused by several processes, of which respiration and primary production are considered to be the most important ones (Odum, 1956; Staehr et al., 2012). During respiration, DO is consumed by aerobic metabolism, whereas primary production leads to an increase of DO in the stream by photosynthesis. As such, both respiration and primary production provide information concerning the vitality and health of the ecosystem (Fellows et al., 2006; Young et al., 2008). The net ecosystem productivity is the difference between respiration and gross primary production and thus denotes the metabolism of a stream. It is usually measured either with the help of in-stream respiration chambers (McIntire et al., 1964; Uzarski et al., 2001) or via the open-water exchange method (Hoellein et al., 2013; Odum, 1956) based on oxygen measurements at one or two stations. Chamber measurements rely on recirculating water around a substrate sample, enabling controlled and replicable measurements. However, artifacts may be caused by non-representative sampling, community disruption and unnatural environments (Bothwell, 1985, 1988, 1989; Horner et al., 1990) preventing upscaling of the results to the whole stream (Bott et al., 2006; Marzolf et al., 1994). The open-water exchange method on the other hand determines metabolic rates from diurnal changes of dissolved-oxygen concentrations. As such, it integrates metabolism over the studied reach and is performed in a natural, undisturbed environment. However, this approach can only be applied where groundwater inflow is negligible (Marzolf et al., 1994; Tank et al., 2010). Furthermore, an independent measurement of reaeration is required in order to determine metabolism rates from oxygen data.

Reaeration changes the DO concentration in the stream towards the saturation concentration, describing the equilibrium with the atmosphere. In case of under-saturation, oxygen is introduced into

* Corresponding author.
E-mail address: olaf.cirpka@uni-tuebingen.de (O.A. Cirpka).

http://dx.doi.org/10.1016/j.watres.2015.06.032
0043-1354/© 2015 Elsevier Ltd. All rights reserved.

the stream by reaeration, but if the stream is over-saturated, oxygen is lost to the atmosphere by the same process. The direction and magnitude of this process is thus highly variable and for accurately calculating metabolic turnover rates, an accurate estimation of reaeration rates is vital. These reaeration rate coefficients, however, are difficult to determine, as all known approaches suffer from inherent shortcomings: Expressions approximating reaeration coefficients from readily available stream data, such as discharge, water depth, and bottom slope, are only applicable under very specific conditions and outcomes calculated by different expressions may differ greatly (Bennett and Rathbun, 1972). Methods relying on longitudinal DO-profiles (e.g., Odum, 1956) are often biased, especially if influenced by varying temperature and non-linear photosynthesis effects (Kosinski, 1984). According to Marzolf et al. (1994) and Wanninkhof et al. (1990), the determination of reaeration coefficients by gas-tracer tests is the most reliable method. In this approach, a volatile compound is continuously injected into the stream and its concentration is measured at one or more downstream locations after steady-state conditions have been reached. From the observed decrease in tracer concentrations along the reach, the reaeration rate coefficient can be directly determined. Propane has frequently been applied as gas tracer (e.g., Marzolf et al., 1994; Young and Huryn, 1999), because the reaeration rate coefficients obtained for this compound can easily be transferred to those of oxygen due to similar Henry's law and molecular diffusion coefficients (Rathbun et al., 1978).

Thus, gas-tracer tests have become a standard evaluation tool for the assessment of oxygen cycling in streams, and the analysis as described by Genereux and Hemond (1990) and Wanninkhof et al. (1990), among others, is relatively simple and easy to implement. Unfortunately, the standard approach is also based on a series of simplifying assumptions that are often not questioned: (i) transport is considered to be strictly advective which, as we will show, leads to systematic underestimation of the reaeration coefficient, (ii) the input of the gas tracer must be steady, which is difficult to achieve with standard field equipment, (iii) if a temperature correction is applied, a constant temperature is assumed over the course of the experiment, (iv) a rigorous uncertainty analysis is typically missing.

The aims of this paper are: (1) to assess the impact of dispersion, unsteady input signals, and temperature changes on the estimation of reaeration rate coefficients and metabolic rates from gas-tracer tests, (2) to quantify the uncertainty of the estimated reaeration rate coefficient and its propagation to respiration and photosynthesis rates when conducting and analyzing gas-tracer tests, and (3) to suggest improvements for the calculation of reaeration rate coefficients from gas-tracer tests at different levels of complexity. Towards this end, we conducted a propane gas-tracer test in a small stream in Southwest Germany, sampling propane concentrations at four measurement stations. To investigate the stability of the propane signal, we conducted repeated sampling at the first station. From the break-through curves (BTCs) of a concurrent conservative-tracer test using fluorescein, we obtained complete travel time distributions as well as characteristic moments of the distributions for the individual sections.

We present analyses of the data according to different methods with increasing complexity to determine the impact of dispersion and an unsteady input signal on the estimation of reaeration rate coefficients in comparison to the standard approach. The uncertainty analysis is based on an ensemble approach applied to both travel time and the propane concentration with 5000 realizations. To show the effect of the different approaches on the calculation of metabolic rates, we used measured time series of DO and temperature to obtain respiration and photosynthesis rates for the different distributions of reaeration rate coefficients.

2. Theory

2.1. Estimation of reaeration rate coefficient

We consider linear transport of compounds in a stream with steady-state flow. The BTC $c_i^{down}(t)$ [ML^{-3}] of compound i at a downstream location can be computed from that at an upstream location $c_i^{up}(t)$ [ML^{-3}] by convolution with the transfer function $g_i(\tau)$ [T^{-1}]:

$$c_i^{down}(t) = \int_0^\infty g_i(\tau) c_i^{up}(t-\tau) d\tau \tag{1}$$

in which τ [T] is the travel time. The transfer function $g_i(\tau)$, also denoted unit-response function, is identical to the breakthrough curve at the downstream location for a pulse injection, multiplied with the discharge at the upstream location and divided by the injected mass. The transfer function between two stations downstream of an injection point can also be inferred from the corresponding measured BTCs by deconvolution without relying on a particular functional shape (Cirpka et al., 2007; Payn et al., 2008). In the following, we will denote the transfer function of a non-volatile, conservative compound $g(\tau)$ (without index), and that of a gas tracer $h(\tau)$, where we assume that the saturation concentration of the gas tracer is zero. The integral $R = \int_0^\infty g(\tau) d\tau \leq 1$ [−] is the recovery of the conservative tracer, indicating dilution by lateral inflow over the stretch of the stream.

The normalized transfer function of the conservative tracer is the travel time distribution $p(\tau) = g(\tau)/R$ between the up- and downstream stations. If we assume Fickian, advective-dispersive transport with uniform coefficients, $p(\tau)$ is the inverse Gaussian distribution with the mean and standard deviation of travel time $\mu_\tau = x/v$ and $\sigma_\tau = \sqrt{2Dx/v^3}$, respectively (Kreft and Zuber, 1978), in which v [LT^{-1}] is the in-stream velocity, D [L^2T^{-1}] is the dispersion coefficient, and x [L] denotes the distance. At many streams, however, deviations from Fickian dispersion, notably extended tailing, have been observed (Cheong and Seo, 2003; Hunt, 1999).

If we follow a water parcel, the concentration c_g of a gas tracer with saturation concentration of zero undergoes linear loss to the atmosphere:

$$\frac{dc_g}{dt} = -k_2 c_g \tag{2}$$

with the gas-exchange or reaeration rate coefficient k_2 [T^{-1}]. From this, we can follow that the transfer function $h(\tau)$ of the gas tracer is:

$$h(\tau) = g(\tau)\exp(-k_2\tau) \tag{3}$$

If $g(\tau)$ is known from conservative-tracer BTCs, the reaeration rate coefficient k_2 can be estimated from up- and downstream concentrations $c_g^{up}(t)$ and $c_g^{down}(t)$ of the gas tracer by substituting Eq. (3) into Eq. (1) and fitting the resulting expression to $c_g^{down}(t)$.

In the standard approach to evaluate the reaeration rate coefficient, the inflow concentration $c_g^{up}(t)$ is assumed constant so that it can be factored out of the integral in Eq. (1). Also, rather than assuming a travel-time distribution, a single value is assumed. This yields after some rearrangement (Wanninkhof et al., 1990):

$$k_2 = \frac{1}{\mu_{\tau_{down}} - \mu_{\tau_{up}}} \ln\left(R\frac{c_g^{up}}{c_g^{down}}\right) \tag{4}$$

in which $\mu_{\tau_{up}}$ [T] and $\mu_{\tau_{down}}$ [T] denote the mean travel times

between the injection point and the up- and downstream stations, respectively. The transfer of k_2 from propane to oxygen is done by multiplication with a factor of 1.39 (Rathbun et al., 1978). This approach of calculating the reaeration rate coefficient has been frequently applied in the past (e.g., Benson et al., 2014; Marzolf et al., 1994; Reid et al., 2007; Soares et al., 2013).

We first consider the effect of neglecting the full travel-time distribution. If transport could be described by the advection-dispersion equation with first-order loss and constant coefficients, the correct expression for the reaeration rate coefficient, provided that $c_g^{up}(t)$ is constant, would be:

$$\begin{aligned} k_2 &= \frac{1}{x}\ln\left(R\frac{c_g^{up}}{c_g^{down}}\right)v + \frac{1}{x^2}\ln^2\left(R\frac{c_g^{up}}{c_g^{down}}\right)D \\ &= \frac{1}{\mu_\tau}\ln\left(R\frac{c_g^{up}}{c_g^{down}}\right) + \frac{\sigma_\tau^2}{2\mu_\tau^3}\ln^2\left(R\frac{c_g^{up}}{c_g^{down}}\right) \end{aligned} \tag{5}$$

implying that k_2 is systematically underestimated in the standard approach, in which dispersion is neglected. The magnitude of the underestimation is proportional to D/x^2. While the validity of Eq. (5) depends on the legitimacy of Fickian dispersion, also any other travel-time distribution leads to values of k_2 that are larger than estimated by the standard approach.

The second effect is related to unsteady injection of the gas tracer. Field equipment used to release the gas tracer into the stream is required to be robust and easy to manage. For instance, Marzolf et al. (1994) attached a weighted air stone to a commercially available propane cylinder, whereas Young and Huryn (1999) replaced the air-stone with a series of fish-tank aerators. In this method significant signal variations may occur, because the pressure and temperature in the propane cylinder changes over the course of the experiment. If we account for a linearly trending input signal, we arrive at:

$$c_g^{down}(t) = \int_0^\infty g(\tau)\exp(-k_2\tau)\left(c_g^0 + s(t-\tau)\right)d\tau \tag{6}$$

in which c_g^0 [ML^{-3}] denotes the upstream gas-tracer concentration at time zero, and s [$ML^{-3}T^{-1}$] is the constant time derivative of c_g^{up}.

Temperature correction is needed to compare rates obtained at different temperatures. The reaeration rate coefficient is usually assigned to the mean stream temperature during the test, and then corrected either to 20 °C or any other temperature (i.e., the stream temperature at a different time). The normalization is achieved with the simplified Arrhenius equation, with $\theta = 1.0241$ [−] (see the critical review of Demars and Manson, 2013):

$$k_{2,T} = k_{2,20^\circ C}\cdot\theta^{(T-20^\circ C)} \tag{7}$$

However, the observed temperature may change significantly over the course of the gas-tracer experiment, so that simple averaging of temperature can introduce a non-negligible error compared to a method that explicitly accounts for the temperature time series:

$$\begin{aligned} c_g^{down}(t) &= \int_0^\infty g(\tau)\exp\left(-k_{2,T(t)}\int_{t-\tau}^{t}\theta^{(T(\tau_*)-T(t))}d\tau_*\right)c_g^{up}(t-\tau)d\tau \\ &\approx \int_0^\infty g(\tau)\exp\left(-k_{2,T(t)}\theta^{(T(t-\tau/2)-T(t))}\tau\right)c_g^{up}(t-\tau)d\tau \end{aligned} \tag{8}$$

The reaeration rate coefficient $k_{2,T(t)}$ at temperature $T(t)$, measured when the downstream sample is taken, is now obtained by fitting the complete expression, Eq. (8), to the measured downstream concentration $c_g^{down}(t)$.

The approach depends on field measurements, which are all uncertain. Nonetheless, even in the standard approach an uncertainty analysis is often not conducted at all (e.g., Bott et al., 2006; Jin et al., 2012; Morse et al., 2007). Because the resulting expression to obtain $k_{2,T(t)}$ depends on the measurements in a nonlinear way, we refrain from linearized uncertainty analysis and apply an ensemble approach instead, in which the full statistical distribution of $k_{2,T(t)}$ is estimated by analyzing an ensemble of measurements perturbed with random measurement error. The uncertain reaeration rates are merged with oxygen data to evaluate metabolic rates (see below), so that a rigorous uncertainty propagation is essential to assess the predictive power of these estimated rates.

2.2. Oxygen balance

The calculated reaeration rate coefficients can be used to estimate respiration and photosynthesis rates. For this, the oxygen balance of a moving water parcel (Odum, 1956) is used as starting point:

$$\frac{dc_{DO}(t)}{dt} = r_{photo}(t) - r_{resp}(t) + k_2(c_{sat}(t) - c_{DO}(t)) \tag{9}$$

in which $c_{DO}(t)$ [ML^{-3}] is the measured concentration of dissolved oxygen, $c_{sat}(t)$ [ML^{-3}] is the saturation concentration of DO depending on the stream temperature at time t, r_{resp} [$ML^{-3}T^{-1}$] denotes the respiration rate, and r_{photo} [$ML^{-3}T^{-1}$] is the photosynthesis rate. The difference $c_{sat}(t)-c_{DO}(t)$ is known as the saturation deficit of DO.

3. Materials and methods

3.1. Site description

We performed a tracer test in the night from June 25 to June 26, 2014 at the Himbach creek, a small second-order stream close to Tübingen, Germany (see Fig. 1). The streambed consists mostly of loamy sediments, with some sandy and gravelly sections. Due to its low discharge (approx. 5–20 L/s), the stream is narrow and shallow, with most sections being no deeper than 30 cm and no wider than 1 m. Typical in-stream velocities at average discharge are about 5 cm/s. The course of the river is marked by a number of easy bends and some larger pools, but features otherwise no great changes in its morphology. For the most part, the Himbach runs through meadows and crop fields. The riverbanks are densely vegetated with a mixture of trees and shrubs, protecting the stream from direct sunlight. For the experiment, a section near its mouth was chosen, with a total length of approximately 780 m and a relatively constant slope of 1.8%.

3.2. Sampling and analysis of field data

As gas tracer, we used propane provided in a commercially available 11 kg cylinder. A hose of approximately 8 m length was attached to the gas cylinder with an interposed pressure reducer (set to 1.5 bar) as well as a rotameter (setting the outflow of propane to 10 L/min). The hose was sealed at the other end and had been perforated with a number of small holes, allowing for a relatively uniform gas injection over the entire width of the stream. While the gas tracer was injected continuously, the conservative tracer fluorescein was injected as a slug at the same location about

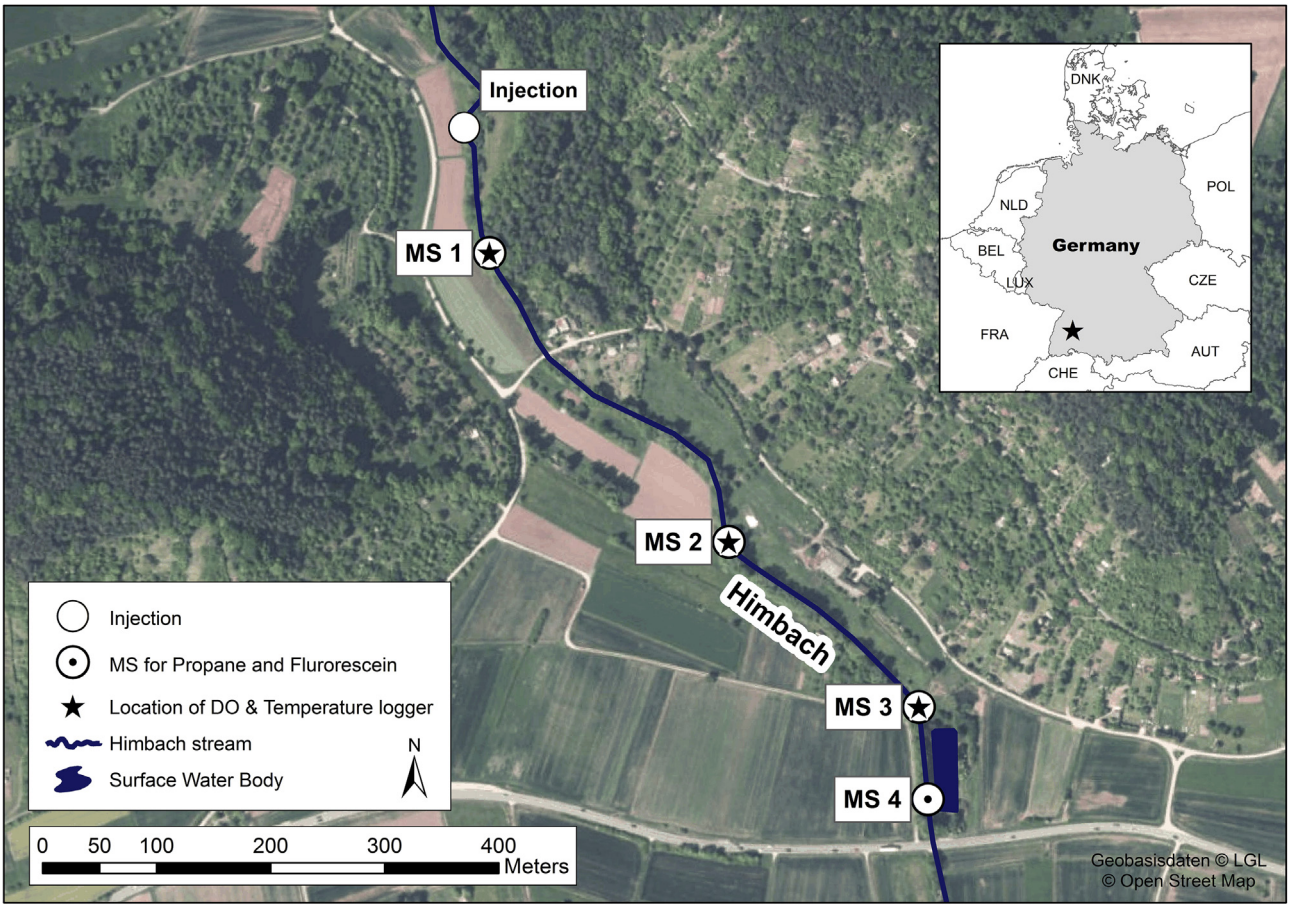

Fig. 1. Map of the Himbach with MS of propane, fluorescein, dissolved oxygen, and temperature.

45 min after the start of the propane injection. 0.57 g of fluorescein were pre-dissolved in approximately 10 L of river water and then poured across the width of the stream.

We monitored the tracers at four measurement stations (MS) downstream of the injection point. By this, the study reach was divided into three different sections (I, II, III), defined as the stretch between two consecutive MS. In addition, we analyzed the entire stretch from MS 1 to MS 4. The first MS was chosen 120 m downstream of the injection point in order to ensure complete mixing. A description of the individual sections is given in Table 1.

The fluorescence signal was measured with a GGUN-FL 30 in-situ fluorometer (Lemke et al., 2014) at each MS with a time resolution of 10 s. The fluorometers were calibrated to known fluorescein concentrations with river water just before the test. Propane samples were taken at all MS after the fluorescence signal had returned to baseline values at the respective locations, indicating full breakthrough. At MS 1, we took a time series of propane samples to obtain information about a potential trend in the outflow of propane from the gas cylinder. For this, three simultaneous samples were taken approximately every 30 min. At each of the other three MS, only one sample set (consisting of three individual samples taken simultaneously) was obtained.

For each sample, about 3/4 of a 200 ml headspace vial were filled with river water at least 10 cm below the water surface to avoid influence by the atmosphere. Each vial was immediately sealed with an aluminum cap with a PTFE septum. The vials were stored upside-down to prevent degassing and analyzed within 8 h of sampling by gas chromatography with flame ionization detection at 85 °C (Varian CP 38000). The exact air and water volumes of each sample were determined and concentrations of gas in the stream water at the time of sampling were calculated with Henry's law from peak areas obtained by gas chromatography. As only relative differences in peak areas are required for the calculation of reaeration rate coefficients, no absolute concentrations of dissolved propane were determined.

DO concentrations and temperature were measured in the stream at 10 min intervals for a duration of approximately 48 h, starting about 24 h before the conduction of the gas tracer test, with an optode-based sensor (miniDOT from PME) at MS 1. At MS 2 and MS 3, DO concentrations were measured additionally, to detect possible deviations from measurements at MS 2. Shortwave solar radiation was measured every minute at a nearby station and Savitzky-Golay filtered for noise reduction.

3.3. Calculation of reaeration rate coefficients

We calculated the reaeration rate coefficients for the stream sections I, II, III, and for the complete stretch from MS 1 to MS 4 applying approaches with increasing complexity. In all approaches, we first determined the transfer function $g(\tau)$ of fluorescein from the up- and downstream BTCs of the respective section by non-parametric deconvolution (Cirpka et al., 2007). In the following, we make use of the temporal moments of the transfer functions as defined in Appendix A.

For the standard evaluation of k_2 (A1), which neglects dispersion and assumes a constant propane signal over time, we calculated the recovery rates R as the zeroth moment of $g(\tau)$, $R = \mu_0(g)$, and the mean travel times as the first over the zeroth moments,

Table 1
Description and general characteristics of the Himbach sections used for analysis.

Stream section	Upstream MS	Downstream MS	Section length [m]	Description
I	1	2	345	Shallow and narrow stream (approx. 0.1 m depth, 1.5 m width)
II	2	3	227	Deeper and narrower than previous section, two small pools
III	3	4	88	Similar to previous section, no pools. Pond on the eastern bank with partially higher hydraulic potential than the stream
MS 1-4	1	4	660	All three sections together

$(\mu_{\tau down} - \mu_{\tau up}) = \mu_1(g)/\mu_0(g)$. Together with the measured concentrations of propane, they were used to calculate the reaeration rate coefficients of the individual sections by the standard approach according to Eq. (4). As the time-dependence of the input signal is neglected in this approach, we considered the first sample set at MS 1 as the presumed steady-state concentration of propane at this location.

In the second approach (A2), we considered a linear trend in the input signal by linear regression of the time series at MS 1. The slope and intercept at the downstream locations was calculated recursively with:

$$c_0^{down} = (c_0^{up} - s^{up} \cdot t_g) \cdot m_0 \tag{10}$$

$$s^{down} = s^{up} \cdot m_0 \tag{11}$$

In this approach (A2), t_g denotes the advective travel time between the stations and is calculated from the temporal moments of the conservative-tracer transfer function by:

$$t_g = \mu_1(g)/\mu_0(g) \tag{12}$$

whereas m_0 represents the zeroth moment of the transfer function of the gas tracer and is calculated as:

$$m_0 = R \cdot \exp(-k_2 \cdot t_g) \tag{13}$$

The propane concentrations at the upstream and downstream locations at time zero are denoted c_0^{up} [ML^{-3}] and c_0^{down} [ML^{-3}], respectively, whereas s^{up} [$ML^{-3}T^{-1}$] and s^{down} [$ML^{-3}T^{-1}$] refer to the corresponding time derivatives. In this approach, we substituted the time-corrected upstream concentration for each section into Eq. (4), which accounts only for the mean travel time between the two stations.

In a third approach (A3), we considered the mean and standard deviations of the travel-time distribution from station to station, and used the expression derived for Fickian dispersion, Eq. (5), to evaluate the reaeration rate coefficient from the measured propane concentrations. The linear trend is accounted for in a similar way as above, with the advective travel time t_g as defined in Eq. (12) and the zeroth moment:

$$m_0 = R \cdot \exp\left(\frac{\mu_\tau}{\sigma_\tau^2}\left(\mu_\tau - \sqrt{\mu_\tau^2 - 2\mu_\tau\sigma_\tau^2 k_2}\right)\right) \tag{14}$$

In the fourth and last approach (A4), we considered the entire travel-time distribution and the linear trend in the gas-tracer signals according to Eq. (6), which was fitted to the measured propane concentrations using the non-linear least-square function lsqnonlin of MATLAB. In the recursive calculation of the linear trend, the entire travel-time distribution was incorporated:

$$m_0 = \int_0^\infty g(h)\exp(-k_2 \cdot \tau) d\tau \tag{15}$$

$$t_g = \frac{\int_0^\infty g(h)\exp(-k_2 \cdot \tau)\ \tau\ d\tau}{\int_0^\infty g(h)\exp(-k_2 \cdot \tau) d\tau} \tag{16}$$

accounting for the full travel-time distribution rather than relying on a particular functional shape.

Subsequently, the reaeration rate coefficients for oxygen were calculated from those of propane by multiplication with 1.39

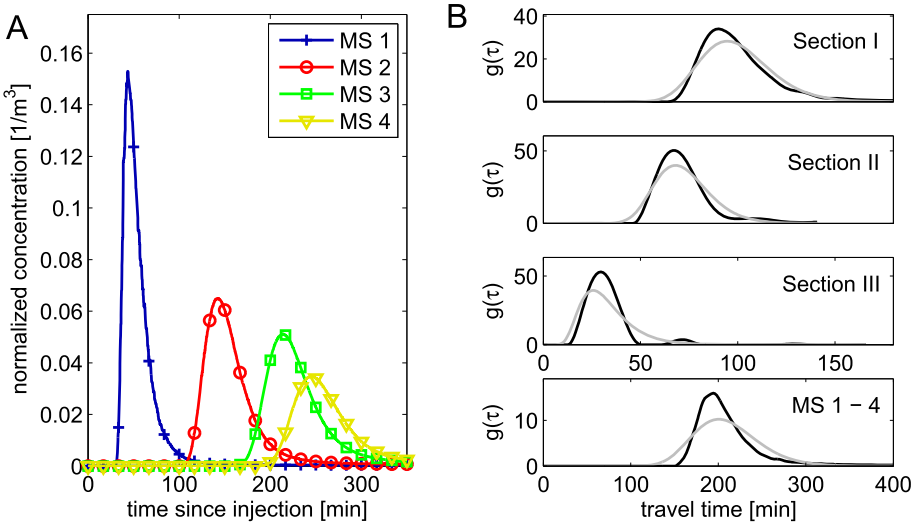

Fig. 2. A: Breakthrough curves of fluorescein, normalized by the injected mass; B: section-wise transfer functions $g(\tau)$ of fluorescein derived from the BTCs (black lines) and inverse-Gaussian distributions (grey) with the same recovery, mean, and standard deviation as the transfer functions.

Table 2
General characteristics of the fluorescein and propane BTCs at the sampling locations.

MS	Apparent dispersion coefficient	Cumulative recovery	Mean relative propane concentration: $\frac{\bar{c}}{c_{MS1,max}}$	Coefficient of variation of propane concentrations: $\frac{\sigma_{\bar{c}}}{\bar{c}}$
	[m^2/s]	[%]	[%]	[%]
1	0.71	n.a.	n.a.	1.4–10.4
2	0.87	91.6	4.5	2.0
3	0.97	87.4	1.3	1.8
4	1.29	67.5	0.6	1.3

(Rathbun et al., 1978). For every approach and all stream sections, the respective water temperatures were additionally determined and the calculated reaeration rate coefficients were corrected to 20 °C.

3.4. Uncertainty estimation of reaeration rate coefficients

We performed uncertainty calculations for every approach based on ensemble calculations of the conservative transfer function $g(\tau)$ and the propane measurements. Towards this end, 5000 conditional realizations of $g(\tau)$ honoring the measured fluorescein BTCs were generated with the non-parametric deconvolution approach of Cirpka et al. (2007). For each realization of $g(\tau)$ we also generated a realization of the up- and downstream propane concentrations assuming a log-normal distribution with the mean and standard deviation of the triple measurements of propane at the corresponding stations. Each combined realization of $g(\tau)$ and the propane concentrations were treated as single set of measurements, yielding one estimate of the reaeration rate coefficient for each realization, stream section, and analysis approach. We characterized the resulting ensembles of k_2 by their mean and standard deviations.

3.5. Estimation of respiration and photosynthesis rates

With the estimated reaeration rate coefficient k_2, both the respiration rate r_{resp} [$ML^{-3}T^{-1}$] and the photosynthesis rate r_{photo} [$ML^{-3}T^{-1}$] can be determined from measured temperature and oxygen data. Because photosynthesis requires light, this component can be eliminated from Eq. (9) during night, leaving respiration as the only unknown. The estimated reaeration rate coefficients adjusted to the given temperatures at the individual time points were thus used to first calculate respiration rates from nocturnal oxygen data over a period of approximately 48 h. We interpolated the last respiration rate before sunrise and the first one after sunset to obtain daytime respiration rates, leaving the photosynthesis rate as the only unknown during the day.

As before, we obtained the uncertainties for the respiration and photosynthesis rates by the ensemble approach using the 5000 ensemble members of the estimated reaeration rate coefficients.

For better comparison with other studies, we additionally converted the respiration and photosynthesis rates to units of mass oxygen transformed per time and bed area, rather than the water volume. This is done by dividing the respiration and photosynthesis rates of Eq. (9) by the hydraulic radius of the stream (Bott et al., 2006), which approximately equals the mean water depth. By doing so, however, we introduce additional uncertainties since determining the wetted perimeter of small streams with non-uniform profile is difficult. Thus, for comparison of the different approaches determining reaeration and their influence of calculated metabolic rates (which is the main objective of this paper), we use the volume-related rates of Eq. (9).

4. Results and discussion

4.1. General characteristics of the tracer experiments

4.1.1. Breakthrough curves

Fig. 2A shows the BTCs of fluorescein, normalized by the injected mass, for all four MS. Table 2 lists the recovery of fluorescein in comparison to MS 1, the mean relative propane concentration in comparison to the first sample set at MS 1, and the measurement uncertainty of propane for all measurement stations. The tailing of the BTCs, caused by in-stream dispersion and transient storage, increases slightly with increasing distance. Apparent dispersion coefficients obtained from the BTCs, derived from the travel distance and the temporal moments of the BTCs, are close to 1 m^2/s, which is in accordance with literature values for streams of similar discharge (Wallis et al., 2007). The fluorescein recovery decreases along the reach. This is attributed to an increase in discharge, which leads to lower tracer concentrations and thus a smaller zeroth moment. The last section shows the strongest decrease in recovery per travel time, which may be caused by water infiltrating from a small pond with higher hydraulic potential next to the stream (see Fig. 1).

4.1.2. Transfer functions and travel-time distributions

Fig. 2B shows the transfer functions $g(\tau)$ of fluorescein for the individual sections derived from the BTCs by non-parametric deconvolution (Cirpka et al., 2007). Travel times were cut once the weight had reached zero, and later peaks contributed less than 2% to the recovery. Table 3 lists the modes, means, and standard deviations of the section-wise travel time distributions, together with apparent velocities and dispersion coefficients computed from their means and standard deviations. Naturally, the longest mean travel time is obtained for the section spanning over the whole

Table 3
Mode, mean, and standard deviation of travel time for each section derived from the transfer functions $g(\tau)$ of fluorescein, as well as apparent velocities and dispersion coefficients.

Section	Peak travel time	Mean travel time μ_τ	Standard deviation of the travel time σ_τ	Apparent velocity v	Apparent dispersion coefficient D
	[min]	[min]	[min]	[m/s]	[m^2/s]
I	90.1	99.6	18.3	0.058	0.34
II	50.4	72.2	14.3	0.052	0.23
III	29.5	32.5	12.9	0.045	0.31
MS 1-4	194.5	210.2	37.2	0.052	0.54

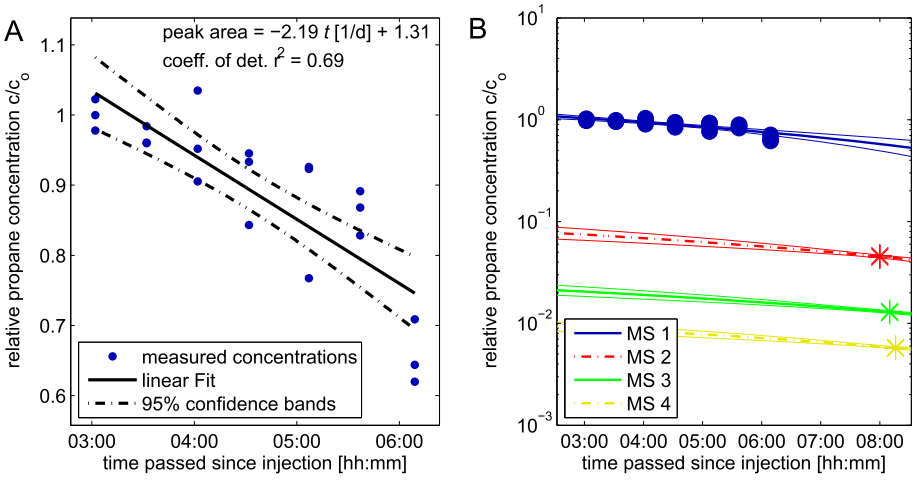

Fig. 3. Relative concentrations of propane measured over time. Propane concentrations are normalized with the mean concentration of the first sample set at MS 1. Bold and dotted lines represent a linear fit and its 95%-confidence bands, respectively. A: Measurements at MS 1. B: Relative propane concentrations at all measurement locations and the calculated (recursive) time-dependence.

stream. Between the individual sections, the mean travel time is greatest for Section I (between MS 1 and MS 2) which is the longest section. The shortest mean travel time is found for the shortest stretch, Section III. The transfer functions of Section I and the entire stream section feature significant tailing, whereas Section III shows a secondary peak, which may be an artefact caused by the deconvolution method. The transfer function of Section II exhibits a distinct shoulder.

The transfer functions derived from inverse-Gaussian distributions, which would be consistent with Fickian dispersion, match the ones derived from the BTCs by non-parametric deconvolution relatively well, except for the entire stream.

4.1.3. Time dependence of propane concentration

Fig. 3A shows the measured concentration of propane at MS 1 as function of time, indicating a clear decrease although no changes in pressure or flux were recorded at the outflow of the propane cylinder. We fitted a linear function to the concentrations ($r^2 = 0.69$).

Fig. 3B shows the measured concentrations and the recursively calculated time-dependences of propane at all measurement stations in a semi-logarithmic scale (Eqs. (10) and (11)). The mean relative concentrations and the coefficients of variation are listed in Table 2. The concentrations decrease along the stretch, and the largest error in propane concentrations is approx. 10% (measured at MS 1).

4.1.4. Dissolved oxygen and temperature

Fig. 4 shows the time series of dissolved oxygen and water temperature continuously measured at MS 1-3. Oxygen data from MS 4 are disregarded because of the low fluorescein recovery. The magnitude and diurnal variations of both variables are very similar at all MS. As the purpose of this study is the comparison of different approaches for the calculation of reaeration rate coefficients, the differences in DO between the individual MS can be neglected in this context. For this reason, using only measurements of DO and temperature from MS 2 for the calculation of reaeration and metabolic rates is legitimate.

The maximum change in temperature at MS 2 during the time of the tracer test amounted to 2.0 °C, with a nearly linear decline from the time of the first sampling at MS 1 (14.1 °C) to the time of

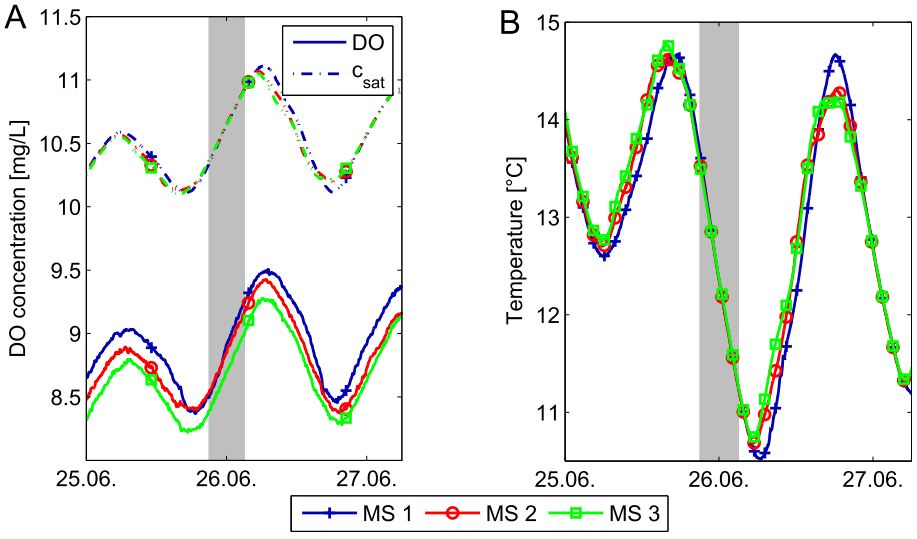

Fig. 4. Time series of dissolved oxygen, the oxygen saturation concentration (A), and temperature (B) at MS 1–3. The area shaded in grey indicates the time of the tracer test.

sampling at the last MS (12.1 °C). Furthermore, concentrations of DO never went above saturation concentrations at any MS, presumably due to dense vegetation and shading from direct sunlight and thus low photosynthesis.

4.2. Estimated reaeration rate coefficients

Fig. 5 shows the reaeration rate coefficients and their standard deviations calculated for each stream section using the four different approaches of increasing complexity. The reaeration rate coefficients are the highest in Section I, independent of the approaches used for their calculation. This is probably due to the larger air–water interface of this section, which leads to a faster reaeration flux. The reaeration rate coefficient for the entire stream is strongly dominated by Section I, covering about half of the length and travel time of the stretch.

The magnitude of the determined reaeration rate coefficients ranges from 40/day to 70/day. This is in agreement with other gas tracer tests in streams of similar size: Wanninkhof et al. (1990) found a reaeration rate coefficient of $k_2 = 134$/day for a stream of 20 L/s discharge and approximately 7 cm/s in-stream velocity. Young and Huryn (1999) determined a reaeration rate coefficient varying between 50/day to 250/day at the Powder Creek, depending on the discharge which ranged from 18 to 40 L/s. And Soares et al. (2013) found a reaeration rate coefficient between 60/day to 200/day for comparable streams.

Estimating reaeration rate coefficients with expressions of O'Connor and Dobbins (1958) and Tsivoglou and Wallace (1972), we obtain much smaller values (see Table 4). Similar findings were made in the studies cited above, where empirical relationships underpredicted the reaeration rate coefficients especially in smaller streams. This suggests, that these relationships do not adequately represent the turbulence and bathymetry influencing reaeration in most smaller streams (as compared to larger streams, for which these relationships have been derived).

Due to the low uncertainty in the propane concentrations, the uncertainties of all rates are relatively small. The highest uncertainty is obtained for Section III, which is the shortest, has the smallest travel time, and the smallest relative decrease of propane concentration, causing the worst signal-to-noise ratio in the propane data.

The estimated reaeration rate coefficients significantly depend on the approach taken for their calculation. The standard approach (A1) yields results that are up to 10% higher or lower than the other approaches: Neglecting the trend of the input signal in A1 leads to both under- and overestimation of the reaeration rate coefficient, depending on the time of sampling relative to the travel time of the sampled water parcel. Ideally, the same water parcel is sampled at the up- and downstream locations. If the downstream sampling is too late, concentrations have dropped by the unconsidered trend of the input signal. In this case reaeration is overestimated, like in Section I. If downstream sampling is too early, like for Sections II and III, the reaeration rate coefficient is underestimated. The magnitude of unsteadiness in the gas-tracer injection depends on the individual tracer test. If recognized by time-dependent measurements, it can be accounted for in the estimation of reaeration rate coefficients, as done in approaches A2-A4, which will be discussed in the following.

The two approaches accounting for dispersion (A3 and A4) consistently yield larger reaeration rate coefficients than the one neglecting it (A2), as was expected from Eq. (5). This difference is largest for Section I and the entire stream, as these exhibit the largest spread of the travel-time distribution.

The magnitude of the differences between A3 (assuming Fickian dispersion) and A4 (not relying on a particular shape of the travel-time distribution) is very small for the individual stream sections, as would have been expected from the relatively good fit of the inverse Gaussian distribution to the non-parametric travel time distributions (see Fig. 2). The direction of the effect depends on how well the Gaussian distribution is able to represent the travel times: If the weight put on the longer travel times is too great or the one

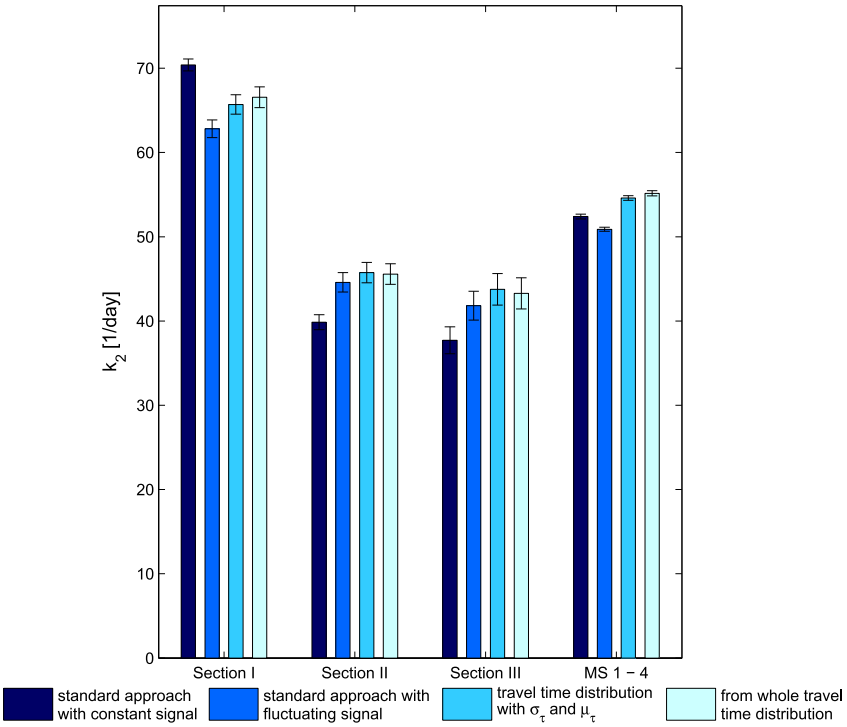

Fig. 5. Reaeration coefficients of oxygen of different sections corrected to 20 °C, calculated according to the four different approaches. The error bars are calculated based on an ensemble based uncertainty analysis with 5000 realizations, taking into account the uncertainties of the travel time as well as the uncertainty in the propane concentrations.

Table 4
Reaeration rate coefficients k_2 estimated for the Himbach by literature expressions.

Expression	Reference	k_2 [1/day]	Remarks
$k_2 = 31.6 \cdot v \cdot (1000 \cdot S)$	Tsivoglou and Wallace (1972)	28.44	$Q < 0.3$ m^3/s
$k_2 = \frac{D_m^{0.5} \cdot v^{0.5}}{h^{1.5}}$	O'Connor and Dobbins (1958)	9.90	isotropic turbulence
$k_2 = \frac{D_m^{0.5} \cdot S^{0.25} \cdot g^{0.25}}{\kappa \cdot h^{1.25}}$	O'Connor and Dobbins (1958)	29.97	anisotropic turbulence

v: in-stream velocity ($\approx$0.05 m/s); S: slope ($\approx$0.018 m/m); h: water depth ($\approx$0.2 m); D_m: molecular Diffusion coefficient of oxygen in water ($\approx$2.1e-9 m^2/s); κ: von Kármán constant ($=$ 0.41); g: gravitational acceleration ($=$ 9.81 m/s^2); Q: discharge.

put on the shorter travel times is too low, the reaeration rate coefficient is overestimated by approach A3 compared to A4. This is the case for Section III. For Section I and the entire stream, the opposite is the case as shorter travel times are overemphasized by the inverse-Gaussian distribution. Hence, the better the non-parametric and inverse-Gaussian distributions correspond, the smaller is the deviation. In our experiment, an approximation of the travel time distribution by its characteristic moments could be considered an acceptable simplification, as differences between A3 and A4 are not significant. Only if dispersion deviated significantly from the Fickian behavior would we have expected strong discrepancies between the outcomes of approaches A3 and A4.

4.3. Estimated respiration and photosynthesis rates

We evaluated the respiration and photosynthesis rates as outlined in Section 3.5 using the reaeration rate coefficients of the different approaches. Fig. 6 illustrates the estimated respiration and photosynthesis rates in units of oxygen mass converted per unit area and time for a duration of approximately 48 h, including the time of the tracer tests. We calculated the metabolic rates for all sections using identical oxygen and temperature time series. Thus, differences between the sections are exclusively caused by differences in reaeration rate coefficients and travel times.

Respiration remains nearly constant during the night, whereas photosynthesis features its highest value near the peak of solar radiation. Due to the longer travel times required for calculations of the section spanning from MS 1-4, rates can only be calculated from the morning of June 25 onwards.

We obtained respiration rates of 8–10 g O_2/m^2/d and photosynthesis rates of approximately 1.5 g O_2/m^2/d for the Himbach stream. These rates reasonably agree with the range of metabolic rates reported in other studies. Rates similar to the Himbach have been found by Mulholland et al. (2001) who measured approximately 8 g O_2/m^2/d in a stream of comparable size and discharge.

The model of Riley and Dodds (2013) fitting calculated to measured DO in streams, obtained values of 2.5–7 g O_2/m^2/d for respiration and 0.8–7 g O_2/m^2/d for primary production for

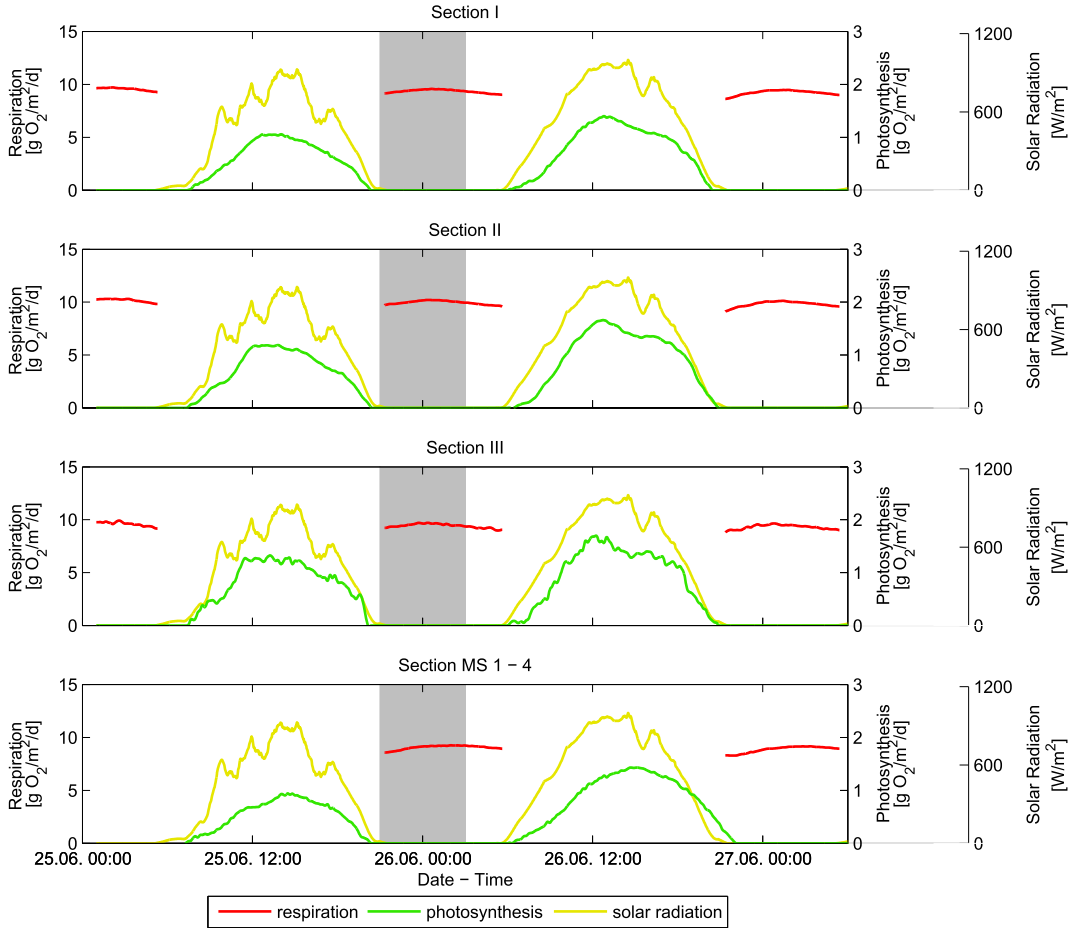

Fig. 6. Respiration rates (night) and photosynthesis rates (day), together with solar radiation data for a time period of approximately 48 h. The shaded area indicates the time of the tracer tests. Ensemble-based uncertainties as well as uncertainties of the conversion are neglected.

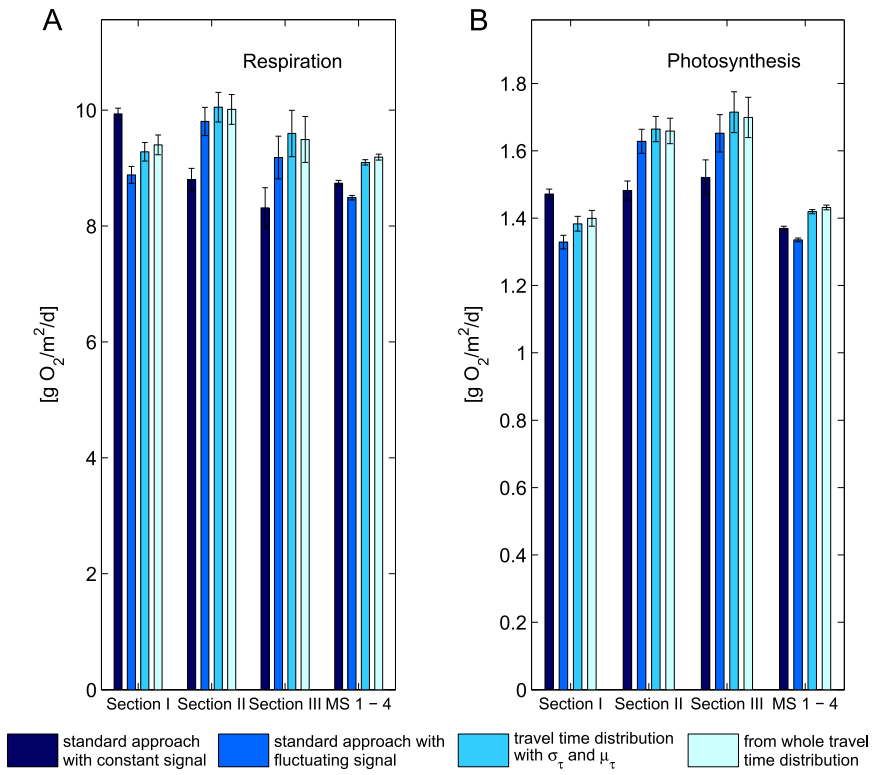

Fig. 7. Respiration and photosynthesis rates for the stream sections using the four different approaches to estimate reaeration. A: Mean respiration rates at the time of the tracer test. B: Maximum photosynthesis rates at the second day. Error bars take into account the uncertainties in the travel time and change in oxygen concentration. For respiration, they represent the standard deviation between the temporal mean of each realization of the respiration rates. Note that units differ from those of Fig. 6.

streams of comparable size. For the already mentioned Powder Creek, Young and Huryn (1999) measured respiration rates between 4 and 8 g $O_2/m^2/d$ and photosynthesis lower than 1.5 g $O_2/m^2/d$.

In the following, we compare the results of the different approaches A1-A4. For this, we use respiration and photosynthesis rates in units of $[ML^{-3}T^{-1}]$ as calculated by Eq. (9), as these do not depend on the highly uncertain wetted perimeter of the stream.

Fig. 7A shows the mean respiration rates in the night of the tracer test for the different stream sections according to the different approaches of estimating reaeration. Respiration is highest for Section I, and the value obtained for the entire stream stretch is the average of the different sections weighted by the respective travel times. The different reaeration rate coefficients obtained by the different approaches are propagated to the estimated respiration rates, with highest rates found for the approach taking into account the entire travel time distribution (A4) for all sections but the entire stream.

The relative uncertainty obtained for the respiration rates is higher than the one calculated for the reaeration rates, as the uncertainty of the travel time associated with the additional components of the oxygen balance has additionally to be considered. As this is very small here, however, the increase in relative uncertainty is also very small.

The pattern of uncertainties between the measurement sections is similar to the one already observed for the calculated reaeration rates, as the main component determining the rates and uncertainties is reaeration. For this reason, the uncertainty is the lowest for the entire stream stretch.

Fig. 7B shows the estimated photosynthesis rates in the middle of the day following the night of the tracer test. The relative uncertainty of these rates increases again slightly compared to the respiration rates, as the calculation of photosynthesis rates depends both on the reaeration coefficient as well as the respiration rate, with the uncertainties of both components adding up.

5. Conclusions and recommendations

This study aimed to highlight sources of error in the estimation of reaeration rates from gas-tracer tests. Towards this end, we conducted a mathematically thorough and more than ordinarily rigorous analysis of the data by investigating the effects of the travel time distribution and unsteady input signals on reaeration and their propagation to the estimation of respiration and photosynthesis rates.

We could show that reaeration is significantly underestimated if travel-time distributions are replaced by only their mean value. Considering the mean and standard deviation of the travel time and using expressions valid for Fickian transport may yield acceptable results. This, however, is only the case if deviations from the inverse Gaussian travel time distribution are negligible. In any case, accounting for the full distribution is computationally not difficult and thus recommended by us.

The error introduced by neglecting unsteady input signal appears to be the most severe one. In practice it is nearly impossible to sample the same water parcel at different measurement stations, and depending on the sign of the time offset and the trend in the gas injection, the sampled concentrations could be too low or too high. We recommend taking a time series of gas-tracer concentrations at the first MS to correct for these effects. As minimum alternative, the first MS may be sampled twice, namely at the beginning and end of the sampling campaign, performing linear interpolation in between. We demonstrated that correcting for a linearly trending input signal is straightforward.

A further reason for accounting for the full distribution of travel times is that it allows for a more accurate way of assigning the calculated reaeration rate coefficient to a certain temperature that also integrates the travel time distribution. The effect in this experiment was rather small, as the temperature difference was relatively small, and it could be approximated by a linear function. If, however, the tracer tests had been conducted during a period spanning over an entire day (thus spanning over the maximum or minimum turning point of the temperature curve), this effect would become more important, since a linear approximation of the temperature time series would not have been possible. This highlights the importance of an accurate application of the temperature correction, which can only be performed when considering the full travel-time distribution.

The propane measurements performed in this study showed some uncertainty as shown in Fig. 3, but we have observed worse measurement errors using the same sampling and analytical techniques in studies at other streams. We believe that the most important error source lies in sampling, which may be avoided with in-situ measurement techniques. Accurate gas-tracer measurements are of course essential in the estimation of reaeration. We also highly recommend taking enough parallel samples to facilitate uncertainty analysis. The applied ensemble approach for error analysis is easy to implement and does not rely on linearization. As the evaluation of the analytical expression presented here is computationally efficient, the computer costs for ensemble-based uncertainty analysis are acceptable.

The accurate determination of reaeration rate coefficients is particularly important when they are used for further assessment of respiration and photosynthesis rates, as the uncertainty accumulates with every calculation step. For this reason, again, it is of great importance to keep the initial uncertainty, originating from the propane detection, as low as possible.

All in all, with the Himbach being of very small size and discharge, our data may be considered as an extreme example. However, as the dimensions of a stream increase, so does dispersion, leading to an even greater significance of the investigated effects.

Acknowledgments

The authors wish to thank Friederike Currle for her help during field work. The Carl Zeiss Stiftung supported the first author by the Ph.D. scholarship “Entwicklung experimenteller und mathematischer Methoden zur Quantifizierung des Stoffumsatzes in der hyporheischen Zone” (Development of experimental and mathematical methods for the quantification of mass transfer in the Hyporheic zone).

Appendix A. Temporal moments

The k-th temporal moment of time signal $y(t)$ is defined as:

$$\mu_k(y) = \int_0^\infty t^k y(t) dt \tag{17}$$

and the k-th central moment is:

$$\mu_{kc}(c) = \int_0^\infty \left(t - \frac{\mu_1(c)}{\mu_0(c)}\right)^k c(t) dt \tag{18}$$

For the BTC of a conservative tracer undergoing Fickian transport, the temporal moments can be interpreted as follows:

- The zeroth moment represents the tracer mass m per discharge Q:

$$\mu_0(c) = \frac{m}{Q} \tag{19}$$

- The second central moment normalized with the zeroth moment is the variance of the travel time and thus denotes the spread of the travel time distribution:

$$\sigma_\tau^2 = \frac{\mu_{2c}(c)}{\mu_0(c)} = \frac{2Dx}{v^3} \tag{20}$$

References

Bennett, J.P., Rathbun, R.E., 1972. Reaeration in Open-channel Flow. U.S. Government Printing Office.
Benson, A., Zane, M., Becker, T.E., Visser, A., Uriostegui, S.H., DeRubeis, E., Moran, J.E., Esser, B.K., Clark, J.F., 2014. Quantifying reaeration rates in alpine streams using deliberate gas tracer experiments. Water 6 (4), 1013–1027.
Bothwell, M.L., 1985. Phosphorus limitation of lotic periphyton growth-rates – an intersite comparison using continuous-flow troughs (Thompson River system, British-Columbia). Limnol. Oceanogr. 30 (3), 527–542.
Bothwell, M.L., 1988. Growth-rate responses of lotic periphytic diatoms to experimental phosphorus enrichment – the influence of temperature and light. Can. J. Fish. Aquat. Sci. 45 (2), 261–270.
Bothwell, M.L., 1989. Phosphorus limited growth dynamics of lotic periphytic diatom communities – areal biomass and cellular growth-rate responses. Can. J. Fish Aquat. Sci. 46 (8), 1293–1301.
Bott, T.L., Newbold, J.D., Arscott, D.B., 2006. Ecosystem metabolism in piedmont streams: reach geomorphology modulates the influence of riparian vegetation. Ecosystems 9 (3), 398–421.
Cheong, T.S., Seo, I.W., 2003. Parameter estimation of the transient storage model by a routing method for river mixing processes. Water Resour. Res. 39 (4), 1074.
Cirpka, O.A., Fienen, M.N., Hofer, M., Hoehn, E., Tessarini, A., Kipfer, R., Kitanidis, P.K., 2007. Analyzing bank filtration by deconvoluting time series of electric conductivity. Ground Water 45 (3), 318–328.
Demars, B.O.L., Manson, J.R., 2013. Temperature dependence of stream aeration coefficients and the effect of water turbulence: a critical review. Water Res. 47 (1), 1–15.
Fellows, C.S., Clapcott, J.E., Udy, J.W., Bunn, S.E., Harch, B.D., Smith, M.J., Davies, P.M., 2006. Benthic metabolism as an indicator of stream ecosystem health. Hydrobiologia 572, 71–87.
Genereux, D.P., Hemond, H.F., 1990. Naturally-occurring Rn-222 as a tracer for streamflow generation - steady-state methodology and field example. Water Resour. Res. 26 (12), 3065–3075.
Hoellein, T.J., Bruesewitz, D.A., Richardson, D.C., 2013. Revisiting Odum (1956): a synthesis of aquatic ecosystem metabolism. Limnol. Oceanogr. 58 (6), 2089–2100.
Horner, R.R., Welch, E.B., Seeley, M.R., Jacoby, J.M., 1990. Responses of periphyton to changes in current velocity, suspended sediment and phosphorus concentration. Freshw. Biol. 24 (2), 215–232.
Hunt, B., 1999. Dispersion model for mountain streams. J. Hydraul. Eng. ASCE 125 (2), 99–105.
Jin, H.S., White, D.S., Ramsey, J.B., Kipphut, G.W., 2012. Mixed tracer injection method to measure reaeration coefficients in small streams. Water Air Soil Pollut. 223 (8), 5297–5306.
Kosinski, R.J., 1984. A comparison of the accuracy and precision of several open-water oxygen productivity techniques. Hydrobiologia 119 (2), 139–148.
Kreft, A., Zuber, A., 1978. Physical meaning of dispersion-equation and its solutions for different initial and boundary conditions. Chem. Eng. Sci. 33 (11), 1471–1480.
Lemke, D., Gonzalez-Pinzon, R., Liao, Z., Wohling, T., Osenbruck, K., Haggerty, R., Cirpka, O.A., 2014. Sorption and transformation of the reactive tracers resazurin and resorufin in natural river sediments. Hydrol. Earth Sys. Sci. 18 (8), 3151–3163.
Marzolf, E.R., Mulholland, P.J., Steinman, A.D., 1994. Improvements to the diurnal upstream-downstream dissolved-oxygen change technique for determining whole-stream metabolism in small streams. Can. J. Fish Aquat. Sci. 51 (7), 1591–1599.
McIntire, C.D., Garrison, R.L., Phinney, H.K., Warren, C.E., 1964. Primary production in laboratory streams. Limnol. Oceanogr. 9 (1), 92–102.
Morse, N., Bowden, W.B., Hackman, A., Pruden, C., Steiner, E., Berger, E., 2007. Using sound pressure to estimate reaeration in streams. J. North Am. Benthol. Soc. 26 (1), 28–37.
Mulholland, P.J., Fellows, C.S., Tank, J.L., Grimm, N.B., Webster, J.R., Hamilton, S.K., Marti, E., Ashkenas, L., Bowden, W.B., Dodds, W.K., McDowell, W.H., Paul, M.J., Peterson, B.J., 2001. Inter-biome comparison of factors controlling stream

metabolism. Freshw. Biol. 46 (11), 1503–1517.
O'Connor, D.J., Dobbins, W.E., 1958. Mechanism of reaeration in natural streams. Trans. Am. Soc. Civ. Eng. 123 (1), 641–666.
Odum, H.T., 1956. Primary production in flowing waters. Limnol. Oceanogr. 1 (2), 102–117.
Payn, R.A., Gooseff, M.N., Benson, D.A., Cirpka, O.A., Zarnetske, J.P., Bowden, W.B., McNamara, J.P., Bradford, J.H., 2008. Comparison of instantaneous and constant-rate stream tracer experiments through non-parametric analysis of residence time distributions. Water Resour. Res. 44 (6), W06404.
Rathbun, R.E., Stephens, D.W., Shultz, D.J., Tai, D.Y., 1978. Laboratory studies of gas tracers for reaeration. J. Environ. Eng. Div. ASCE 104 (2), 215–229.
Reid, S.E., Mackinnon, P.A., Elliot, T., 2007. Direct measurements of reaeration rates using noble gas tracers in the River Lagan, Northern Ireland. Water Environ. J. 21 (3), 182–191.
Riley, A.J., Dodds, W.K., 2013. Whole-stream metabolism: strategies for measuring and modeling diel trends of dissolved oxygen. Freshw. Sci. 32 (1), 56–69.
Soares, P.A., Faht, G., Pinheiro, A., da Silva, M.R., Zucco, E., 2013. Determination of reaeration-rate coefficient by modified tracer gas technique. Hydrol. Process. 27 (19), 2710–2720.
Staehr, P.A., Testa, J.M., Kemp, W.M., Cole, J.J., Sand-Jensen, K., Smith, S.V., 2012. The metabolism of aquatic ecosystems: history, applications, and future challenges. Aquat. Sci. 74 (1), 15–29.
Tank, J.L., Rosi-Marshall, E.J., Griffiths, N.A., Entrekin, S.A., Stephen, M.L., 2010. A review of allochthonous organic matter dynamics and metabolism in streams. J. North Am. Benthol. Soc. 29 (1), 118–146.
Tsivoglou, E.C., Wallace, J.R., 1972. Characterization of Stream Reaeration Capacity, Office of Research and Monitoring. US Environmental Protection Agency (For sale by the Supt. of Docs., US Govt. Print. Off).
Uzarski, D.G., Burton, T.M., Stricker, C.A., 2001. A new chamber design for measuring community metabolism in a Michigan stream. Hydrobiologia 455, 137–155.
Wallis, S., Piotrowski, A., Rowinski, P., Napiorkowski, J., 2007. Prediction of Dispersion Coefficients in a Small Stream Using Artificial Neural Networks, p. 517.
Wanninkhof, R., Mulholland, P., Elwood, J., 1990. Gas exchange rates for a first-order stream determined with deliberate and natural tracers. Water Resour. Res. 26 (7), 1621–1630.
Young, R.G., Huryn, A.D., 1999. Effects of land use on stream metabolism and organic matter turnover. Ecol. Appl. 9 (4), 1359–1376.
Young, R.G., Matthaei, C.D., Townsend, C.R., 2008. Organic matter breakdown and ecosystem metabolism: functional indicators for assessing river ecosystem health. J. North Am. Benthol. Soc. 27 (3), 605–625.

AGU PUBLICATIONS

Water Resources Research

RESEARCH ARTICLE
10.1002/2016WR019393

Tracer-based characterization of hyporheic exchange and benthic biolayers in streams

Julia L. A. Knapp[1,2], Ricardo González-Pinzón[3], Jennifer D. Drummond[4], Laurel G. Larsen[2,5], Olaf A. Cirpka[1], and Judson W. Harvey[2]

[1]Center for Applied Geoscience, University of Tübingen, Tübingen, Germany, [2]National Research Program, U.S. Geological Survey, Reston, Virginia, USA, [3]Department of Civil Engineering, University of New Mexico, Albuquerque, New Mexico, USA, [4]Integrative Freshwater Ecology Group, Center for Advanced Studies of Blanes (CEAB-CSIC), Blanes, Girona, Spain, [5]Department of Geography, University of California, Berkeley, California, USA

Key Points:
- In-stream tracer measurements specify bulk stream reactivity but not biolayer depth
- Streambed profiles identify reactive zones, but not contributions to whole-stream reactivity
- Coupled in-stream and multidepth measurements contextualize hyporheic and reach-scale processing

Supporting Information:
- Supporting Information S1

Correspondence to:
J. L. A. Knapp,
julia.knapp@uni-tuebingen.de

Citation:
Knapp, J. L. A., R. González-Pinzón, J. D. Drummond, L. G. Larsen, O. A. Cirpka, and J. W. Harvey (2017), Tracer-based characterization of hyporheic exchange and benthic biolayers in streams, *Water Resour. Res.*, *53*, doi:10.1002/2016WR019393.

Received 22 JUN 2016
Accepted 21 JAN 2017
Accepted article online 28 JAN 2017

Abstract Shallow benthic biolayers at the top of the streambed are believed to be places of enhanced biogeochemical turnover within the hyporheic zone. They can be investigated by reactive stream tracer tests with tracer recordings in the streambed and in the stream channel. Common in-stream measurements of such reactive tracers cannot localize where the processing primarily takes place, whereas isolated vertical depth profiles of solutes within the hyporheic zone are usually not representative of the entire stream. We present results of a tracer test where we injected the conservative tracer bromide together with the reactive tracer resazurin into a third-order stream and combined the recording of in-stream breakthrough curves with multidepth sampling of the hyporheic zone at several locations. The transformation of resazurin was used as an indicator of metabolism, and high-reactivity zones were identified from depth profiles. The results from our subsurface analysis indicate that the potential for tracer transformation (i.e., the reaction rate constant) varied with depth in the hyporheic zone. This highlights the importance of the benthic biolayer, which we found to be on average 2 cm thick in this study, ranging from one third to one half of the full depth of the hyporheic zone. The reach-scale approach integrated the effects of processes along the reach length, isolating hyporheic processes relevant for whole-stream chemistry and estimating effective reaction rates.

1. Introduction

River corridors convey water over and around fluvial features and exchange water across sediment interfaces, causing mixing between river water and groundwater that creates steep gradients in temperature, pH, redox conditions, and nutrient availability and thereby enhance chemical reactions [*Boulton et al.*, 1998; *Boano et al.*, 2014; *Harvey and Gooseff*, 2015]. River interactions with hyporheic zones are widely important for water quality and for creating unique habitats for aquatic organisms [*Stanford and Ward*, 1988; *Boulton et al.*, 1998; *Boano et al.*, 2014]. Chemical reactions in the hyporheic zone also contribute to the overall health and functions of the stream network, notably influencing nutrient cycling [*Grimm and Fisher*, 1984; *Bardini et al.*, 2012] and metabolic activity [*Brunke and Gonser*, 1997; *Krause et al.*, 2011]. However, not all parts of the hyporheic zone interact equally with the stream. Recently, it has been proposed that the shallow layer at the top of the streambed, or slightly beneath it, is an active area for biotic and abiotic chemical transformations [*Battin et al.*, 2003; *O'Connor and Harvey*, 2008]. This "shallow benthic biolayer" at the uppermost sediments accumulates organics (i.e., organic carbon and other fine particles), algae, periphyton, and microbes and thus influences redox zonation and hyporheic processes [*Boano et al.*, 2014; *Battin et al.*, 2016]. In this biolayer, microorganism abundances are often highest [e.g., *Navel et al.*, 2011; *Harvey et al.*, 2013] and mediate key biochemical reactions across the stream network [*Briggs et al.*, 2015], including aerobic respiration [*González-Pinzón et al.*, 2012, 2014], denitrification [*O'Connor and Hondzo*, 2008; *Harvey et al.*, 2013], and degradation of organic contaminants [e.g., *Conant et al.*, 2004]. Furthermore, environmentally relevant sorption and precipitation reactions take place in this layer [*Fuller and Harvey*, 2000], affecting the transport and reactivity of trace metals and nutrients [*Rodriguez-Freire et al.*, 2016]. The benthic biolayer is described as an extension of the surficial benthic biofilm deeper into the hyporheic zone (Figure 1a) and its

© 2017. American Geophysical Union. All Rights Reserved.

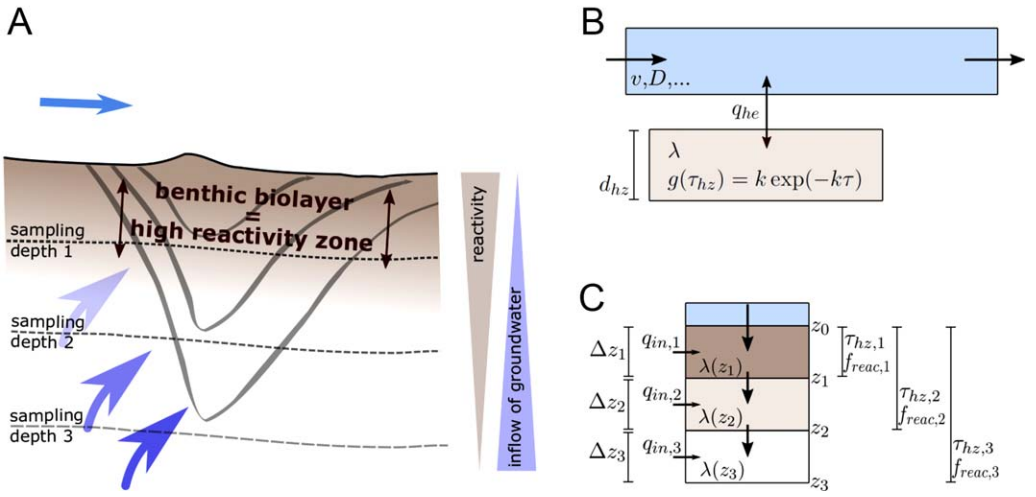

Figure 1. (a) Illustration of hyporheic exchange and reactivity: hypothetical hyporheic flow paths and the gradient of reactivity in the subsurface indicating the extent of the benthic biolayer; (b) conceptual representation of hyporheic processes by the transient storage model (Model I), which captures in-stream processes (advective velocity v, dispersion D, etc.) and assumes one single hyporheic storage zone with an exponential distribution of hyporheic residence times τ and linear reactivity in the hyporheic zone (transformation constant λ), but does not capture individual flow paths into and out of the hyporheic zone; (c) conceptual representation of processes captured by the subsurface model (Model II), which compartmentalizes the hyporheic zone into individual layers with distinct reactivity (transformation constants λ) and different contributions of groundwater (fluxes q_{in}), but only represents the vertical component of the downwelling flow paths, thus quantifying water ages at the different depths (i.e., τ_{hz}) and reaction ratios (f_{reac}), but making no assumptions about how, when and where the water returns to the stream. All parameters are explained in detail in section 2.

depth varies depending on flow and transport, grain-size, redox chemistry, carbon and nutrient sources, and biogeochemical reactions. Little is known about the vertical extent of biolayers, although several field studies identified a layer of some centimeters within a granular and permeable sediment matrix where hyporheic exchange occurred to a depth of tens of centimeters (see discussions in *Arnon et al.* [2013] and *Harvey et al.* [2013]). The potential importance of the benthic biolayer to reactive processing in river networks was highlighted in the recent modeling work by *Gomez-Velez et al.* [2015], who estimated that denitrification occurring beneath small-stream bedforms was of far greater importance to processing of nitrate in the upper Mississippi river than denitrification occurring in longer and deeper hyporheic flow paths through bars and meanders.

Hyporheic processes can be assessed on multiple spatiotemporal scales, from measurements and modeling approaches on the pore-scale (i.e., with microelectrodes) [*O'Connor et al.*, 2012] via studies on the centimeter-scale (e.g., with mini-piezometers) [*Harvey and Fuller*, 1998; *Briggs et al.*, 2013], to tracer-based investigations integrating the effects of hyporheic processes over longer stream reaches [*González-Pinzón et al.*, 2015], or even whole catchments [*Böhlke et al.*, 2009]. While in-stream tracer tests are a well-established tool for characterizing processes on the reach scale, there are fewer examples of measuring small-scale chemical gradients and reaction rates within the benthic biolayer [e.g., *O'Connor and Harvey*, 2008].

In recent years, coinjecting the reactive tracer resazurin into streams along with a conservative solute has become an established method to better understand the interactions between water and sediments [e.g., *Haggerty et al.*, 2008, 2009; *Argerich et al.*, 2011; *González-Pinzón et al.*, 2012; *Lemke et al.*, 2013a]. Resazurin is a fluorescent phenoxazine dye, which is reduced to fluorescent resorufin through reactions within living cells, among others, by aerobic microorganisms [*O'Brien et al.*, 2000; *González-Pinzón et al.*, 2012]. As the abundance of microorganisms in streams is the highest within the hyporheic zone [e.g., *Hendricks*, 1993; *Fischer et al.*, 1996], the transformation of resazurin can be utilized as an indicator of exchange processes with metabolically active transient storage zones [*Haggerty et al.*, 2008, 2009]. Resazurin could therefore potentially serve as a tracer of exchange and reaction within the benthic biolayer.

While results from localized sampling of the hyporheic zone are rarely representative of the general conditions of a greater stream section, reach-scale tracer investigations mainly provide information on bulk

reactivity without localizing where within the streambed the reaction is the greatest [*Harvey et al*., 2013]. Therefore, combining in-stream reactive tracer tests with sampling performed simultaneously in the hyporheic zone potentially improves the interpretation of the data, but there are only few studies in which reach-scale investigations of reactive transport in streams are coupled to detailed investigations within the hyporheic zone [e.g., *Harvey and Fuller*, 1998; *Böhlke et al*., 2009; *Harvey et al*., 2012, 2013]. This holds especially for the resazurin-resorufin tracer [*González-Pinzón et al*., 2015].

Figures 1b and 1c illustrate those aspects of hyporheic exchange and reactivity captured by in-stream and detailed subsurface sampling according to the modeling approaches used here. The measured in-stream concentrations reflect the part of the hyporheic processes that affect the stream itself, but from these data it is impossible to derive the spatial distribution of reactivity within the hyporheic zone. Hence, the transient storage model used to interpret these data (Figure 1b) yields effective bulk estimates of reactivity of an assumed single, fully mixed storage zone. While models with multiple storage zones exist [e.g., *Marion et al*., 2008; *Kerr et al*., 2013], localization of these zones is impossible from in-stream data only. The concentrations measured within depth profiles of the streambed, in contrast to in-stream data, reflect the internal structure of the hyporheic zone. The proposed subsurface model (Figure 1c) considers vertical advective-dispersive-reactive transport and compartmentalizes the hyporheic zone into individual layers, thereby identifying layers of higher and lower reactivity in the subsurface. These layers differ conceptually from the multiple storage zones mentioned above, as we incorporate transport from one layer to the next, whereas the multiple storage zones only interact with the stream. Conversely, the vertical profiles do not provide information on hyporheic water returning to the stream, and thus it is difficult to deduce the large-scale influence of the internal organization of the hyporheic zone on the stream water. These two pieces of information are complementary and cannot be interchanged.

The aim of the present study was to quantify the contribution of the shallow subsurface to reactive turnover within the hyporheic zone and thus quantify the extent of the benthic biolayer. For this, we injected resazurin into a third-order stream (Difficult Run, Virginia, USA) and simultaneously measured the concentrations of resazurin and resorufin in the surface water at several distances from the injection point and in vertical profiles at shallow depths in the streambed, thereby identifying layers of higher and lower reactivity by comparing the full depth of hyporheic exchange with the depth over which reactive turnover effectively takes place. We analyzed in-stream results with the traditional transient-storage model based on the advection-dispersion equation (similar to *Bencala and Walters* [1983]; *Runkel* [1998], but including turnover of the reactive tracer; cf. *Lemke et al*. [2013a]) and the vertical depth profiles with an advection-dispersion-reaction type of model. We show that the two observation methods and models provide information about different aspects of the same system and illustrate how this leads to very different predictions of hyporheic depth and time scales of hyporheic exchange.

2. Methods

2.1. Site Description

Our tracer experiment was conducted within the headwaters of Difficult Run (catchment area of 14 km^2) in Virginia, USA, in a 150 m long study reach with variable topography including riffles, runs, and pools. The geology in the region is dominated by gneiss and schist bedrock. The streambed sediments are mainly composed of coarse sand, gravel, and pebbles interspersed with a relatively fine silty matrix with a porosity of 0.39 (estimated based on 31 shallow core samples taken along the reach). The study reach has an average bed slope of 6‰ and an average channel width and water depth equal to 5.57 and 0.2 m, respectively. On the morning of the injection (13 July 2011), the discharge was 0.027 m^3/s (USGS stream gage 01645704). The conservative tracer bromide and reactive tracer resazurin were coinjected with a constant rate over a period of 5 h. A total of 7850 g of bromide and 187 g of resazurin (codissolved in 175 L of stream water) were injected during the experiment. The in-stream plateau concentrations of the conservative tracer reached 16.5 mg/L.

About 1 h after the injection ended, a thunderstorm caused a spate (peak $Q \cong 0.88$ m^3/s) and raised the stream water level by 26 cm. All tracer measurements were terminated 1 h 45 min after the injection stopped because sampling equipment could not withstand the spate and had to be removed.

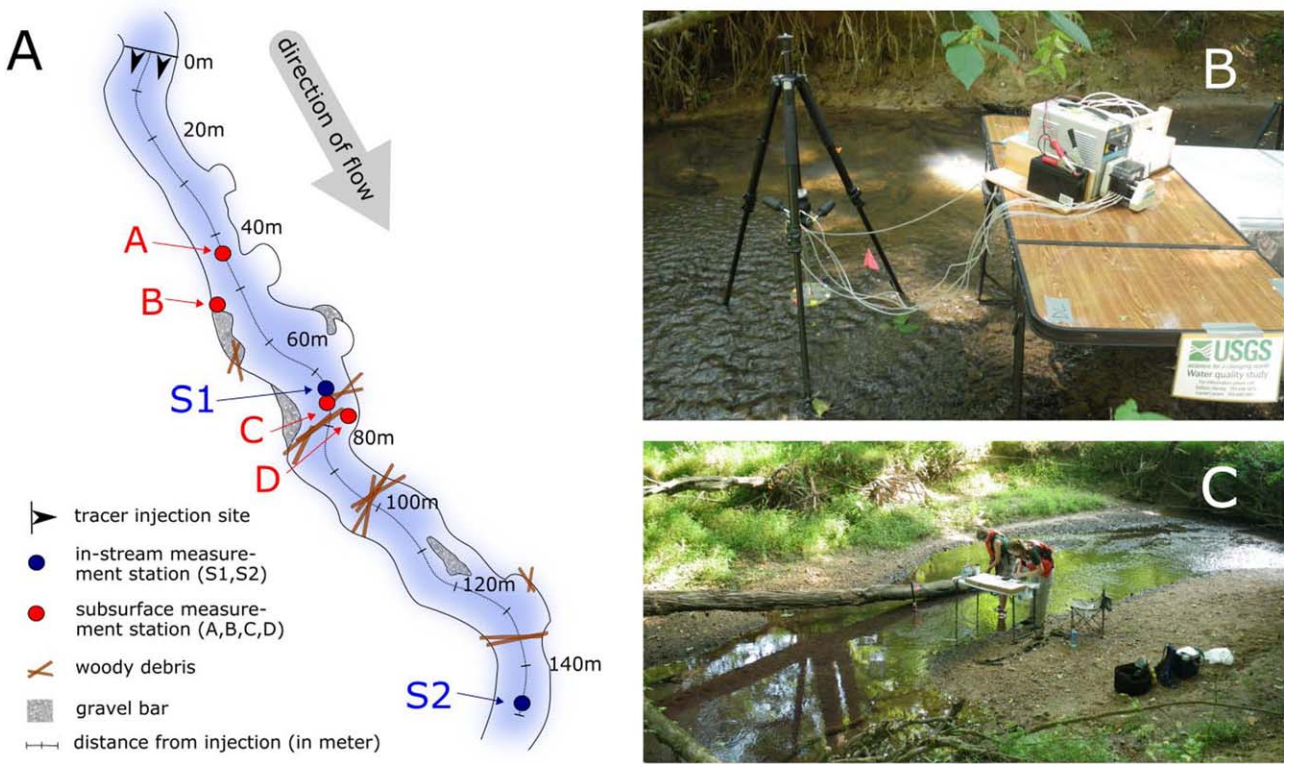

Figure 2. (a) Map of the study area, showing the locations of the injection as well as the different in-stream and subsurface measurement points. (b) Picture of the MINIPOINT setup: MINIPOINT sampler with tripod, peristaltic pump. (c) General overview of the stream with in-stream sampling point.

2.2. Sampling and Analysis of Field Data

The breakthrough curves (BTCs) of bromide, resazurin, and resorufin were recorded within the stream over the course of the experiment at two different locations, from here on referred to as S1 and S2. S1 was located 74.7 and S2 148.7 m downstream of the injection site (see Figure 2a). In-stream samples were collected with a peristaltic pump into syringe barrels fitted with polysulfone filters (0.2 μm pore size, 30 mm diameter, sealed disposable type) from which sample water was filtered directly into 22 mL sample bottles made of high-density polyethylene and capped with Polyseal tops. Bottles were stored cool out of direct sunlight. Sampling intervals ranged from 0.5 min during the rising and falling limbs of the breakthrough to 30 min under tracer-plateau conditions when tracer concentrations were relatively stable. Additionally, water samples from the shallow subsurface were simultaneously collected from several depths using a USGS MINIPOINT sampler as described by *Harvey and Fuller* [1998] and *Harvey et al*. [2013]. In total, four MINIPOINT samplers (labeled as A, B, C, and D in Figure 2a) were emplaced at distances of 44.0, 51.5, 77.4 and 79.7 m, respectively, from the injection site. MINIPOINT sampler A was emplaced in a 5 m long riffle, B in a lateral cavity of the stream near the right bank (oriented downstream), C in a channel thalweg between riffles, and D in a large pool near the left bank of the stream. MINIPOINT sampler B was omitted from the results because very little tracer entered the lateral cavity, leading to insufficient precision of the subsurface tracer concentrations to estimate reactive-transport parameters.

Each MINIPOINT sampler collected water samples of small volume (15 mL) at low rates (1.5 mL/min) from 1 cm slotted ports in 1/8 inch (nominal outside diameter) stainless-steel tubes situated approximately 2 cm above the bed and from four additional ports situated between 0.5 and 9 cm below the stream bed. Water samples were collected approximately every 10 min during the rising and falling limb of the tracer breakthrough in the stream, with longer intervals (30–40 min) between sampling during the period of stable conditions. The water samples were pumped through Masterflex size 13 tygon tubing and filtered inline by pumping through 0.2 μm pore size, 25 mm, *Pall* polysulfone filters and then directly into 22 mL high-density polyethylene (HDPE) scintillation vials supplied with HDPE polyseal caps.

Bromide concentrations of all samples were measured by ion chromatography (Dionex DX-120) with a Dionex AS-14 analytical column, AG-14 guard column, conductivity detector, 50 μL sample loop, and 3.4 mM sodium carbonate/L mM sodium bicarbonate eluent. Using this system, the detection limit of bromide is 15 μg/L. Concentrations of resazurin and resorufin were determined by fluorescence analysis with a Cary Eclipse Fluorescence Spectrophotometer (Agilent Technologies) at excitation/emission wavelengths of 602 nm/632 nm (resazurin) and 571 nm/584 nm (resorufin). The limit of quantification (LOQ) for resorufin is $<$0.05 nmol/L and $<$0.62 nmol/L for resazurin in DI water. Due to the overlap in spectra of the two compounds and the stronger fluorescence of resorufin, the LOQ of resazurin decreases if resorufin is present. The LOQ for both compounds is approximately five times greater in natural water than in DI water. All samples were kept cold in the dark until analysis, which was completed within a week of sampling. Due to a possible interference between the fluorescent signals of resazurin/resorufin and a fluorescent particle tracer that was coinjected with the dissolved tracers, the effect of the particles on the detection of resazurin was analyzed in the laboratory. The interference was found to be negligible at particle plateau concentrations because the particles (nominal 4 μm diameter) were nearly completely removed by filtering. In spite of filtering, however, some surface-water samples had high particle concentrations during periods of rapid sampling after the tracer injection stopped. For the subset of samples that had become contaminated with particles, the laboratory analysis revealed that the peak wavelength of the fluorescence spectrum of particles coincided with the analysis wavelengths of resorufin. For those samples, the resorufin concentrations were overestimated and the resazurin concentrations were slightly underestimated. The latter was caused by the interdependence of resazurin and resorufin concentrations in the matrix calculation used to determine concentrations from fluorescence signals [see *Lemke et al*., 2013b]. Therefore, extreme outliers of the calculated resazurin and resorufin concentrations fitting this pattern were removed. The number of outliers at any location and depth did not exceed 10% of the data points of the respective data set.

2.3. Modeling

In this section, we outline two models fitted to the data, Model I for reach-scale interpretation of surface water transport and subsurface exchange between the measurement stations S1 and S2, and Model II describing subsurface transport as a function of depth in the streambed using the MINIPOINT data sets A, C, and D. Both models were based on the one-dimensional advection-dispersion-reaction equation. Model I was a version of the transient storage model, which has often been applied to simulate conservative solute transport in streams [e.g., *Bencala and Walters*, 1983; *Zaramella et al*., 2003; *Runkel*, 2007]. It accounts for a single transient storage, ideally representing the hyporheic zone, which undergoes linear exchange with the stream [*Runkel*, 1998]. We amended the model with reaction terms for resazurin and resorufin that are only active in the hyporheic zone [see *Haggerty et al*., 2009; *Lemke et al*., 2013a, etc.]. The model cannot differentiate between a near surface benthic biolayer and the deeper hyporheic zone, because the model does not provide any spatial resolution of the hyporheic zone, but rather assumes a single, well-mixed hyporheic storage zone. Therefore, the reaction parameters are effective bulk parameters of the entire hyporheic zone.

Model II for the subsurface assumes one-dimensional, vertical transport underneath the stream, as it is commonly done for shallow hyporheic flow [e.g., *Harvey and Fuller*, 1998; *Bhaskar et al*., 2012]. Both models account for the compound-specific behavior of resazurin in the hyporheic zone including transformation of resazurin to resorufin in the hyporheic zone as well as retardation due to equilibrium sorption of resazurin and resorufin therein.

For the parameter estimation, we used the *DiffeRential Evolution Adaptive Metropolis* algorithm (DREAM(ZS)) [*Vrugt et al*., 2009; *Laloy and Vrugt*, 2012], a Markov chain Monte Carlo algorithm which provides full distributions of parameters conditioned on the measurements, and, thus, determined correlated parameter uncertainties. We constrained the parameters to be nonnegative and for the case of the retardation coefficients the lower limit was constrained to be 1. In a first optimization step, the parameters related to bromide and resazurin were jointly estimated. In a second optimization step, the previously determined parameters were sampled from their obtained distributions and parameters specific to resorufin only were estimated. This approach was chosen to decrease the ambiguity of the estimated parameter sets. To reduce autocorrelation between successively stored chain samples, we applied a thinning rate of 10 to the sets of estimated parameters. The goodness of the fits was determined by calculating the sum of squared residuals

normalized by the squared theoretical plateau concentration of each tracer. We refer to this quantity as normalized residual sum of squares, *nRSS* [-].

The analysis of in-stream data relies on comparing the change in tracer concentrations between sites S1 and S2 with the travel distance x [L] between these locations. The subsurface data were analyzed layer-wise, i.e., the concentrations recorded at the shallower depth were used as input signals, and those at the greater depth as output signals (e.g., layer 1 ranged from depth 0 to depth 1, layer 2 from depth 1 to depth 2, and so forth). In total, four depth layers were represented per location. In the analysis of the subsurface data, the travel distance Δz_k [L] is considered to be the vertical distance $d_{hz,k}$ [L] between the upper and lower MINIPOINT port of layer k (see Figure 1c). All concentrations reported from here on are corrected for background concentrations of the tracer compounds.

Calculating reaction rate coefficients from steady state concentrations by the approaches presented by *Harvey and Fuller* [1998], *Harvey et al*. [2013], and *González-Pinzón and Haggerty* [2013] was not feasible at most sampling depths because plateau concentrations were not reached at all subsurface measurement points. Also, dilution was significant and the sampling ended too early to capture the entire tail of the BTCs at these points. Instead, we fitted models to the time series of measured concentrations to obtain smooth simulated BTCs with complete tails and based our analysis on the moments and metrics of these simulated BTCs. We used temporal moment analysis, a common tool used to estimate central tendencies and model parameters in transport problems [e.g., *Kucera*, 1965; *Sardin et al*., 1991; *Harvey and Gorelick*, 1995], and details on their derivation can be found in the supporting information (Text S3).

Based on these model outcomes, we determined the depth and reactivity of the hyporheic zone as well as hyporheic residence times. Uncertainties of all metrics were calculated from an ensemble approach with 3125 realizations, by drawing parameters from their respective (thinned) distributions. Further details and derivations can be found in the supporting information.

2.3.1. Model I: In-Stream Transport With Hyporheic Exchange

Model I described the one-dimensional in-stream transport of the tracer compounds undergoing hyporheic exchange and hyporheic reactions (Figure 1b). Here, the hyporheic zone was considered a well-mixed transient-storage zone, characterized by a single concentration value for each compound at a given in-stream coordinate and time. As reach-based dilution was found to be insignificant between S1 and S2 (i.e., the conservative mass remained unchanged, see X^{br}_{reach} in Table 3), it was not included in the equations. The coupled governing equations were:

$$\frac{\partial c_i}{\partial t}+\frac{A_s}{A}R_i\frac{\partial c_{hz,i}}{\partial t}+v\frac{\partial c_i}{\partial x}-D\frac{\partial^2 c_i}{\partial x^2}=\frac{A_s}{A}r_{hz,i} \tag{1}$$

$$R_i\frac{\partial c_{hz,i}}{\partial t}=k\left(c_i-c_{hz,i}\right)+r_{hz,i} \tag{2}$$

subject to the following initial and boundary conditions:

$$c_i(x,t=0)=c_{hz,i}(x,t=0)=0\ \ \forall x \tag{3}$$

$$c_i(x=0,t)=c_{ini,i}(t);\ \ \lim_{x\to\infty}\frac{\partial^j c_i}{\partial x^j}=0\ \ \forall j\in\mathbb{N}_0. \tag{4}$$

in which c_i [ML^{-3}] denotes the in-stream concentration of compound i (0: bromide, 1: resazurin, 2: resorufin) and $c_{hz,i}$ [ML^{-3}] the corresponding concentration in the hyporheic zone; x [L] is the distance between S1 and S2; t [T] is time; the advective in-stream velocity is given by v [LT^{-1}]; D [L^2T^{-1}] is the longitudinal dispersion coefficient in the stream; $\frac{A_s}{A}$ [-] represents the ratio of the cross-sectional area of the storage zone A_s [L^2] to that of the stream A [L^2]; k [T^{-1}] is the first-order mass transfer rate coefficient between the stream and the transient storage zone. Our reference volume of the mass-transfer coefficient was that of the transient storage zone, whereas in other works [e.g., *Bencala and Walters*, 1983] the reference volume typically is that of the stream. Conversion implies that our coefficient k equals $\frac{A}{A_s}\alpha$ in *Bencala and Walters* [1983]. Furthermore, R_i [-] represents the retardation factor of compound i in the hyporheic zone, assuming linear sorption at local equilibrium; and $r_{hz,i}$ [$ML^{-3}T^{-1}$] is the reaction rate of compound i in the hyporheic zone. Bromide is considered an ideal tracer that neither sorbs nor undergoes transformations, therefore

$$R_0 = 1 \text{ and } r_{hz,0} = 0$$

whereas both resazurin and resorufin may sorb within the streambed ($R_1 \geq 1;\ R_2 \geq 1$). The chemical transformations of resazurin and resorufin within the hyporheic zone were assumed to follow linear reaction kinetics, resulting in the following reaction rates:

$$r_{hz,1} = -\lambda_1 c_{hz,1} \tag{5}$$

$$r_{hz,2} = \lambda_{12} c_{hz,1} - \lambda_2 c_{hz,2} \tag{6}$$

in which λ_1 [T^{-1}] is the rate coefficient of total resazurin transformation; λ_{12} [T^{-1}] is the rate coefficient describing the transformation of resazurin to resorufin; and λ_2 [T^{-1}] is the rate coefficient of resorufin transformation. The transformation of resazurin to resorufin cannot exceed the total transformation of resazurin, thus requiring $\lambda_{12} \leq \lambda_1$.

The equations above were analytically solved in the Laplace domain and back-transformed numerically [*Hollenbeck*, 1998]. A detailed derivation is given in the supporting information (Text S1).

As presented above, the transient-storage model assumed a perfectly mixed hyporheic zone. As there is no mixed reactor in the subsurface in reality, the physical interpretation of fitted parameters may thus be misleading. The set of equations presented above, however, can also be interpreted in a different way [e.g., *Wörman*, 1998; *Liao and Cirpka*, 2011; *Lemke et al*., 2013a]. Based on a mass balance of the solutes in the stream alone, with a partial retention of the solutes caused by hyporheic exchange, the stream-transport equations for bromide and resazurin (equations (1) and (2)) can be represented as:

$$\frac{\partial c_i}{\partial t} + v\frac{\partial c_i}{\partial x} - D\frac{\partial^2 c_i}{\partial x^2} = q_{he,reach}\left(\int_0^\infty \frac{k}{R_i}\exp\left(-\left(\frac{k}{R_i}+\lambda_i\right)\tau\right)c_i(t-\tau)d\tau - c_i(t)\right) \tag{7}$$

in which τ [T] is the time that a solute particle has spent in the hyporheic zone when coming back into the stream, and the hyporheic exchange rate $q_{he,reach}$ [T^{-1}] can be interpreted as the fraction of stream water undergoing hyporheic exchange per time [see *Liao and Cirpka*, 2011 for a more detailed explanation]. $q_{he,reach}$ in equation (7) was computed from the coefficients of the previous formulation of Model I by:

$$q_{he,reach} = \frac{A_s}{A}k. \tag{8}$$

Equations (1) and (7) merely differ in the conceptualization of the hyporheic zone. Whereas equation (1) conceptualizes a defined size of the storage zone, equation (7) parameterizes the effects of hyporheic exchange on in-stream transport by an exchange coefficient $q_{he,reach}$ and the distribution of hyporheic travel times, here assumed to follow the exponential distribution $k\exp(-k\tau)$. Sorption within the hyporheic zone is expressed as retardation of the travel-time distribution, and first-order transformation by the exponential loss of solute mass as function of time spent in the hyporheic zone.

2.3.2. Model II: Transport Within the Hyporheic Zone

For comparability, Model II for reactive transport in the subsurface was also based on the one-dimensional advection-dispersion-reaction equation, adapted for admixture of groundwater (Figure 1c):

$$\frac{\partial c_{0,hz}}{\partial t} + v_z\frac{\partial c_{0,hz}}{\partial z} - D_z\frac{\partial^2 c_{0,hz}}{\partial z^2} = q_{in}\left(c_{0,GW} - c_{0,hz}\right) \tag{9}$$

$$R_{1z}\frac{\partial c_{1,hz}}{\partial t} + v_z\frac{\partial c_{1,hz}}{\partial z} - D_z\frac{\partial^2 c_{1,hz}}{\partial z^2} = -\lambda_1 c_{1,hz} + q_{in}\left(c_{1,GW} - c_{1,hz}\right) \tag{10}$$

$$R_{2z}\frac{\partial c_{2,hz}}{\partial t} + v_z\frac{\partial c_{2,hz}}{\partial z} - D_z\frac{\partial^2 c_{2,hz}}{\partial z^2} = -\lambda_2 c_{2,hz} + \lambda_{12} c_{1,hz} + q_{in}\left(c_{2,GW} - c_{2,hz}\right) \tag{11}$$

in which z [L] denotes the spatial coordinate along the hyporheic flow path, simplified as depth; q_{in} [T^{-1}] is a rate coefficient accounting for mixing with groundwater, which can be interpreted as the groundwater discharge added to the river-borne water per volume of pore space. $c_{i,GW}$ [ML^{-3}] is the concentration of compound i in groundwater—note that in the present application $c_{i,GW} = 0$ for all compounds, because the admixed groundwater does not contain any tracer compound added into the stream. The net effect of mixing with groundwater is therefore dilution, which is mathematically identical to first-order transformation

with the rate coefficient q_{in}. In reality, mixing with groundwater is affected by complicated three-dimensional flow fields that cannot be resolved in a 1-D model considering only vertical transport. Thus, in our model, groundwater dilution is treated as lateral inflow, affecting concentrations at every depth section of the hyporheic zone and not just the lowest layer. This dilution term acts to the same extent on the conservative compound bromide as on the reactive compound and its product, whereas the effects of reaction of resazurin and resorufin (i.e., λ_1 and λ_2, respectively) are exclusive to the non-conservative compounds. All other terms are as previously defined for Model I, but for vertical subsurface transport. Because z is a depth coordinate, the transport parameters v_z and D_z should be referred to as apparent parameters of vertical transport.

The equations of hyporheic transport were solved between two consecutive layers (i.e., shallower BTCs become fixed-concentration upstream boundary conditions). To solve these equations, we assumed a semi-infinite domain and solved the system of equations analytically in the Laplace domain, followed by numerical back-transformation into the time domain. A detailed derivation of the above equations is given in the supporting information (Text S2). All parameters are estimated as function of depth z, meaning that they were allowed to differ between the different depth compartments. A depth compartment is defined here as the depth section between two consecutive MINIPOINT ports.

Model II only simulates the water entering the hyporheic zone and makes no assumptions about the fate of the water remaining in the channel. However, the exchange rate q_{he} [T^{-1}] between stream and hyporheic zone was evaluated from the topmost layer, analogous to the one obtained from the reach-scale approach (equation (8)):

$$q_{he} = \frac{v_z}{\theta w_{hz}} \tag{12}$$

in which θ [-] denotes the porosity of the streambed, and w_{hz} [L] is the width of the hyporheic zone (approximated by the measured active channel width).

2.4. Comparison of Surface and Subsurface Results

A direct interpretation of model parameters is typically regarded with skepticism, because assessing the validity of the obtained parameters is not straightforward, particularly in light of noisy data and missing tracer tails in conjunction with BTCs not reaching steady state (plateau) values. As a result it is difficult to estimate tracer recovery and the appropriate hyporheic residence time directly from the data. The selection of the residence time distribution, however, influences the estimated model parameters. To improve our interpretation, we instead used the model to generate smooth, complete BTCs—the validity of which is easily assessed by comparing the measured and simulated concentrations. We then based our interpretation on temporal moments of these fitted BTCs or, to be more explicit, on BTCs that would be obtained if the stream signal was a perfect Dirac delta pulse. We reasoned that by fitting a model, the truncated BTCs could be extrapolated in a manner that was consistent with the observed data. The measured part of the BTC did not need to approach the base value again, but it did need to include a peak and at least the beginning of the falling limb, in order to obtain reliable model parameters and temporal moments. Of course, if the true tracer BTCs exhibited a contribution with a rapid drop and a very elongated tail with low values we would have missed that, but, very likely, we would have missed it also with extended sampling as low values tend to disappear in the noise of base line, which can lead to errors in tracer recovery.

2.4.1. Analysis of Tracer Recovery

Tracer recovery in the stream was evaluated from ratios of plateau concentrations $c_{plateau}$ at the upstream and downstream locations, because stable plateau concentrations were reached in the stream at both measurement locations:

$$X_{reach} = \frac{c_{plateau}(\mathrm{S2})}{c_{plateau}(\mathrm{S1})}. \tag{13}$$

For subsurface data, a decrease in reactive tracer concentrations with depth can be caused by both dilution (through mixing of river-borne water with groundwater) and transformation, whereas the conservative tracer is only affected by dilution. Dilution, reaction, and dispersion not only influence concentrations, but also affect the propagation velocity of concentration fronts, termed celerity. Thus, the celerity v_* is usually larger

than the advective velocity v, because it accounts for the effects of dilution and transformation. For the conservative tracer bromide, the celerity v_{0*} [LT^{-1}] was calculated as follows:

$$v_{0*} = \sqrt{v^2 + 4Dq_{in}} \tag{14}$$

whereas for the reactive tracer resazurin, the celerity v_{1*} [LT^{-1}] became:

$$v_{1*} = \sqrt{v^2 + 4D(q_{in} + \lambda_1)}. \tag{15}$$

A derivation of equations (14) and (15) is given in the supporting information (Text S3).

We identified the fraction of river-borne water in the hyporheic zone at depth z as the recovery $X_{rec}^{br}(z)$ [-] of the conservative tracer. It is related to the transport coefficients of the subsurface-transport model by:

$$X_{rec}^{br}(z) = \exp\left(-\int_0^z \frac{v_{0*} - v}{2D}\, d\zeta\right) = \exp\left(-\int_0^z \frac{2q_{in}}{v + \sqrt{v^2 + 4Dq_{in}}}\, d\zeta\right) \tag{16}$$

which can be derived from analyzing the zeroth temporal-moment of the conservative tracer (see supporting information Text S3). The integral with the variable of integration ζ in equation (16) and in following expressions was determined from fitted constant transport parameters for each layer. In steady state transport, the recovery $X_{rec}^{br}(z)$ would be the concentration of the conservative tracer at depth z divided by the concentration in the river.

The recovery of the conservative tracer in the subsurface profile was used to determine an equivalent depth $\tilde{d}_{hz}$ [L] of the hyporheic zone at the different MINIPOINT sampler locations. For this purpose, values of the tracer recovery $X_{rec}^{br}(z)$ at sampling depths were exponentially interpolated layer-wise and also exponentially extrapolated. Then, the equivalent depth $\tilde{d}_{hz}$ [L] of the hyporheic zone is the depth-integral of the recovery profile:

$$\tilde{d}_{hz} = \int_{z=0}^{\infty} X_{rec}^{br}(z)\, dz. \tag{17}$$

This equivalent depth quantifies the theoretical extent of the hyporheic zone if it contained only stream water. It is necessary to quantify the hyporheic depth in this way instead of using other definitions (i.e., $\geq$10% surface water recovery, as defined by *Triska et al.* [1989]) to obtain comparability to the size of the transient-storage zone assumed by the in-stream-transport model (i.e., A_s), because the transient-storage model does not account for mixing with groundwater within the transient-storage zone, but assumes that the storage zone only contains river-borne water.

We compared the equivalent depth d_{hz} to the apparent depth of the hyporheic zone $\tilde{d}_{hz,reach}$ [L] calculated from the relative hyporheic storage area of the reach-scale transient storage Model I:

$$\tilde{d}_{hz,reach} = \frac{A_s}{A}\, A_{meas}\, \frac{1}{w_{hz}\theta} \tag{18}$$

In this, the measured cross-sectional area of the stream, A_{meas} [L^2], is multiplied by the relative storage zone size to estimate the full hyporheic zone depth in sediment.

While the analysis of the bromide profiles in the subsurface provided information on mixing with groundwater and the extent of the hyporheic zone, the depth profiles of the reactive tracer gave information about subsurface reactivity. We directly assessed the reactivity using an estimated rate coefficient λ_{Raz} [T^{-1}] describing total resazurin transformation. We also computed the recovery $X_{rec}^{raz}(z)$ [-] of resazurin as function of depth, which can be interpreted as the steady-state plateau concentration of resazurin at depth z normalized by the river concentration if the latter was constant. To do so, we repeat the operation of equation (15) using the celerity v_{1*} of resazurin (equation (14)) rather than the one of bromide, v_{0*}:

$$X_{rec}^{raz}(z) = \exp\left(-\int_0^z \frac{v_{1*} - v}{2D}\, d\zeta\right) = \exp\left(-\int_0^z \frac{2(q_{in} + \lambda_1)}{v + \sqrt{v^2 + 4D(q_{in} + \lambda_1)}}\, d\zeta\right). \tag{19}$$

We used the recoveries of the conservative and reactive tracers at paired observation depths to compute a reaction factor f_{reac} [-] that expressed the relative mass loss of the reactive tracer occurring over the depth difference Δz corrected for the effect of dilution:

$$f_{reac}(z+\Delta z)=1-\frac{X_{rec}^{raz}(z+\Delta z)}{X_{rec}^{raz}(z)}\cdot\frac{X_{rec}^{br}(z)}{X_{rec}^{br}(z+\Delta z)}. \quad (20)$$

In analogy to the equivalent depth $\tilde{d}_{hz}$ of the hyporheic zone, defined in equation (17), we computed a penetration depth $\tilde{d}_{raz}$ [L] of resazurin by considering the depth-integral of the resazurin recovery:

$$\tilde{d}_{raz}=\int_0^\infty X_{rec}^{raz}(z)dz. \quad (21)$$

$\tilde{d}_{raz}$ is a metric of the depth-distribution of resazurin and quantifies the reactive part of the hyporheic zone and therefore the part of the subsurface with particularly high metabolic activity. There is no equivalence in the transient-storage model for reach-scale transport, as it assumes that the hyporheic zone is perfectly mixed, implying that all constituents reach the same depth.

We compared the total normalized steady state mass of resazurin stored in the hyporheic zone to that of bromide (in which normalization is done with the in-stream concentration). Toward that end, we divided the penetration depth $\tilde{d}_{raz}$ of resazurin by the equivalent depth $\tilde{d}_{hz}$ of the hyporheic zone, resulting in a reaction factor f_{reac}^{tot} [-] for the entire hyporheic zone:

$$f_{reac}^{tot}=1-\frac{\tilde{d}_{raz}}{\tilde{d}_{hz}}. \quad (22)$$

In the reach-scale transient-storage model, the same ratio of masses in the hyporheic zone is the ratio of steady state concentrations in the well-mixed transient storage zone:

$$f_{reac,reach}^{tot}=1-\frac{k}{k+\lambda_{Raz}}=\frac{\lambda_{Raz}}{k+\lambda_{Raz}}. \quad (23)$$

To complete the analysis, for the reach-scale transport analysis we computed the recovery $X_{rec,reach}^{raz}(x)$ [-] of the reactive tracer in the stream using a derivation that considered the steady state solution of the transient-storage model:

$$X_{rec,reach}^{raz}(x)=\exp\left(-\frac{2\lambda_{eff}}{v+\sqrt{v^2+4D\lambda_{eff}}}\,x\right) \quad (24)$$

with the effective first-order transformation coefficient λ_{eff} [T^{-1}] for reach-scale transport:

$$\lambda_{eff}=\frac{A_s}{A}\cdot\frac{k\lambda_{Raz}}{k+\lambda_{Raz}}. \quad (25)$$

That approach was analogous to the calculation of tracer recovery we made for the subsurface. Details are given in the supporting information (Text S4).

2.4.2. Analysis of Hyporheic Water Ages

The mean hyporheic transport time was assessed for subsurface BTCs using an analysis of first temporal moments of the conservative tracer (see supporting information Text S3), which yielded the mean hyporheic water age $\tau(z)$ [T] as a function of depth:

$$\tau(z)=\int_0^z\frac{1}{v_{0^*}(\zeta)}d\zeta. \quad (26)$$

where $\tau(z)$ corresponded to the center of mass of a conservative-tracer BTC if the concentration in the river was a perfect pulse.

The mean age of the stream water in the entire hyporheic zone was estimated as the recovery-weighted average of $\tau(z)$:

$$\tilde{\tau}_{hz}=\frac{1}{\tilde{d}_{hz}}\int_0^\infty\tau(z)X_{rec}^{br}(z)\;dz. \quad (27)$$

We compare this value to the reach-scale apparent mean hyporheic water age $\tilde{\tau}_{hz,reach}$ [T] evaluated by the fitted transient-storage model, which was estimated as the inverse of the first-order exchange coefficient k [T^{-1}]:

$$\tilde{\tau}_{hz,reach} = \frac{1}{k}. \tag{28}$$

This residence time applies to the conservative and the reactive tracer, due to the assumption of a perfectly mixed single storage zone of the transient storage model. From the subsurface data, on the other hand, an apparent age $\tau_{raz}(z)$ [T] of the metabolically active resazurin can be calculated in analogy to equation (26):

$$\tau_{raz}(z) = \int_0^z \frac{R_1}{v_{1*}(\zeta)} d\zeta. \tag{29}$$

2.4.3. Analysis of Solute Spreading

We furthermore analyze the spreading of the solute time series, for both hyporheic and in-stream transport, which was calculated for the hyporheic zone as:

$$\sigma_\tau^2(z) = \int_0^z \frac{2D}{v_{0*}^3} d\zeta. \tag{30}$$

For the reach-scale approach, the mean in-stream arrival times were obtained from temporal moments of the BTCs using:

$$\tau_{reach} = \frac{\mu_1(t)}{\mu_0(t)} \tag{31}$$

with the zeroth temporal moment $\mu_0(t) = \int_0^\infty c(t)\ dt$ and the first temporal moment $\mu_1(t) = \int_0^\infty c\ t\ dt$. The travel time between the stations S1 and S2 was calculated as the difference between the arrival times and the spreading of the BTC (i.e., the variance of in-stream travel times) was calculated as follows:

$$\sigma_{\tau,reach}^2 = 2\left(\frac{D}{v^2}\left(\frac{A_s}{A}+1\right)^2 + \frac{A_s}{Ak}\right)\frac{x}{v}. \tag{32}$$

The square root of the equations (30) and (32) denote the standard deviations and thus define the range of arrival times and water ages, i.e., the solute spreading.

3. Results and Discussion

In this section we first present the stream characteristics and all of the in-stream results, then we focus on the outcomes from the analysis of the subsurface data, and we close with a comparison across scales. The characteristic parameters obtained from in-stream data were compared to subsurface parameters to analyze if in-stream tracer tests are able to provide good information on the depth of the hyporheic zone, hyporheic water ages, and the distribution and rates of reactivity in the hyporheic zone.

3.1. Stream Characteristics and In-Stream Results

The fit between simulated and measured in-stream concentrations (Figure 3) was generally good as indicated by the low magnitude of the normalized residual sum of squares $nRSS_{br}$ and $nRSS_{raz}$ (Table 1), and all obtained parameters lay in the expected ranges (i.e., similar to values obtained, e.g., by *Haggerty et al.* [2009]; *Lemke et al.* [2013a]; and *Liao et al.* [2013]). The quality of the fit of the tailing and thus the longer residence times were represented less accurately because sampling was stopped at the beginning of the spate. Although we acknowledge that previous data sets have shown that hyporheic residence time distributions may be better fitted with broader than exponential tailing, i.e., power-law or nonparametric residence time distributions [i.e., *Wörman et al.*, 2002; *Gooseff et al.*, 2003; *Liao and Cirpka*, 2011], our simple transient storage model with a single storage zone with an exponential residence time distribution was able to capture the main processes observed. Thus, the application of a more complex model would not have been justified for our data.

The full mass of bromide found at S1 was recovered at S2 and therefore dilution was insignificant along the reach. Also, the transformation of resazurin along the reach resulted in a recovery of only 88% of the mass found at S1 (see Table 1). Arrival times between bromide and resazurin did not differ greatly (see vertical lines in Figure 3) and the BTCs generally exhibited a low amount of solute spreading ($\sigma_\tau = 20.0 \pm 6.4$ min).

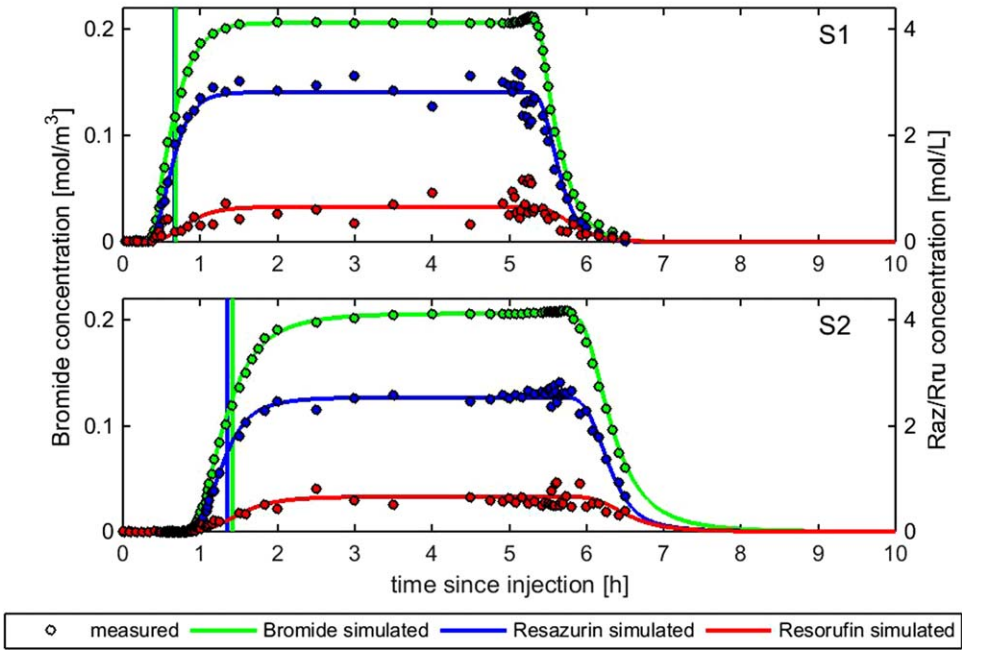

Figure 3. Measured and simulated in-stream tracer breakthroughs for Difficult Run at stream sites S1 and S2 with tracer concentrations. Points indicate measured concentrations and lines show simulated concentrations for the joint fit of bromide, resazurin, and resorufin. Vertical lines indicate the mean arrival times of the rising limbs for bromide and resazurin as calculated from moments of the BTCs.

The measured cross-sectional area of the channel, A_{meas}, was approximately 22% larger than the one calculated from streamflow discharge, distance, and travel time (Table 1). This indicates that tracer transport primarily occurred through a cross-sectional area that was smaller than the observable active channel, which already excluded areas of still or recirculating flow. The advective in-stream velocities v obtained from

Table 1. Results From the Stream Survey, Calculated Characteristics, Metrics, and Estimated Parameters for the In-Stream Sections From Model Fitting[a]

Parameter	Description	Units	Survey	Calculated	Model Fit
θ	Porosity		0.39		
x	Longitudinal distance between S1 and S2	(m)	74.0		
τ	Conservative in-stream travel time	(min)		44.6	
σ_τ	Conservative in-stream solute spreading	(min)		20.1 ± 6.4	
X^{br}_{reach}	Bromide recovery			1.00	
X^{raz}_{reach}	Resazurin recovery			0.88	
v	Advective velocity	(m/s)		2.8e-2[b]	3.3e-2 ± 1.6e-4
Q	Discharge	(m^3/s)		0.027	
w_{hz}	Width of the hyporheic zone	(m)	5.57[c]		
A_{meas}, A	Channel cross-sectional area	(m^2)	1.26[c]	0.98[d]	
D	Dispersion coefficient	(m^2/s)			5.3e-2 ± 2.2e-3
k	First-order mass transfer rate coefficient	(1/s)			6.0e-4 ± 2.5e-5
A_s/A	Relative size of the storage zone				1.9e-1 ± 4.9e.3
R_1	Retardation factor of resazurin				1.45 ± 8.7e-2
λ_1	Total transformation coefficient of resazurin	(1/s)			4.0e-4 ± 3.5e-5
R_2	Retardation factor of resorufin				1.36 ± 1.5e-1
λ_{12}	Resazurin to resorufin transformation coefficient	(1/s)			3.2e-4 ± 1.8e-5
λ_2	Transformation coefficient of resorufin	(1/s)			7.6e-4 ± 1.2e-4
$nRSS_{br}$	Normalized RSS for bromide				1.8e-2
$nRSS_{raz}$	Normalized RSS for resazurin				7.5e-2
$nRSS_{rru}$	Normalized RSS for resorufin				2.51

[a]The modal value of each obtained parameter distribution is given with its respective standard deviation.
[b]Calculated as $v = x/\tau$.
[c]Assumed to be identical to the measured width of the active channel ignoring zones with still or recirculating flow, denoted A_{meas} in equation (18).
[d]Calculated as $A = Q\tau/x$.

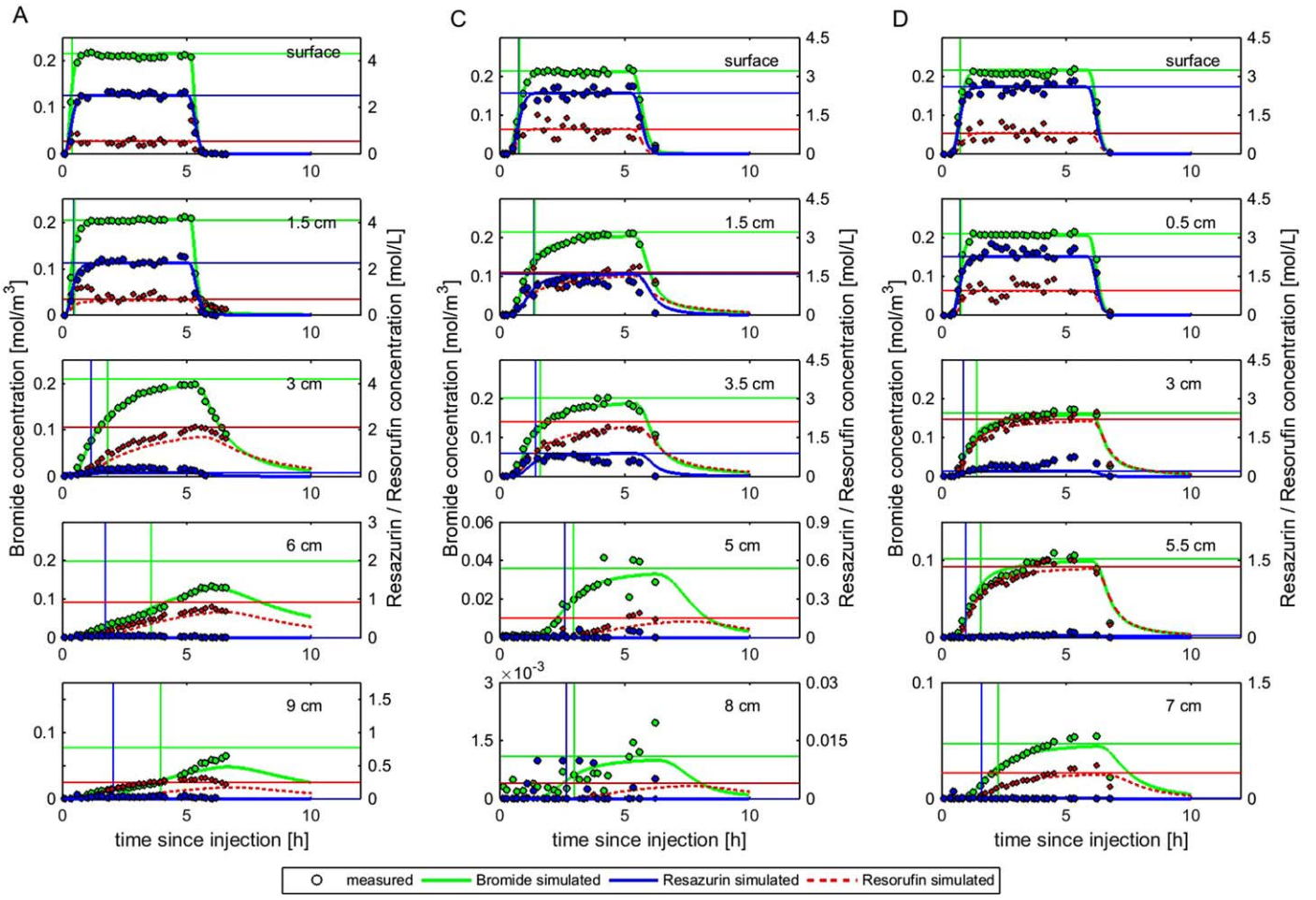

Figure 4. Measured (points) and fitted (lines) subsurface data for A (first column), C (second column) and D (third column). Horizontal lines indicate the theoretical plateau concentrations of the different compounds that would be obtained for a longer constant injection. The vertical lines indicate mean arrival times of the rising limb (obtained by subtracting half the injection duration from first temporal moments of the complete, simulated BTCs).

calculations and inverse modeling agree, and the uncertainties of all parameters related to the conservative and reactive tracer are relatively low. However, because the fitted rate coefficients of resazurin-to-resorufin transformation, λ_{12}, and transformation of resorufin, λ_2, are usually highly correlated (visible, i.e., in the correlation plot found in the supporting information Figures S1–S13), we chose to interpret hyporheic processes based on the transformation of resazurin alone. Resorufin measurements, on the other hand, are used to confirm the validity of the estimated parameters, by verifying that the measured resorufin curves can be reproduced with the estimated parameters.

3.2. Subsurface Results

The goodness of fit of the simulated BTCs decreased with depth in the hyporheic zone (Figure 4), but the generally good fits indicate the validity of the model used. All obtained parameters also lay in the expected ranges (see supporting information Table S1–S3). However, it should be noted here that the amount of missing part of the tails of the measured BTCs was greater with depth, and thus the quality of simulations decreased with depth and all calculations became less certain at greater depths.

The concentrations of bromide and resazurin decreased with depth, leading to lower theoretical plateau concentrations in deeper layers. Consequently, the concentrations of resorufin increased slightly until the third or fourth depths. Furthermore, the bromide BTCs became increasingly wider with depth to the point that plateau values could not be reached with the given injection time. Resazurin curves showed less spreading and tailing than bromide curves due to its transformation, which led to earlier mean arrival times for this compound than for bromide (see vertical lines in Figure 4). The spreading in the BTCs reveal an

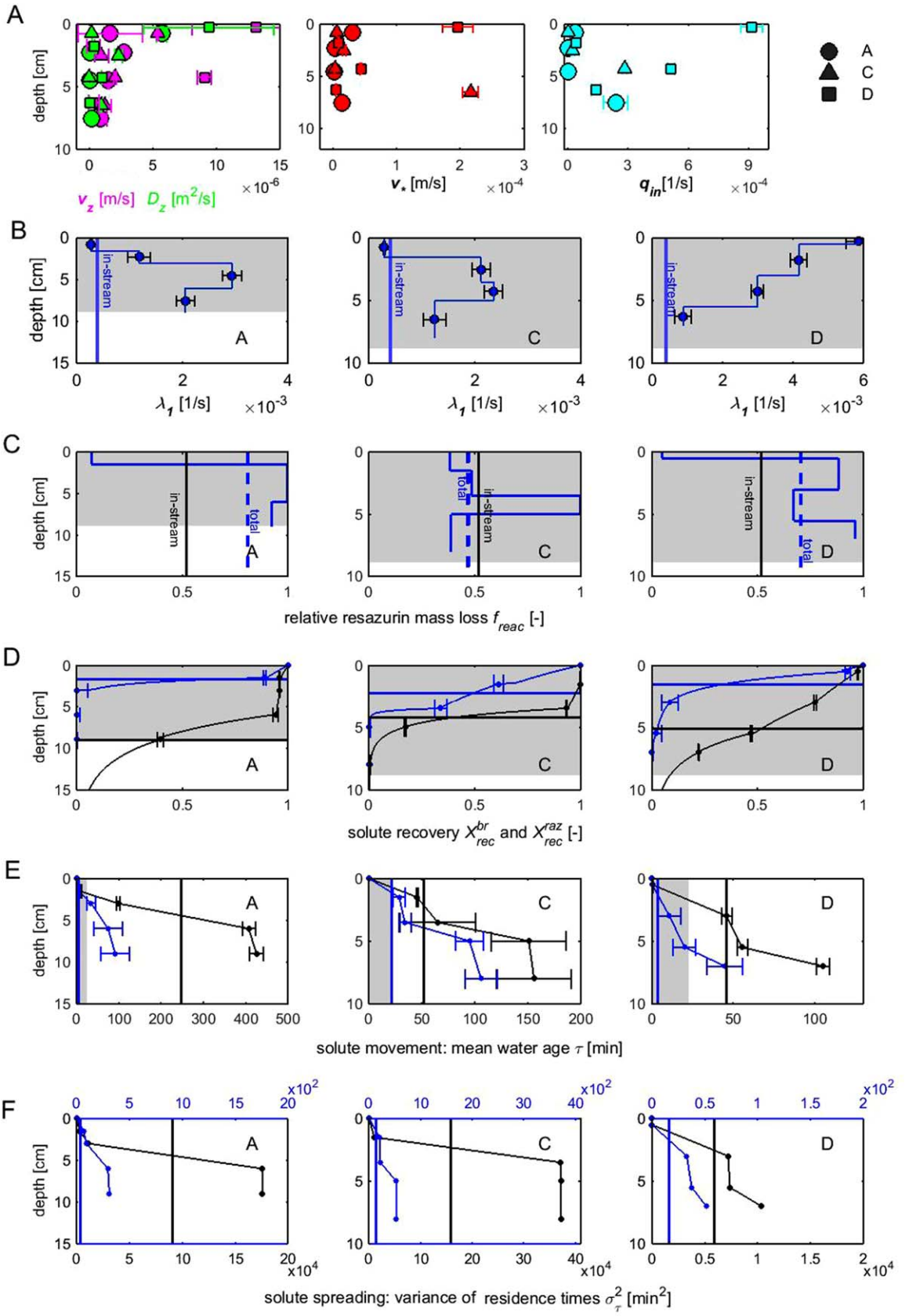
A
depth [cm]
v_z [m/s] D_z [m²/s]
$\times 10^{-6}$
v_* [m/s]
$\times 10^{-4}$
q_{in} [1/s]
$\times 10^{-4}$
A
C
D
B
in-stream
λ_1 [1/s]
$\times 10^{-3}$
C
in-stream
total
relative resazurin mass loss f_{reac} [-]
D
solute recovery X_{rec}^{br} and X_{rec}^{raz} [-]
E
solute movement: mean water age τ [min]
F
$\times 10^2$
$\times 10^4$
solute spreading: variance of residence times σ_τ^2 [min²]

Figure 5.

increasing distribution of mean water ages with depth (Figures 5e and 5f). For bromide, the decrease in concentration with depth was caused by mixing with tracer-free groundwater. For resazurin, the concentration decrease was even stronger, because it underwent transformation in addition to dilution. For resorufin, the concentration only decreased once the effect of dilution became stronger than production. The decrease in tracer concentrations with depth was described well by the calculated recovery rates (see Table 2 and Figure 5d).

The relative mass loss of resazurin f_{reac} due to transformation was generally higher in the upper layers of the hyporheic zone than in the lower layers (see Figure 5c), leading to a fast disappearance of the reactive tracer with depth (see Figure 5d). The relative reactive mass loss f_{reac} (Figure 5c) expresses which fraction of the reactive tracer is lost by reaction, corrected for dilution and regardless of the time needed, whereas the reaction rate constants λ_1 [T^{-1}] (Figure 5b) is a reaction rate [$ML^{-3}T^{-1}$] scaled by the concentration. The two profiles differ because the time increments in the various layers differs.

This is in agreement with the concept of the benthic biolayer, which postulates that higher transformation potential and more pronounced transformation processes occur not only at the stream-sediment interface, but throughout the upper, highly reactive layer of the hyporheic zone. This is consistent with studies recording strong metabolic activity and steep gradients in the upper layer of the sediment [e.g., *Arnon et al.*, 2013]. Interestingly, however, only at MINIPOINT sampler D did we observe the highest transformation coefficient λ_1 directly at the top of the streambed, whereas for both A and C the layer of highest reactivity was located at slightly greater depths. These differences between locations are likely higher than those between layers and may be due to different processes at the sampling locations. While D was positioned in a pool towards the bank of the stream, both A and C had been placed in the channel center. Possibly, the increased turbulence in the channel led to a disturbance of the upper sediment, whereas calmer conditions in the pool created favorable conditions for higher metabolic activity at the stream-sediment interface.

Figure 5a illustrates the decrease of the apparent velocity v_z and the apparent dispersion coefficient D_z with depth. Due to the model-implicit assumption of vertical flow paths, these values should not be confused with actual parameter values observed along the true (unknown) flow paths, which are reduced here to their vertical component. Nevertheless, they followed an expected decrease with depth. For the celerity v_{0*} this decreasing trend was less pronounced, due to the adjustment for increasing discharge q_{in}, which is also shown in the same figure.

For MINIPOINT profiles C and D, the tracer recovery X_{rec}^{br} at the deepest ports amounted to less than 20%, suggesting large influence of groundwater at great depths. Therefore, the sampled profiles span the whole range from stream water dominated to groundwater dominated BTCs, yielding informative metrics of transport and reactivity. In contrast, for the MINIPOINT profile A the subsurface sampling did not reach deep enough to get close to the depth where groundwater dominates. Instead, the recovery trend toward greater depths had to be approximated, yielding less informative results.

3.3. Comparison of the Results

So far, in-stream and subsurface results were discussed separately. Here we compare reach-scale and subsurface parameters which allows for an increased understanding of the different information gained from the two approaches.

The transformation rate coefficients λ_1 determined for the hyporheic zone by the reach-scale analysis were lower than those determined directly in the subsurface (Figure 5b), particularly at the shallower depths. This

Figure 5. (a) Depth-wise illustration of the estimated vertical parameters obtained from model fitting of the subsurface data for profiles A (circles), C (triangles), and D (squares) of apparent velocity v (m/s), celerity v_{0^*} (m/s) according to equation (14), apparent dispersion coefficient D (m^2/s) and discharge rate coefficient q_{in} (1/s); (b) first-order transformation coefficient λ_1 [T^{-1}] of resazurin; the vertical line represent the equivalent estimated reach-scale processing rate coefficient; (c) relative resazurin mass loss f_{reac} according to equation (20), total mass loss according to equation (22) (blue vertical line), and in-stream mass loss according to equation (23) (black vertical line); (d) calculated recovery rates for the conservative tracer X_{rec}^{br} according to equation (16) (black) and reactive tracer X_{rec}^{raz} according to equation (19) (blue) with the subsurface estimated hyporheic zone depth $\bar{d}_{hz}$ according to equation (17) (horizontal black line) and in-stream tracer estimated hyporheic zone depth $\bar{d}_{hz,reach}$ according to equation (18) (grey areas) and the reactive depth $\bar{d}_{raz}$ according to equation (21) (blue line); (e) mean water age τ as calculated for the conservative tracer according to equation (26) (black markers) and the reactive tracer according to equation (29) (blue markers). The average age for the location is given by the vertical black line, the patched area indicates the mean water age as calculated from the reach-scale fit according to equation (28) (13 min); (f) solute spreading σ_{tau}^2 with depth according to equation (30).

Table 2. Lengths of the Hyporheic Depth Layers Δz, Layer-Wise Calculated Mean Water Ages $\Delta\tau$, Cumulative Mean Water Age at the Bottom of the Given Layer, $\tau_{hz}(z_{bot})$, Layer-Wise Reaction Rates of Resazurin, f_{reac}, and Fractions of River-Borne Bromide and Resazurin Recovery at the Different Subsurface Depths, $X^{br}_{rec}(z_{bot})$ and $X^{raz}_{rec}(z_{bot})$

	A (Channel Center)				C (Channel Center)				D (Pool)			
	Sec 1	Sec 2	Sec 3	Sec 4	Sec 1	Sec 2	Sec 3	Sec 4	Sec 1	Sec 2	Sec 3	Sec 4
Δz (cm)	1.5	1.5	3	3	1.5	2	1.5	3	0.5	2.5	2.5	1.5
$\Delta\tau$ (min)	6.8 ± 4.5	91.3 ± 0.4	306.7 ± 15.4	14.0 ± 8.2	45.5 ± 0.8	13.4 ± 36.6	89.6 ± 2.7	2.2 ± 8.2	0.4 ± 0.3	45.5 ± 3.2	9.1 ± 0.4	47.5 ± 2.4
$\tau_{hz}(z_{bot})$(min)	6.8 ± 4.5	98.8 ± 4.4	406.9 ± 15.4	425.4 ± 16.6	45.5 ± 0.8	64.9 ± 35.7	151.2 ± 35.2	156.1 ± 35.3	0.4 ± 0.3	46.0 ± 3.2	55.5 ± 3.2	105.0 ± 4.0
f_{reac}	0.07 ± 5e-3	0.996 ± 6e-2	0.998 ± 5.4e-2	0.92 ± 5.4e-2	0.38 ± 2e-2	0.49 ± 3e-2	0.998 ± 6e-2	0.39 ± 4e-2	0.05 ± 1e-2	0.88 ± 5e-2	0.67 ± 4e-2	0.96 ± 6e-2
$X^{br}_{rec}(z_{bot})$	0.96 ± 2e-3	0.96 ± 2e-3	0.94 ± 1.4e-2	0.40 ± 1.4e-2	1.00 ± 2e-3	0.93 ±4e-3	0.17 ± 3e-2	0.01 ± 4e-4	0.97 ± 2e-3	0.77 ± 5e-3	0.47 ± 3e-3	0.22 ± 3e-3
$X^{raz}_{rec}(z_{bot})$	0.89 ± 6e-3	3.5e-3 ± 5e-2	4.7e-4 ± 1.4e-2	1.2e-4 ± 3.4e-3	0.61 ± 2e-2	0.34 ± 3e-3	2.7e-4 ± 8e-3	6.4e-6 ± 2e-4	0.93 ± 1e-2	0.08 ± 4e-2	0.02 ± 2e-2	2.1e-4 ± 6e-3

was similar for the total mass loss f^{tot}_{reac} (Table 3), i.e., while approximately 50% of the resazurin entering the hyporheic zone was lost according to the in-stream results, up to 80% mass loss was detected along the subsurface flow paths, leading to much lower resazurin concentrations at the deeper subsurface ports than measured by the in-stream analysis. These findings indicate that while the flux of water through the main channel at any given time is much higher than the one through the hyporheic zone, a shallow benthic layer with enhanced turnover controls most of the biochemical processing observed at the reach-scale.

From the three MINIPOINT profiles (A, C and D), we determined the extent of the hyporheic zone $\tilde{d}_{hz}$ according to equation (17) and found depths of 9.1, 4.3, and 5.1 cm, respectively (see Table 3). From the reach-scale modeling results, the hyporheic zone was estimated to be on average 8.8 cm deep. Due to the assumptions of the transient storage model, the extent of the reactive storage zone $\tilde{d}_{raz}$ is identical to the total storage zone size if estimated from in-stream results, because the model conceptualizes one single, fully mixed storage zone. However, the subsurface analysis clearly showed that the concentration of resazurin decreased much faster with depth than that of bromide, and the calculated extent of the reactive zone was only about one third of the total depth (approximately 2 cm, see Table 3). This is in agreement with the idea of a highly reactive benthic biolayer close to the streambed, where the majority of compound transformations take place. In our case, this benthic biolayer therefore extended to approximately 2 cm below the streambed, but the actual extent was location-dependent. This also explains why the apparent water ages of resazurin $\tilde{\tau}_{reac}$ are much smaller than those of the conservative tracer $\tilde{\tau}_{hz}$ (Table 3).

Conceptual differences between the two models can also explain why the values obtained for water ages differ greatly (see Table 3). While the in-stream model provides information on the hyporheic travel time distribution (i.e., the age of the water returning to the stream), the subsurface approach determines the hyporheic residence time distribution (i.e., the age of the water at a specific observation point within the hyporheic zone). The obtained quantities of the water ages therefore provide information on how long solute particles have stayed in the hyporheic zone when they return to the stream, or how long a solute particle has stayed in the hyporheic zone while it is still therein, but never both. Because most of the old solute particles found at the deepest ports of the MINIPOINT samplers probably never made it back to the stream (at least not within the timeframe of our experiment), the water age from the in-stream results was much lower than the ages obtained from the subsurface approach. Thus, the majority of the hyporheic exchange

Table 3. Calculated Mean Water Age in the Hyporheic Zone of the Conservative and Reactive Tracer, $\tilde{\tau}_{hz}$ and $\tilde{\tau}_{reac}$, Mean Hyporheic Zone Depths, $\tilde{d}_{hz}$ and $\tilde{d}_{raz}$, Fractions of Tracer loss, f^{tot}_{reac}, Highest Decay Coefficients of Resazurin Obtained for the Given Sampler, $\lambda_{1,max}$, and Hyporheic Exchange Rates at the Stream-Bed Interface, q_{he}[a]

	In-Stream	A	C	D
$\tilde{\tau}_{hz}$ (min)	21.9 ± 2.2	246.8 ± 15.7	51.8 ± 15.1	45.8 ± 2.6
$\tilde{\tau}_{reac}$ (min)	(21.9 ± 2.2)[a]	4.9 ± 7.1	21.2 ± 4.3	3.4 ± 4.4
$\tilde{d}_{hz}$ (cm)	8.8 ± 0.2	9.1 ±0.2	4.3 ± 0.01	5.1 ± 0.03
$\tilde{d}_{raz}$ (cm)	(8.8 ± 0.2)[a]	1.7 ± 0.1	2.2 ± 0.1	1.5 ± 0.2
f^{tot}_{reac}	0.52 ± 2.9e-2	0.81 ± 1.3e-2	0.47 ± 2.1e-2	0.71 ± 2.9e-2
$\lambda_{1,max}$ (1/s)	4.0e-4 ± 3.5e-5	2.9e-3 ± 1.7e-4	2.4e-3 ± 1.7e-4	5.9e-3 ± 3.5e-4
q_{he} (1/s)	1.1e-4 ± 8.9e-6	7.6e-7 ± 1.2e-6	2.5e-6± 4.0e-8	6.0e-6 ± 2.3e-6

[a]The in-stream model does not differentiate between total and reactive depth, but rather assumes a perfectly mixed hyporheic storage zone, for which reason a reactive depth cannot be calculated from this model.

likely happened across the top few centimeters of the streambed, which is also the biolayer portion of the hyporheic zone.

Contributions of the longer flow paths in the subsurface, on the other hand, were of small significance to the reach-scale mass balance. Even though the hyporheic zone is in reality made up of layers with water of different ages and concentrations, the theoretical transient storage model samples water from different ages with the same probability. For catchment-scale transport, it has been recognized that the outlet of a system selects water of different ages within the system in a nonuniform manner, explaining differences between residence and travel-time distributions [*Botter et al*., 2011; *Rinaldo et al*., 2015]. It should also be expected that streams select the age distribution of the hyporheic zone in a nonuniform way. However, the conceptual model of the hyporheic zone as a well-mixed reactor does not allow that.

The hyporheic exchange rates q_{he} differed greatly between in-stream and subsurface analysis, and also among the subsurface results (see Table 3). The difference between the in-stream and subsurface rates was mainly due to a conceptual difference of how hyporheic exchange is quantified. For the subsurface profiles, this exchange rate is related to the advective velocity only, whereas the in-stream approach implicitly lumps advective, dispersive effects, and effect of pressure gradients caused by surface water flow patterns.

In summary, neither in-stream nor subsurface analyses can provide a full picture of the relevant processes. Instead, each approach provides a snapshot of two different parts of the system (see also Figures 1b and 1c). The subsurface analysis revealed that biogeochemical reactions were concentrated in shallow biolayers and indicated how reaction rates decreased with depth. This extent of the benthic biolayer, however, could not be identified from the in-stream analysis because it could not separate the reactive part of the hyporheic zone from nonreactive parts. Nonetheless, it was able to identify the part of the hyporheic reactions essential for reach-scale water chemistry, whereas the subsurface analysis could not provide any information about the relevance of the detected processes on in-stream conditions. These findings are in agreement with a study by *Harvey et al*. [1996] who used a combined surface and subsurface analysis and found that the in-stream tracer was able to characterize the relatively fast exchange between the stream and gravel streambed but failed to account for slower exchange with deeper alluvium. Similarly, *Harvey et al*. [2013], *González-Pinzón et al*. [2015], and *Zarnetske et al*. [2015] concluded that hyporheic zone characteristics cannot be inferred from reach-scale tracer tests alone.

Therefore, subsurface and in-stream results inform about two different parts of the system. Depth profiles provide detailed information about in-situ conditions but contain no information about what the river sees. In-stream results, on the other hand, tell us nothing about the specific location of reaction, but provide integrated information about the reaction zones which have the largest impact on downstream water chemistry.

4. Conclusions

This study contrasted reach-scale tracer tests using bromide (conservative) and resazurin (bioreactive) with simultaneous multisite and multidepth subsurface sampling to quantify coupled transport and reaction at the reach and centimeter-scale. The subsurface approach provided a detailed look at the vertical resolution of hyporheic processes, enabling us to identify layers of higher and lower reactivity from the reaction rates of resazurin, which indicates the importance of the benthic biolayer in controlling substrate supply and subsequent microbial metabolism. While our data helped us to localize layers with increased turnover, they did not allow us to quantitatively resolve the relationship between biomass abundance and function, and hydrological substrate supply.

Even though the benthic biolayer was found to be on average 2 cm thick based on the integrative approach of the reaction depth $\tilde{d}_{raz}$ (according to equation (21)), our analysis showed that the regions of highest metabolic activity are not necessarily located at very shallow depths of the subsurface, but may be found slightly beneath the stream bed at some locations. This pattern and its magnitude is highly location-dependent, and further research is needed to determine whether spatial variations are linked to variations in streambed morphology, or rather an effect of depth-dependent biomass and organic carbon content.

Subsurface profiles alone only resolve a part of the flow paths, and therefore provide little information about water returning to the stream. For this reason, they cannot separate subsurface processes relevant

for whole-stream conditions from those without great significance on the reach scale. The reach-scale approach, on the other hand, is often favored for its spatial integration as it determines an effective reaction rate for the stream reach, but it cannot resolve the importance of specific subsurface processes such as biolayer dynamics that may be relevant for evaluating restoration projects. This outcome agrees with the conclusions of *Harvey et al*. [2013] that reach-scale tracer tests alone are not a suitable tool to quantify the depth of the reaction and the reaction rate in the subsurface, and is also in agreement with studies by *Lemke et al*. [2013a], *González-Pinzón et al*. [2015], and others who showed that in-stream tracer tests are very effective for the determination of bulk reaction rates.

Thus, the subsurface data detects profiles of reactivity within the hyporheic zone, while the reach-scale data reliably estimates whole-stream effects. Conversely, the reach-scale approach cannot constrain the distribution of reactivity in the subsurface when used alone, while depth profiles tell us nothing about water returning from the subsurface to the stream and have therefore little relevance for reach-scale chemistry. Combining approaches adds information about hydrologic and chemical process variability on the different scales, thus illustrating the fundamental discrepancies of the two approaches, owing to the complementary information about hyporheic transport gained by combining the two different types of observation. Combining both types of information with process models of river and hyporheic flow has the potential to vastly improve understanding about the controlling processes and cumulative effects of hyporheic-zone reactions in large drainage basins [*Gomez-Velez et al*., 2015], which will be needed to forecast how changing land use will affect river water quality and to prioritize effective management [*Hester and Gooseff*, 2010; *Mortensen et al*., 2016].

Acknowledgments

J.L.A.K. was supported as a visiting scientist at the U.S. Geological Survey in Reston, VA, USA by the German Academic Exchange Service (DAAD) through a DAAD Doctoral Scholarship and by a Carl Zeiss Stiftung scholarship for Ph.D. research. Further support came from NSF grants EAR 08-38338 and HRD-1345169 (R.G.P.), NSF grant EAR 08-10140 (J.D.D.), and NSF grant EAR 08-14990, and the USGS National Water Quality and Water Availability and Use Programs (J.W.H. and L.G.L.). We thank Roy Haggerty for his collaboration with logistics and early discussions regarding this work and Alexandra Gessner for many helpful comments on this manuscript and we are grateful to Fulvio Boano and three anonymous reviewers for their helpful comments and constructive suggestions. The authors also wish to thank the following people for help with field and laboratory work: Jay Choi, Morgan Maglio, Trevor Langston, Craig Snyder, and Melissa Reardon. The data used are available upon request from the first or last author. Any use of trade, firm, or product names is for descriptive purposes only and does not imply endorsement by the U.S. Government.

References

Argerich, A., R. Haggerty, E. Marti, F. Sabater, and J. Zarnetske (2011), Quantification of metabolically active transient storage (MATS) in two reaches with contrasting transient storage and ecosystem respiration, *J. Geophys. Res.*, *116*, G03034, doi:10.1029/2010JG001379.

Arnon, S., K. Yanuka, and A. Nejidat (2013), Impact of overlying water velocity on ammonium uptake by benthic biofilms, *Hydrol. Processes*, *27*(4), 570–578.

Bardini, L., F. Boano, M. B. Cardenas, R. Revelli, and L. Ridolfi (2012), Nutrient cycling in bedform induced hyporheic zones, *Geochim. Cosmochim. Acta*, *84*, 47–61.

Battin, T. J., L. A. Kaplan, J. D. Newbold, and C. M. Hansen (2003), Contributions of microbial biofilms to ecosystem processes in stream mesocosms, *Nature*, *426*(6965), 439–442.

Battin, T. J., K. Besemer, M. M. Bengtsson, A. M. Romani, and A. I. Packmann (2016), The ecology and biogeochemistry of stream biofilms, *Nat. Rev. Microbiol.*, *14*(4), 251–263.

Bencala, K. E., and R. A. Walters (1983), Simulation of solute transport in a mountain pool-and-riffle stream: A transient storage model, *Water Resour. Res.*, *19*(3), 718–724.

Bhaskar, A. S., J. W. Harvey, and E. J. Henry (2012), Resolving hyporheic and groundwater components of streambed water flux using heat as a tracer, *Water Resour. Res.*, *48*, W08524, doi:10.1029/2011WR011784.

Boano, F., J. W. Harvey, A. Marion, A. I. Packman, R. Revelli, L. Ridolfi, and A. Wörman (2014), Hyporheic flow and transport processes: Mechanisms, models, and biogeochemical implications, *Rev. Geophys.*, *52*, 603–679, doi:10.1002/2012RG000417.

Böhlke, J. K., R. C. Antweiler, J. W. Harvey, A. E. Laursen, L. K. Smith, R. L. Smith, and M. A. Voytek (2009), Multi-scale measurements and modeling of denitrification in streams with varying flow and nitrate concentration in the upper Mississippi River basin, USA, *Biogeochemistry*, *93*(1-2), 117–141.

Botter, G., E. Bertuzzo, and A. Rinaldo (2011), Catchment residence and travel time distributions: The master equation, *Geophys. Res. Lett.*, *38*, L11403, doi:10.1029/2011GL047666.

Boulton, A. J., S. Findlay, P. Marmonier, E. H. Stanley, and H. M. Valett (1998), The functional significance of the hyporheic zone in streams and rivers, *Annu. Rev. Ecol. Syst.*, *29*, 59–81.

Briggs, M. A., L. K. Lautz, D. K. Hare, and R. González-Pinzón (2013), Relating hyporheic fluxes, residence times, and redox-sensitive biogeochemical processes upstream of beaver dams, *Freshwater Sci.*, *32*(2), 622–641.

Briggs, M. A., F. D. Day-Lewis, J. P. Zarnetske, and J. W. Harvey (2015), A physical explanation for the development of redox microzones in hyporheic flow, *Geophys. Res. Lett.*, *42*, 4402–4410, doi:10.1002/2015GL064200.

Brunke, M., and T. Gonser (1997), The ecological significance of exchange processes between rivers and groundwater, *Freshwater Biol.*, *37*(1), 1–33.

Conant, B., J. A. Cherry, and R. W. Gillham (2004), A PCE groundwater plume discharging to a river: Influence of the streambed and near-river zone on contaminant distributions, *J. Contamin. Hydrol.*, *73*(1), 249–279.

Fischer, H., M. Pusch, and J. Schwoerbel (1996), Spatial distribution and respiration of bacteria in stream-bed sediments, *Arch. Hydrobiol.*, *137*(3), 281–300.

Fuller, C. C., and J. W. Harvey (2000), Reactive uptake of trace metals in the hyporheic zone of a mining-contaminated stream, Pinal Creek, Arizona, *Environ. Sci. Technol.*, *34*(7), 1150–1155.

Gomez-Velez, J. D., J. W. Harvey, M. B. Cardenas, and B. Kiel (2015), Denitrification in the Mississippi River network controlled by flow through river bedforms, *Nat. Geosci.*, *8*, 941–945.

González-Pinzón, R., and R. Haggerty (2013), An efficient method to estimate processing rates in streams, *Water Resour. Res.*, *49*, 6096–6099, doi:10.1002/wrcr.20446.

González-Pinzón, R., R. Haggerty, and D. D. Myrold (2012), Measuring aerobic respiration in stream ecosystems using the resazurin-resorufin system, *J. Geophys. Res.*, *117*, G00N06, doi:10.1029/2012JG001965.

Gonzalez-Pinzon, R., R. Haggerty, and A. Argerich (2014), Quantifying spatial differences in metabolism in headwater streams, *Freshwater Sci.*, *33*(3), 798–811.
González-Pinzón, R., A. S. Ward, C. E. Hatch, A. N. Wlostowski, K. Singha, M. N. Gooseff, R. Haggerty, J. W. Harvey, O. A. Cirpka, and J. T. Brock (2015), A field comparison of multiple techniques to quantify groundwater–surface-water interactions, *Freshwater Sci.*, *34*(1), 139–160.
Gooseff, M. N., S. M. Wondzell, R. Haggerty, and J. Anderson (2003), Comparing transient storage modeling and residence time distribution (RTD) analysis in geomorphically varied reaches in the Lookout Creek basin, Oregon, USA, *Adv. Water Resour.*, *26*(9), 925–937.
Grimm, N. B., and S. G. Fisher (1984), Exchange between interstitial and surface water: Implications for stream metabolism and nutrient cycling, *Hydrobiologia*, *111*(3), 219–228.
Haggerty, R., A. Argerich, and E. Marti (2008), Development of a "smart" tracer for the assessment of microbiological activity and sediment-water interaction in natural waters: The resazurin-resorufin system, *Water Resour. Res.*, *44*, W00D01, doi:10.1029/2007WR006670.
Haggerty, R., E. Marti, A. Argerich, D. von Schiller, and N. B. Grimm (2009), Resazurin as a "smart" tracer for quantifying metabolically active transient storage in stream ecosystems, *J. Geophys. Res.*, *114*, G03014, doi:10.1029/2008JG000942.
Harvey, C. F., and S. M. Gorelick (1995), Temporal moment-generating equations: Modeling transport and mass-transfer in heterogeneous aquifers, *Water Resour. Res.*, *31*(8), 1895–1911.
Harvey, J. W., and C. C. Fuller (1998), Effect of enhanced manganese oxidation in the hyporheic zone on basin-scale geochemical mass balance, *Water Resour. Res.*, *34*(4), 623–636.
Harvey, J. W., and M. Gooseff (2015), River corridor science: Hydrologic exchange and ecological consequences from bedforms to basins, *Water Resour. Res.*, *51*, 6893–6922, doi:10.1002/2015WR017617.
Harvey, J. W., B. J. Wagner, and K. E. Bencala (1996), Evaluating the reliability of the stream tracer approach to characterize stream-subsurface water exchange, *Water Resour. Res.*, *32*(8), 2441–2451.
Harvey, J. W., et al. (2012), Hydrogeomorphology of the hyporheic zone: Stream solute and fine particle interactions with a dynamic streambed, *J. Geophys. Res.*, *117*, G00N11, doi:10.1029/2012JG002043.
Harvey, J. W., J. K. Bohlke, M. A. Voytek, D. Scott, and C. R. Tobias (2013), Hyporheic zone denitrification: Controls on effective reaction depth and contribution to whole-stream mass balance, *Water Resour. Res.*, *49*, 6298–6316, doi:10.1002/wrcr.20492.
Hendricks, S. P. (1993), Microbial ecology of the hyporheic zone: A perspective integrating hydrology and biology, *J. N. Am. Benthol. Soc.*, *12*(1), 70–78.
Hester, E. T., and M. N. Gooseff (2010), Moving beyond the banks: Hyporheic restoration is fundamental to restoring ecological services and functions of streams, *Environ. Sci. Technol.*, *44*(5), 1521–1525.
Hollenbeck, K. (1998), *INVLAP. M: A Matlab Function for Numerical Inversion of Laplace Transforms by the de Hoog Algorithm*. [Available at https://www.mathworks.com/matlabcentral/answers/uploaded_files/1034/invlap.m.]
Kerr, P. C., M. N. Gooseff, and D. Bolster (2013), The significance of model structure in one-dimensional stream solute transport models with multiple transient storage zones: Competing vs. nested arrangements, *J. Hydrol.*, *497*, 133–144.
Krause, S., D. Hannah, J. Fleckenstein, C. Heppell, D. Kaeser, R. Pickup, G. Pinay, A. Robertson, and P. Wood (2011), Inter-disciplinary perspectives on processes in the hyporheic zone, *Ecohydrology*, *4*(4), 481–499.
Kucera, E. (1965), Contribution to theory of chromatography linear non-equilibrium elution chromatography, *J. Chromatogr.*, *19*(2), 237–248.
Laloy, E., and J. A. Vrugt (2012), High-dimensional posterior exploration of hydrologic models using multiple-try DREAM (ZS) and high-performance computing, *Water Resour. Res.*, *48*, W01526, doi:10.1029/2011WR010608.
Lemke, D., Z. J. Liao, T. Wohling, K. Osenbruck, and O. A. Cirpka (2013a), Concurrent conservative and reactive tracer tests in a stream undergoing hyporheic exchange, *Water Resour. Res.*, *49*, 3024–3037, doi:10.1002/wrcr.20277.
Lemke, D., P. A. Schnegg, M. Schwientek, K. Osenbruck, and O. A. Cirpka (2013b), On-line fluorometry of multiple reactive and conservative tracers in streams, *Environ. Earth Sci.*, *69*(2), 349–358.
Liao, Z. J., and O. A. Cirpka (2011), Shape-free inference of hyporheic travel time distributions from synthetic conservative and "smart" tracer tests in streams, *Water Resour. Res.*, *47*, W07510, doi:10.1029/2010WR009927.
Liao, Z. J., D. Lemke, K. Osenbruck, and O. A. Cirpka (2013), Modeling and inverting reactive stream tracers undergoing two-site sorption and decay in the hyporheic zone, *Water Resour. Res.*, *49*, 3406–3422, doi:10.1002/wrcr.20276.
Marion, A., M. Zaramella, and A. Bottacin-Busolin (2008), Solute transport in rivers with multiple storage zones: The STIR model, *Water Resour. Res.*, *44*, W10406, doi:10.1029/2008WR007037.
Mortensen, J. G., R. Gonzalez-Pinzoń, C. N. Dahm, J. Wang, L. H. Zeglin, and D. J. Van Horn (2016), Advancing the Food-Energy–Water Nexus: Closing Nutrient Loops in Arid River Corridors, *Environ. Sci. Technol.*, *50*(16), 8485–8496.
Navel, S., F. Mermillod-Blondin, B. Montuelle, E. Chauvet, L. Simon, and P. Marmonier (2011), Water–sediment exchanges control microbial processes associated with leaf litter degradation in the hyporheic zone: A microcosm study, *Microb. Ecol.*, *61*(4), 968–979.
O'Brien, J., I. Wilson, T. Orton, and F. Pognan (2000), Investigation of the Alamar Blue (resazurin) fluorescent dye for the assessment of mammalian cell cytotoxicity, *Eur. J. Biochem.*, *267*(17), 5421–5426.
O'Connor, B. L., and J. W. Harvey (2008), Scaling hyporheic exchange and its influence on biogeochemical reactions in aquatic ecosystems, *Water Resour. Res.*, *44*, W12423, doi:10.1029/2008WR007160.
O'Connor, B. L., and M. Hondzo (2008), Dissolved oxygen transfer to sediments by sweep and eject motions in aquatic environments, *Limnol. Oceanogr.*, *53*(2), 566–578.
O'Connor, B. L., J. W. Harvey, and L. E. McPhillips (2012), Thresholds of flow-induced bed disturbances and their effects on stream metabolism in an agricultural river, *Water Resour. Res.*, *48*, W08504, doi:10.1029/2011WR011488.
Rinaldo, A., P. Benettin, C. J. Harman, M. Hrachowitz, K. J. McGuire, Y. van der Velde, E. Bertuzzo, and G. Botter (2015), Storage selection functions: A coherent framework for quantifying how catchments store and release water and solutes, *Water Resour. Res.*, *51*, 4840–4847, doi:10.1002/2015WR017273.
Rodriguez-Freire, L., S. M. Avasarala, A.-M. S. Ali, D. Agnew, J. H. Hoover, K. Artyushkova, D. E. Latta, E. J. Peterson, J. Lewis, and L. J. Crossey (2016), Post Gold King Mine spill investigation of metal stability in water and sediments of the Animas River watershed, *Environ. Sci. Technol.*, *50*(21), 11539–11548.
Runkel, R. L. (1998), One-dimensional transport with inflow and storage (OTIS): A solute transport model for streams and rivers, *U.S. Geol. Sur. Water Resour. Invest. Rep.*, 98-4018, 73 pp.
Runkel, R. L. (2007), Toward a transport-based analysis of nutrient spiraling and uptake in streams, *Limnol. Oceanogr. Methods*, *5*(1), 50–62.
Sardin, M., D. Schweich, F. J. Leij, and M. T. Vangenuchten (1991), Modeling the nonequilibrium transport of linearly interacting solutes in porous-media: A review, *Water Resour. Res.*, *27*(9), 2287–2307.
Stanford, J., and J. Ward (1988), The hyporheic habitat of river ecosystems, *Nature*, *335*, 64–66.

Triska, F. J., V. C. Kennedy, R. J. Avanzino, G. W. Zellweger, and K. E. Bencala (1989), Retention and transport of nutrients in a third-order stream in northwestern California: Hyporheic processes, *Ecology*, *70*, 1893–1905.

Vrugt, J. A., C. Ter Braak, C. Diks, B. A. Robinson, J. M. Hyman, and D. Higdon (2009), Accelerating Markov chain Monte Carlo simulation by differential evolution with self-adaptive randomized subspace sampling, *Int. J. Nonlinear Sci. Numer. Simul.*, *10*(3), 273–290.

Wörman, A. (1998), Analytical solution and timescale for transport of reacting solutes in rivers and streams, *Water Resour. Res.*, *34*(10), 2703–2716.

Wörman, A., A. I. Packman, H. Johansson, and K. Jonsson (2002), Effect of flow-induced exchange in hyporheic zones on longitudinal transport of solutes in streams and rivers, *Water Resour. Res.*, *38*(1), 1001, doi:10.1029/2001WR000769.

Zaramella, M., A. I. Packman, and A. Marion (2003), Application of the transient storage model to analyze advective hyporheic exchange with deep and shallow sediment beds, *Water Resour. Res.*, *39*(7), 1198, doi:10.1029/2002WR001344.

Zarnetske, J. P., R. Haggerty, and S. M. Wondzell (2015), Coupling multiscale observations to evaluate hyporheic nitrate removal at the reach scale, *Freshwater Sci.*, *34*(1), 172–186.

AGU PUBLICATIONS

Water Resources Research

RESEARCH ARTICLE
10.1002/2017WR020734

Key Points:
- The estimation of transport parameters is coupled with the inference of a continuous travel time distribution
- The nested local-in-global approach provides the joint posterior distribution of all parameters
- The presented approach is applied to reactive stream-tracer data to determine hyporheic exchange processes

Supporting Information:
- Supporting Information S1
- Data Set S1
- Data Set S2
- Data Set S3
- Data Set S4
- Data Set S5
- Data Set S6
- Data Set S7
- Data Set S8
- Data Set S9
- Data Set S10
- Data Set S11

Correspondence to:
J. L. A. Knapp,
julia.knapp@uni-tuebingen.de

Citation:
Knapp, J. L. A., and O. A. Cirpka (2017), Determination of hyporheic travel time distributions and other parameters from concurrent conservative and reactive tracer tests by local-in-global optimization, *Water Resour. Res.*, *53*, doi:10.1002/2017WR020734.

Received 10 MAR 2017
Accepted 31 MAY 2017
Accepted article online 2 JUN 2017

© 2017. American Geophysical Union. All Rights Reserved.

Determination of hyporheic travel time distributions and other parameters from concurrent conservative and reactive tracer tests by local-in-global optimization

Julia L. A. Knapp[1] and Olaf A. Cirpka[1]

[1]Center for Applied Geoscience, University of Tübingen, Tübingen, Germany

Abstract The complexity of hyporheic flow paths requires reach-scale models of solute transport in streams that are flexible in their representation of the hyporheic passage. We use a model that couples advective-dispersive in-stream transport to hyporheic exchange with a shape-free distribution of hyporheic travel times. The model also accounts for two-site sorption and transformation of reactive solutes. The coefficients of the model are determined by fitting concurrent stream-tracer tests of conservative (fluorescein) and reactive (resazurin/resorufin) compounds. The flexibility of the shape-free models give rise to multiple local minima of the objective function in parameter estimation, thus requiring global-search algorithms, which is hindered by the large number of parameter values to be estimated. We present a local-in-global optimization approach, in which we use a Markov-Chain Monte Carlo method as global-search method to estimate a set of in-stream and hyporheic parameters. Nested therein, we infer the shape-free distribution of hyporheic travel times by a local Gauss-Newton method. The overall approach is independent of the initial guess and provides the joint posterior distribution of all parameters. We apply the described local-in-global optimization method to recorded tracer breakthrough curves of three consecutive stream sections, and infer section-wise hydraulic parameter distributions to analyze how hyporheic exchange processes differ between the stream sections.

Plain Language Summary Compounds, dissolved in river water, are transported along the river, but also to some extent into the sediments and back into the river. While being in the sediments, they may react. In reactive stream-tracer tests, we add easy-to-detect reactive compounds into a stream and measure time-series of concentration in the river further downstream. We present an approach of analyzing such tracer tests in a flexible, yet reliable manner, which also provides the uncertainty of our interpretation. This can be useful in the assessment of river-water quality

1. Introduction

Hyporheic exchange has been the subject of intensive research over the last two decades. As our knowledge and scientific understanding of the underlying hydrological processes increases, so does the complexity of the models used to describe transport of solutes undergoing hyporheic exchanges. One of the first quantitative descriptions of hyporheic exchange was made by *Bencala and Walters* [1983], who extended the well-known advection-dispersion equation for solute transport in streams by a linear exchange term between the mobile water in the stream and a well-mixed, immobile hyporheic zone ("transient storage model"). Most hyporheic exchange models up to date are generally based on this approach, but include additional processing of varying complexity. As example, multirate mass transfer models [e.g., *Haggerty and Gorelick*, 1995] subdivide the immobile zone into several subzones, each of which linearly exchanges solutes with the mobile domain with a different exchange rate coefficient.

The transport equations of the transient storage model have also been expanded to address reactions of solutes that are transformed in the metabolically active hyporheic storage zone. These models can be used to interpret reactive, "smart" stream-tracer tests [e.g., *Haggerty et al.*, 2009, 2008], in which the reactive compound resazurin is injected into a stream together with a conservative tracer compound. Resazurin is a weakly fluorescent, phenoazine dye [*O'Brien et al.*, 2000], which is transformed into the reaction product resorufin by metabolically active bacteria in the hyporheic zone. The resazurin-to-resorufin transformation

can thus be used as a proxy for microbial activity, particularly aerobic respiration [*O'Brien et al*., 2000; *González-Pinzón et al*., 2014, 2015, 2012]. In order to quantify the reactivity of the metabolically active transient-storage zone and its exchange with the stream, reactive transport models are fitted to concentration time series of the conservative and reactive tracers as well as the reaction product.

All models mentioned above require the description of the residence or travel time distribution in the hyporheic zone. In the most simple case, a single well-mixed transient storage zone is assumed [e.g., *Bencala and Walters*, 1983; *Runkel*, 1998], which is equivalent to choosing an exponential hyporheic travel time distribution. As alternative parameterizations, lognormal [e.g., *Wörman et al*., 2002] and (truncated) power law [e.g., *Gooseff et al*., 2003] distributions are commonly applied. These distributions are fully described by a few parameters, which are usually estimated by fitting models to measured concentration breakthrough curves within the stream.

When fitting these models, the functional shape of the hyporheic residence-time or travel time distribution is fixed, and nontraditional features such as broad or multiple peaks remain unnoticed. Conversely, *Liao and Cirpka* [2011] and *Liao et al*. [2013] used a shape-free approach to infer hyporheic travel time distributions from conservative and reactive tracer breakthrough curves. In the latter approach, the only constraints on the continuous hyporheic travel time distributions are that they must be nonnegative and exhibit a certain smoothness (for details see *Cirpka et al*. [2007]). The shape-free approach is more flexible but, given more degrees of freedom, the uncertainty of the inferred hyporheic travel time distributions may be higher. When fitting models of stream transport and hyporheic exchange to in-stream tracer data, the inferred parameters are not independent of each other. That is, choosing different values of dispersion coefficients, in-stream velocities, or reactive parameters within their uncertainty bounds can be compensated by different parameters of hyporheic exchange. Even when fitting the simplest linear transient-storage model, the ambiguity of the parameters and the existence of multiple local minima in the objective function, used for parameter estimation, requires global-search methods to obtain reliable parameter values and their uncertainty [e.g., *Lemke et al*., 2013]. The higher flexibility of the shape-free approach calls even more for global-search methods, but the associated computational costs have so far been considered unacceptable so that *Liao et al*. [2013] used a gradient-based method to estimate the hyporheic travel time distribution and other parameters of stream-tracer transport coupled to hyporheic exchange.

For the estimation of hydrological model parameters, different search algorithms of varying complexity are available. The simplest choice are gradient-based methods like the Gauss-Newton method and its stabilized Levenberg-Marquardt modification [e.g., *Press et al*., 1992, chap. 15]. These methods are usually very efficient for unimodal problems with a single optimum solution and a smooth objective function, but are rarely able to find the global optimum in case of multimodality. They tend to get stuck in a local optimum ("premature convergence"), which typically depends on the initial guess. Closing in on the global optimum thus requires multiple optimization runs with different initial guesses. It is easily imaginable that in the complex case of simultaneously fitting a shape-free hyporheic transfer function in addition to a number of hydrological parameters described above, most common optimization procedures reach their limits. Furthermore, the solutions obtained from these algorithms yield no reliable information on how good the encountered parameter set actually is, that is, the typical guess of the a posteriori distribution of the parameters based on linearized uncertainty propagation is not trustworthy. This holds in particular for transient storage models, where different combinations of parameters can reproduce measured instream BTCs [e.g., *Harvey et al*., 1996; *Wagener et al*., 2002]. This equifinality leads to a lack of parameter identifiability, resulting in possibly false interpretation of physical parameters.

For this reason, global-search algorithms have been developed that are able to systematically search the parameter space in order to find the global optimum. One group of such global-search methods are evolutionary algorithms, that mimic evolution processes to separate more successful parameter sets (called "individuals") from less successful ones and achieve convergence (referred to as optimum "fitness") according to Darwin's principle of "survival of the fittest." These evolutionary algorithms are generally very flexible and can be employed for objective functions of different shapes (for an overview of evolutionary algorithms see *Bäck and Schwefel* [1993]). However, they only supply the parameter set with the highest fitness value, but are generally not able to generate a posterior distribution and thus a measure of uncertainty of the estimated parameters. This problem has been tackled by a number of algorithms combining evolutionary

algorithms with Bayesian methods in a Markov-Chain Monte Carlo procedure. The Differential Evolution Markov Chain (DE-MC) method of *Ter Braak* [2004] and the Differential Evolution Adaptive Metropolis (DREAM) algorithm of *Vrugt et al*. [2008, 2009] are examples of these algorithms, that run several chains of parameter sets in parallel. The DREAM algorithms and further developments of the algorithm (e.g., DREAM(ZS) and DREAM(D)) have been applied to a number of hydrological optimization problems in the past, like the posterior exploration of hydrologic models, including a 241-parameter groundwater model [*Laloy and Vrugt*, 2012], the parameterization of the "Soil and Water Assessment Tool" (SWAT), a basin-scale, semidistributed, precipitation-runoff hydrologic model [*Joseph and Guillaume*, 2013], as well as a snow model [*He et al*., 2011]. In these applications, the global optimization algorithm is commonly used to find the "fittest" parameter set and evaluate the sensitivity of the same by providing an a posteriori distribution of the estimated parameters. This approach was tested successfully for hyporheic exchange processes by *Lemke et al*. [2013], who obtained posterior parameter probability density functions using an adaptive Markov chain Monte Carlo scheme to fit measured breakthrough curves of a reactive stream-tracer test. The applied model, however, only employed an exponential hyporheic travel time distribution and was therefore not able to correctly fit tracer concentrations at late arrival times (tailing), a common problem encountered when applying the single transient-storage model, which is equivalent to assuming an exponential hyporheic travel time distribution [*Gooseff et al*., 2003].

In this study, we present a new approach for the inference of hyporheic exchange, in-stream transport, and reactive parameters from breakthrough curves of reactive and conservative tracer tests employing shape-free hyporheic travel time distributions. The approach is based on nesting a local search method for the detection of the hyporheic travel time distribution into a global search for all remaining parameters, namely the in-stream velocity and dispersion coefficient, the strength of hyporheic exchange, reactivities and sorptivities of the reactive compounds, and the smoothness parameter of the hyporheic travel time distribution. As global-search method, we apply DREAM(ZS) [*Laloy and Vrugt*, 2012], whereas the nested local method for updating the hyporheic travel time distribution, keeping all other parameters constant, is based on the Gauss-Newton method. Similar to *Liao et al*. [2013], we consider transformation of resazurin to resorufin as well as two-site sorption of the reactive compound and reaction product, and apply the data to a stream-tracer test in the Goldersbach, a stream within the Neckar catchment in Southwest Germany. Applying DREAM(ZS) instead of a standard or adaptive genetic algorithms allows obtaining the posterior distributions of all parameters rather than only the best parameter set.

2. Description of the Predictive Model

In this study, we adapt the model of *Liao et al*. [2013] solving advective-dispersive transport in the stream coupled to hyporheic exchange, described by an exchange rate and a shape-free hyporheic travel time distribution. The reactive tracer also undergoes a first-order chemical transformation to a degradation product, presumably only during the hyporheic passage. Both the reactant and the product undergo two-site sorption within the hyporheic zone. The system of partial differential equations is solved in the Laplace domain. In the present application, we assume section-wise constant coefficients, that we infer from breakthrough curves of the conservative tracer fluorescein, the reactive tracer resazurin, and the reaction product resorufin.

2.1. In-Stream Transport Equations Subject to Hyporheic Processes

In total, the model requires three governing equations, one each for the conservative ($i = 0$) and reactive ($i = 1$) tracer as well as one for the reaction product ($i = 2$):

$$\frac{\partial c_{i,k}}{\partial t} + v_k \frac{\partial c_{i,k}}{\partial x_k} - D_k \frac{\partial^2 c_{i,k}}{\partial x_k^2} = q_k^{he}\left(\int_0^t g_{i,k}(\tau) c_{i,k}(t-\tau) d\tau - c_{i,k}(t)\right), \quad i=0,1 \tag{1}$$

$$\frac{\partial c_{2,k}}{\partial t} + v_k \frac{\partial c_{2,k}}{\partial x_k} - D_k \frac{\partial^2 c_{2,k}}{\partial x_k^2} = q_k^{he}\left(\int_0^t \left(g_{12,k}(\tau) c_{1,k}(t-\tau) + g_{2,k}(\tau) c_{2,k}(t-\tau)\right) d\tau - c_{2,k}(t)\right) \tag{2}$$

in which the index k stands for the kth stream sections ($1 < k < n$ with the total number of sections n), and v_k [$L\ T^{-1}$] is the in-stream advective velocity, D_k [$L^2\ T^{-1}$] denotes the dispersion coefficient and x_k [L] the travel distance of section k. τ [T] denotes the hyporheic travel time and t [T] the absolute time since

injection. The concentration of compound i in section k is denoted $c_{i,k}$ [$M\,L^{-3}$], and q_k^{he} [T^{-1}] represents the rate coefficient of hyporheic exchange (exchanged discharge per volume of stream water).

The functions $g_{0,k}(\tau)$, $g_{1,k}(\tau)$, $g_{2,k}(\tau)$, and $g_{12,k}(\tau)$ [T^{-1}] are hyporheic transfer functions in section k, expressing the concentration time series in the water returning into the stream as a function of the time difference τ in response to a hypothetical Dirac-pulse of concentration in the water entering the hyporheic zone. While $g_{i,k}(\tau)$ with a single index expresses the response of compound i to a pulse input of the same compound, $g_{12,k}(\tau)$ is a cross-component transfer function, quantifying the response of compound 2 (resorufin) in the returning water to a pulse of compound 1 (resazurin) in the water entering the hyporheic zone. For the conservative tracer, $i = 0$, the hyporheic transfer function $g_{0,k}(\tau)$ essentially equals the distribution of times that a water parcel has spent in the hyporheic zone when returning into the stream, denoted hyporheic travel time distribution in this paper. For all other compounds, the sorption and transformation processes within the hyporheic zone alter the hyporheic transfer functions. Further explanations of the hyporheic transfer functions are given below.

The transport equations are subject to the following initial and boundary conditions:

$$c_{i,k}(x, t_0) = 0 \forall x_k \tag{3}$$

$$v_1 c_{i,1} - D_1 \frac{\partial c_{i,1}}{\partial x_1}\bigg|_{x_1=0} = \frac{m_i}{A}\delta(t) \tag{4}$$

$$c_{i.k}(0, t) = c_{i.k-1}(L_{k-1}, t) \quad \text{for} \quad k > 1 \tag{5}$$

with the tracer mass m_i [M] of compound i injected at the upstream end of the first stream section ($k = 1$) and $m_2 = 0$. t_0 denotes time zero when the tracers are injected, L_{k-1} [L] is the length of the preceding stream section $k - 1$. A [L^2] is the effective cross-sectional area of the first stream section, which is chosen such that the conservative tracer exhibits a perfect mass recovery over the first section:

$$A = \frac{m_0}{v_1 \int_{t_0}^{\infty} c_{0,1}^{meas}(L_1, t)dt} \tag{6}$$

in which $c_{0,1}^{meas}(L_1, t)$ [$M\,L^{-3}$] is the measured concentration of the conservative tracer at the end of the first stream section. To derive equation (6), we used the estimate of the total stream discharge Q [$L^3\,T^{-1}$] by the tracer-dilution method, applied to the first stream section, and divided Q by the stream velocity v_1 of the first section.

Liao et al. [2013] exclusively considered sections starting at the injection point, which implied that the simulated stream sections overlapped, when sequential sampling locations were considered. Consequently, the associated parameters were bulk parameters over the entire length from the injection point up to the sampling locations. In the present study, we have altered the model to account for different sections in a sequence: the simulated breakthrough curves at the downstream end of the upper section is the fixed-concentration boundary condition at the upstream end of the lower section (equation (5)).

Equations (1) and (2) can be solved in the Laplace domain, which has the advantage that the time derivative becomes a multiplication with the complex Laplace frequency parameter s [T^{-1}], and the convolution integral becomes a multiplication of two Laplace-transformed functions:

$$\tilde{c}_{i,k}(s)\left(s + q_k^{he} - q_k^{he}\tilde{g}_{i,k}(s)\right) + v_k \frac{d\tilde{c}_{i,k}(s)}{dx} - D_k \frac{d^2\tilde{c}_{i,k}(s)}{dx^2} = 0, \quad i = 0, 1 \tag{7}$$

$$\tilde{c}_{2,k}(s)\left(s + q_k^{he} - q_k^{he}\tilde{g}_{2,k}(s)\right) - \tilde{c}_{1,k}(s) q_k^{he}\tilde{g}_{12,k} + v_k \frac{d\tilde{c}_{2,k}(s)}{dx} - D_k \frac{d^2\tilde{c}_{2,k}(s)}{dx^2} = 0 \tag{8}$$

subject to:

$$v_1 - D_1 \frac{d\tilde{c}_{i,1}}{dx_1}\bigg|_{x_k=0} = \frac{m_i}{A} \tag{9}$$

$$\tilde{c}_{i.k}(0, s) = \tilde{c}_{i.k-1}(L_{k-1}, s) \tag{10}$$

with the Laplace-transformed hyporheic transfer functions $\tilde{g}_{i,k}(s)$ and the Laplace-transformed concentrations, $\tilde{c}_{i,k}(s)$.

2.2. Hyporheic Transfer Functions $g_i(\tau)$

The hyporheic transfer functions $g_{0,k}(\tau)$, $g_{1,k}(\tau)$, $g_{2,k}(\tau)$, and $g_{12,k}(\tau)$ are the result of physical transport of the tracer compounds through the hyporheic zone, as well as sorption and chemical transformations therein. For the conservative tracer, the corresponding transfer function $g_{0,k}(\tau)$ can be interpreted as hyporheic travel time distribution times the recovery of the tracer. Recoveries smaller than unity indicate that some water returning into the stream does not originate from the stream itself (at least not on time scales observed by the tracer test), whereas recoveries larger than unity are physically impossible as they violate the mass balance. In the first stream section, the application of equation (6) enforces a perfect recovery of 100%.

The hyporheic transfer functions of the reactive compounds can be derived from the transfer function of the conservative tracer. Identical to *Liao et al.* [2013], we assume five processes coupled to transport through the hyporheic zone: (1) linear decay of resazurin with the decay coefficient $\lambda_{1,k}$ [T^{-1}], (2) linear decay of resazurin to resorufin with the decay coefficient $\lambda_{12,k}$ [T^{-1}], with $\lambda_{12,k} < \lambda_{1,k}$, (3) linear decay of resorufin with the decay constant $\lambda_{2,k}$ [T^{-1}], (4) linear equilibrium sorption of resazurin and resorufin in the hyporheic zone with the retardation coefficients $R_{1,k}$ and $R_{2,k}$, respectively, and (5) linear kinetic sorption of both compounds with the sorption coefficients $K_{1,k}$ and $K_{2,k}$ the mass transfer rate coefficients $k_{1,k}$ [T^{-1}] and $k_{2,k}$ [T^{-1}]. Together, we obtain the following governing equations for reactive transport in the hyporheic zone for resazurin ($i = 1$) and resorufin ($i = 2$) [*Liao et al.*, 2013]:

$$R_{i,k}\frac{\partial c_{i,k}^{HZ}}{\partial \tau_k}+K_{i,k}\frac{\partial c_{i,k}^{*}}{\partial \tau_k}+\frac{\partial c_{i,k}^{HZ}}{\partial \tau_k^{*}}=r_{i,k}^{HZ} \tag{11}$$

$$\frac{\partial c_{i,k}^{*}}{\partial \tau_k}=k_{i,k}\left(c_{i,k}^{HZ}-c_{i,k}^{*}\right) \tag{12}$$

$$c_{i,k}^{HZ}(\tau,0)=b_{i,k}\delta(\tau) \tag{13}$$

with

$$r_{1,k}^{HZ}=-\lambda_{1,k}c_{1,k}^{HZ} \tag{14}$$

$$r_{2,k}^{HZ}=\lambda_{12,k}c_{1,k}^{HZ}-\lambda_{2,k}c_{2,k}^{HZ} \tag{15}$$

with the tracer concentration in the hyporheic zone, $c_{i,k}^{HZ}$ [$M\,L^{-3}\,T^{-1}$], and at the kinetically sorbing sites, $c_{i,k}^{*}$ [$M\,L^{-3}\,T^{-1}$]. The delta function $\delta(\tau)$ represents the tracer concentration within the hyporheic zone for a pulse injection and the dimensionless coefficient b_i represents how much tracer mass is introduced into the hyporheic zone at time $\tau = 0$.

This leads to the following Laplace-transformed hyporheic transfer functions $\tilde{g}_{i,k}(s)$ according to *Liao et al.* [2013, equation (12)]:

$$\tilde{g}_{0,k}(s)=\int_0^{\infty} g_{0,k}(\tau^{*})\,\exp\left(-s\tau^{*}\right)d\tau^{*} \tag{16}$$

$$\tilde{g}_{1,k}(s)=\int_0^{\infty} g_{0,k}(\tau^{*})\,\exp\left(-\beta_{1,k}\tau^{*}\right)d\tau^{*} \tag{17}$$

$$\tilde{g}_{2,k}(s)=\int_0^{\infty} g_{0,k}(\tau^{*})\,\exp\left(-\beta_{2,k}\tau^{*}\right)d\tau^{*} \tag{18}$$

$$\tilde{g}_{12,k}(s)=\int_0^{\infty} g_{0,k}(\tau^{*})\frac{\lambda_{12}}{\beta_{1,k}-\beta_{2,k}}\exp\left(-\beta_{2,k}\tau^{*}\right)-\exp\left(-\beta_{1,k}\tau^{*}\right)d\tau^{*}. \tag{19}$$

with the coefficients $\beta_{1,k}$ and $\beta_{2,k}$ incorporating compound-specific behavior:

$$\beta_{1,k}=R_{1,k}s+\lambda_{1,k}+K_{1,k}s\frac{k_{1,k}}{s+k_{1,k}} \tag{20}$$

$$\beta_{2,k}=R_{2,k}s+\lambda_{2,k}+K_{2,k}s\frac{k_{2,k}}{s+k_{2,k}} \tag{21}$$

Table 1. Overview of the Eight Different Model Parameters Estimated During the Local and Global Optimization Procedure[a]

Symbol	Unit	Definition
v^*	$[L\,T^{-1}]$	In-stream velocity
D^*	$[L^2\,T^{-1}]$	In-stream dispersion coefficient
q^{he*}	$[T^{-1}]$	Hyporheic exchange rate
λ_1^*	$[T^{-1}]$	Decay rate coefficient of resazurin
λ_2	$[T^{-1}]$	Decay rate coefficient of resorufin
λ_{12}	$[T^{-1}]$	Transformation rate coefficient from resazurin to resorufin, $\lambda_{12} \leq \lambda_1$
R_1^*		Equilibrium sorption coefficient of resazurin
R_2		Equilibrium sorption coefficient of resorufin
K_1^*		Kinetic sorption coefficient of resazurin
K_2		Kinetic sorption coefficient of resorufin
k_1^*	$[T^{-1}]$	First-order mass transfer rate coefficient of kinetic sorption of resazurin
k_2	$[T^{-1}]$	First-order mass transfer rate coefficient of kinetic sorption ofresorufin
Θ^*	$[T^{-3}]$	Slope of the linear variogram, smoothness parameter for the transfer function

[a]Parameters marked with an asterisk are estimated during the joint fluorescein + resazurin optimization.

3. Description of the Inverse Problem

All in all, the model requires the hyporheic transfer function of the conservative tracer $g_{0,k}(\tau)$ and 13 additional parameters per stream section (see Table 1). These parameters need to be estimated from the measured breakthrough curves. Of the 13 parameters, 8 are inherent to the joint estimation of the conservative tracer fluorescein and the reactive tracer resazurin. The other five parameters are purely associated with the reaction product, resorufin. Among the parameters listed in Table 1, those associated with the conservative tracer fluorescein and the reactive tracer resazurin are marked with an asterisk.

We subdivide the optimization of the parameters for jointly fitting the data of the conservative tracer and the reactive tracer resazurin into two, nested subproblems: In an outer global optimization loop, performed with the DREAM(ZS) algorithm [*Laloy and Vrugt*, 2012], different combinations of the eight parameters listed in Table 1 are tested and evaluated for their fitness, leading to the joint posterior probability density function of the different parameter solutions. Nested within is a local optimization procedure by a Gauss-Newton algorithm, adapting the hyporheic transfer function $g_{0,k}(\tau)$ of the conservative tracer, keeping the other eight parameters selected by the outer loop. Both optimization procedures are explained in more detail below and the complete procedure is illustrated in Figure 1.

After obtaining the parameters for fluorescein and resazurin, we estimate the remaining five parameters related to resorufin in a separate step. This is explained in more detail in section 4.2.

3.1. Overall Objective Function

In the following we consider one stream section at a time, and the subscript k is dropped for readability. For each section, the eight parameters marked with an asterisk in Table 1 are concatenated to the parameter vector $\mathbf{p}$. Applying Bayes' Theorem, the conditional probability density function $f(\mathbf{p}, \mathbf{g}|\mathbf{c}_{\text{meas}})$ of the parameters $\mathbf{p}$ and the discretized hyporheic transfer function $\mathbf{g}$ of the conservative tracer given the measured concentrations $\mathbf{c}_{\text{meas}}$ is computed as:

$$f(\mathbf{p}, \mathbf{g}|\mathbf{c}_{\text{meas}}) = \frac{f(\mathbf{c}_{\text{meas}}|\mathbf{p}, \mathbf{g}) f(\mathbf{p}) f(\mathbf{g}|\mathbf{p})}{f(\mathbf{c}_{\text{meas}})} \tag{22}$$

where $f(\mathbf{c}_{\text{meas}}|\mathbf{p}, \mathbf{g})$ is the likelihood of the measurements $\mathbf{c}_{\text{meas}}$ given the input parameters $\mathbf{p}$ and $\mathbf{g}$, $f(\mathbf{p})$ is the prior probability density of $\mathbf{p}$, $f(\mathbf{g}|\mathbf{p})$ that of $\mathbf{g}$ given $\mathbf{p}$, and $f(\mathbf{c}_{\text{meas}})$ is known as Bayesian model evidence, which does not depend on $\mathbf{p}$ or $\mathbf{g}$. We assume that $f(\mathbf{c}_{\text{meas}}|\mathbf{p}, \mathbf{g})$ is a multi-Gaussian distribution, whereas the prior of $\mathbf{p}$ is diffuse:

$$f(\mathbf{c}_{\text{meas}}|\mathbf{p}, \mathbf{g}) = \frac{1}{\sqrt{(2\pi)^{n_{meas}}||\mathbf{C}||}} \exp\left(-\frac{1}{2}(\mathbf{c}_{\text{meas}} - \mathbf{c}_{\text{sim}})^T \mathbf{C}^{-1} (\mathbf{c}_{\text{meas}} - \mathbf{c}_{\text{sim}})\right) \tag{23}$$

$$f(\mathbf{p}) = \text{constant} \tag{24}$$

in which $\mathbf{C}$ is the covariance matrix expressing the measurement error, $||\mathbf{A}||$ is the determinant of matrix $\mathbf{A}$, and n_{meas} is the number of measurements. $\mathbf{C}$ is considered a diagonal matrix, which implies no correlation

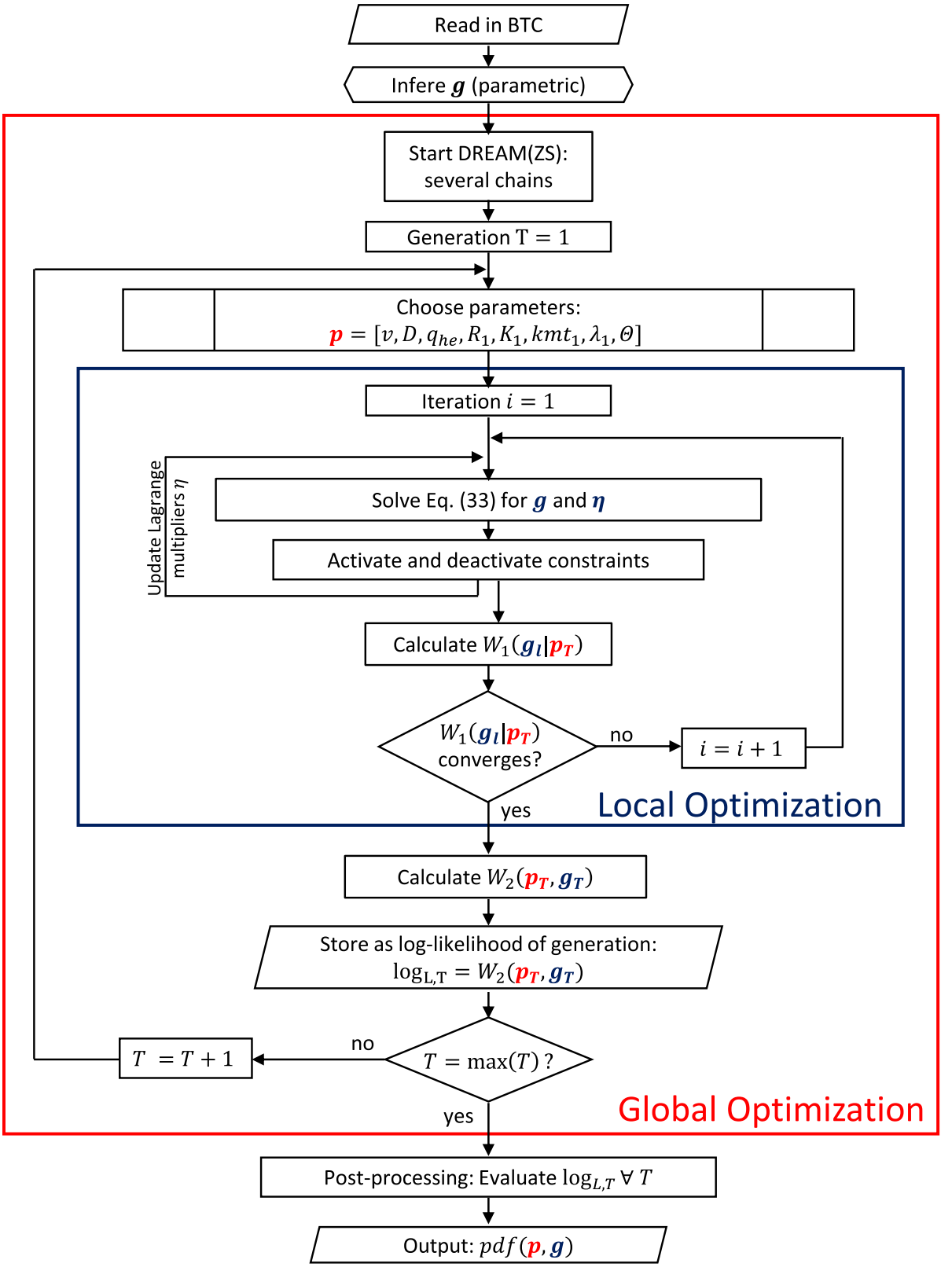

Figure 1. Illustration of the optimization procedure applied: in the global optimization (using the DREAM(ZS) algorithm), different combination of the parameter sets are tested and evaluated. This requires a local optimization (Gauss-Newton algorithm) of a parameter set-specific travel time distribution $g(\tau)$. The goodness of each estimations is quantified by the respective fitness function $W_1(\mathbf{g})$ and $W_2(\mathbf{p})$.

of the measurement errors. The corresponding standard deviation σ_i of measurement i constitutes of a relative and an absolute error, ε_{rel} and ε_{abs}:

$$\sigma_i = \varepsilon_{rel} c_i + \varepsilon_{abs} \tag{25}$$

in which ε_{rel} and ε_{abs} depend on the compound.

Contrary to parametric expressions commonly used, we assume that $g_{0,k}(\tau)$ is a continuous function of the hyporheic travel time τ without enforcing a predefined parametric shape. It is only constrained to be nonnegative for all values of τ (which will be enforced later), and its smoothness is described by a linear semivariogram function γ_{gg}:

$$\gamma_{gg}(\tau_i - \tau_j) = \frac{1}{2} E\left[\left(g_{0,k}(\tau_i) - g_{0,k}(\tau_j)\right)^2\right] = \Theta|\tau_i - \tau_j| \tag{26}$$

in which $E[\cdot]$ is the expected-value operator, and the slope Θ $[T^{-3}]$ of the semivariogram function is included in the parameter set $\mathbf{p}$. We assume that the expected value of $g_{0,k}(\tau)$ does not depend on τ, but its prior knowledge is diffuse. Then, the prior probability density of the discretized hyporheic transfer function $\mathbf{g}$ is a quasi multi-Gaussian distribution:

$$f(\mathbf{g}|\mathbf{p}) \propto \sqrt{\frac{1}{\Theta^{n_g-1}}} \exp\left(-\frac{1}{2}\mathbf{g}^T\mathbf{G}\mathbf{g}\right) \tag{27}$$

in which n_g is the number of elements in the transfer function and $\mathbf{G}$ is the inverse generalized covariance matrix of $\mathbf{g}$ corresponding to the linear variogram function and an unknown mean. $\mathbf{G}$ is a tridiagonal matrix with elements:

$$\begin{aligned}
G(1,1) &= \frac{1}{2\Theta}\frac{1}{\tau_2 - \tau_1} \\
G(i,i) &= \frac{1}{2\Theta}\left(\frac{1}{\tau_{i+1} - \tau_i} - \frac{1}{\tau_i - \tau_{i-1}}\right) \forall i > 1 \wedge i < n_g \\
G(n_g, n_g) &= \frac{1}{2\Theta}\frac{1}{\tau_{n_g} - \tau_{n_g-1}} \\
G(i, i-1) = G(i-1, i) &= \frac{1}{2\Theta}\frac{1}{\tau_i - \tau_{i-1}} \forall i > 1 \\
G(i, i+1) = G(i+1, i) &= \frac{1}{2\Theta}\frac{1}{\tau_{i+1} - \tau_i} \forall i < n_g
\end{aligned} \tag{28}$$

It may be noted that $\mathbf{G}$ is a singular matrix by construction, in which the vector of ones spans the nullspace. The $(n_g - 1)$ nonzero eigenvalues are proportional to Θ^{-1}, explaining the prefactor of equation (27). As discussed by *Kitanidis* [1997], assuming a linear variogram function in 1-D applications is identical to first-order Tikhonov regularization.

Taking the negative logarithm of equation (22) yields the following objective function to be minimized in the optimization procedure:

$$W_2(\mathbf{p}, \mathbf{g}) = \frac{1}{2}(\mathbf{c}_{\text{meas}} - \mathbf{c}_{\text{sim}}(\mathbf{p}, \mathbf{g}))^T \mathbf{C}^{-1} (\mathbf{c}_{\text{meas}} - \mathbf{c}_{\text{sim}}(\mathbf{p}, \mathbf{g})) + \frac{1}{2}\mathbf{g}^T\mathbf{G}\mathbf{g} + \frac{n_g - 1}{2}\ln\Theta + constant \tag{29}$$

in which we have substituted the distribution functions into equation (22). The first term of equation (29) penalizes large residuals between measured and simulated concentrations and the second term penalizes strong fluctuations in the hyporheic transfer function $g_{0,k}(\tau)$ of the conservative tracer. The third term stems from the smoothness parameter Θ appearing in the factor preceding the exponential term of equation (27). Because we make Θ a parameter to be estimated, we can minimize the second term, which is proportional to Θ^{-1}, by maximizing Θ, which would be equivalent to assuming that $g_{0,k}(\tau)$ is a strongly fluctuating function. The third term of equation (29) thus penalizes choosing particularly large slopes Θ of the semivariogram function $\gamma_{gg}(\triangle\tau)$.

The key idea of our local-in-global optimization is to split the objection function $W_2(\mathbf{p}, \mathbf{g})$ into two parts. In the outer loop, the parameters $\mathbf{p}$ are optimized assuming that the optimal values of $\mathbf{g}$, required to compute

the second term of equation (27), are a unique function of the chosen values of **p**. In the inner loop, the optimal values of **g** for given values of **p** are determined. For the outer loop, we use a global optimization method, whereas a gradient-based optimization method is used for the inner loop.

3.2. Global Optimization With DREAM(ZS)

We estimated the parameter vector **p** (see above) for each section using DREAM(ZS) [*Laloy and Vrugt*, 2012]. This algorithm is an adaptation of the DiffeRential Evolution Adaptive Metropolis (DREAM) algorithm [*Vrugt et al*., 2008, 2009], a multichain Markov Chain Monte Carlo method that automatically tunes the orientation and scale of the proposal distribution. Furthermore, it maintains detailed balance and ergodicity and is also very efficient in sampling high-dimensional search spaces. It runs several chains in parallel, and jumps in each chain are created by adding a fixed multiple of the difference between two other, randomly chosen chains. The Metropolis ratio is used to determine whether a parent individual is to be replaced by its child parameter set, and the evolutionary mechanisms are incorporated by estimating a distribution of crossover probabilities during a burn-in period (the period until which the generated states have become independent of the initial state) to speed up convergence. For details on the DREAM algorithm, see *Vrugt et al*. [2008, 2009].

DREAM(ZS), unlike DREAM, samples from an archive of past states to generate new parameter sets, thereby reducing the number of required chains and increasing the efficiency by shortening the burn-in period [*Laloy and Vrugt*, 2012]. The number of total function evaluations required for model convergence is therefore reduced.

In our approach, DREAM(ZS) is not used directly to modify the discretized hyporheic transfer function **g** of the conservative tracer. Instead, we obtain optimal values of **g** for given values of **p** by a nested optimization step, leading to a unique relationship $\mathbf{g}(\mathbf{p})$. The corresponding values of **g** are substituted into the objection function of equation (29). Because the local optimization is computationally expensive, the reduction of function calls implemented in DREAM(ZS) is particularly advantageous in our application.

3.3. Inference of the Hyporheic Transfer Function $g_{0,k}(\tau)$ for Given Other Parameters

The objective function to be minimized for the estimation of **g** given **p** reads as:

$$W_1(\mathbf{g}_\ell|\mathbf{p}) = \frac{1}{2}(\mathbf{c}_{\text{meas}} - \mathbf{c}_{\text{sim}}(\mathbf{p},\mathbf{g}_\ell))^T \mathbf{C}^{-1}(\mathbf{c}_{\text{meas}} - \mathbf{c}_{\text{sim}}(\mathbf{p},\mathbf{g}_\ell)) + \frac{1}{2}\mathbf{g}_\ell^T \mathbf{G}\mathbf{g}_\ell \tag{30}$$

$$\approx \frac{1}{2}(\mathbf{c}_* - \mathbf{J}_\ell \mathbf{g}_\ell)^T \mathbf{C}^{-1}(\mathbf{c}_* - \mathbf{J}_\ell \mathbf{g}_\ell) + \frac{1}{2}\mathbf{g}_\ell^T \mathbf{G}\mathbf{g}_\ell \tag{31}$$

with

$$\mathbf{c}_* = \mathbf{c}_{\text{meas}} - \mathbf{c}_{\text{sim}}(\mathbf{p},\mathbf{g}_\ell) + \mathbf{J}_\ell \mathbf{g}_\ell \tag{32}$$

in which equation (31) is the linearization of equation (30), ℓ is the iteration index of the nested optimization, and $\mathbf{J}_\ell$ is the Jacobian with elements $\partial c_{sim,i}/\partial g_j$ (for details see *Liao and Cirpka* [2011]). The first term of equation (31) penalized large residuals between measured and simulated concentrations whereas the second term penalizes strong fluctuations of **g**.

The hyporheic transfer function $g_{0,k}(\tau)$ of the conservative tracer is a continuous function constrained to be nonnegative for all travel times τ, which is achieved in the following using the method of Lagrange multipliers. For the determination of $\mathbf{g}_\ell$, a third term containing the constraint multiplied by the Lagrange multipliers $\boldsymbol{\eta}$ is added to equation (31), and the full expression is minimized by setting the derivatives with respect to $\mathbf{g}_\ell$ and $\boldsymbol{\eta}$ to zero. This results in the following system of linear equations:

$$\begin{bmatrix} \mathbf{J}_\ell \mathbf{C}^{-1} \mathbf{J}_\ell + \mathbf{G} & \mathbf{H}^T \\ \mathbf{H} & 0 \end{bmatrix} \begin{bmatrix} \mathbf{g}_\ell \\ \boldsymbol{\eta} \end{bmatrix} = \begin{bmatrix} \mathbf{J}_\ell \mathbf{C}^{-1} \mathbf{c}_* \\ \mathbf{0} \end{bmatrix} \tag{33}$$

in which the matrix **H** has a value of one in element (*i*, *j*) if the *i*th constraint is that the *j*th element of $\mathbf{g}_\ell$ is forced to be zero. All other elements of **H** are zeros. Setting the constraints is done in yet another nested iteration. If the last solution of equation (33) yields an element of $\mathbf{g}_\ell$ that is smaller than zero, this element is forced to be zero in the next iteration by setting a constraint. Constraints can be removed when elements of $\boldsymbol{\eta}$ are larger than zero [e.g., *Liao and Cirpka*, 2011; *Cirpka et al*., 2007]. This procedure is carried out until

the Lagrange multipliers do not change anymore from one iteration to the next or for a maximum of 10 iterations, after which any remaining negative entries are forced to zero.

We thus end up with three nested loops: The outermost loop is the global optimization by DREAM(ZS), in which different trials of the parameter vector **p** are tested. In each call of the objective function $W_2(\mathbf{p}, \mathbf{g})$, performed by DREAM(ZS), the discretized hyporheic transfer function **g** of the conservative tracer is obtained by the Gauss-Newton method in the intermediate loop, minimizing $W_1(\mathbf{g}_\ell|\mathbf{p})$, which requires linearization because the concentrations depend on **g** in a nonlinear way. Finally, each Gauss-Newton step requires internal iterations (in the innermost loop) to obtain the right set of Lagrange multipliers for a given Jacobian $\mathbf{J}_\ell$.

It should be noted here that opposed to the algorithm of *Liao et al*. [2013], only the hyporheic transfer function of the conservative tracer is optimized by the Gauss-Newton method. *Liao et al*. [2013] combined the estimation of all other parameters **p** with the updating of the hyporheic transfer function **g**, whereas we decompose the problem into two different subproblems tackled individually by the global and local optimization steps. This has the advantage that the estimated parameters **p** depend less on the initial guess as a far greater search space is sampled, and are therefore more reliable. Also, we obtain the posterior distribution of the parameters without relying on linearized uncertainty propagation. The interplay of the combination of global and local optimization is illustrated in Figure 1.

4. Application

4.1. Description of Field Data

We apply the approach to tracer concentrations from a reactive stream-tracer test at River Goldersbach, a second-order stream within the Neckar catchment in South-West Germany near the city of Tübingen. The test was performed in the night from May 12 to 13, 2015. River Goldersbach is a small stream of approximately 9 km length (mean annual discharge 0.25 m^3/s), draining a catchment of close to 72 km^2 [*Grathwohl et al*., 2013] with low anthropogenic influence. The stream flows through the Schönbuch reserve, a large mixed and coniferous forest. The geology of the study section is dominated by sandstones and mudstones of the Upper Triassic. The stream bed is of clayey and sandy consistency, with some gravel sections. The steady bed slope along the 600 m long study section is slightly smaller than 1%, and the discharge at the time of the tracer test was close to 140 L/s with an insignificant increases toward the downstream measurement stations ($<$1%) as determined by tracer dilution.

In total, 2.00 g of fluorescein and 25.61 g of resazurin were injected during a slug injection as conservative and reactive tracers. The first measurement station was located 165 m downstream of the injection site, whereas the second and third sections were 219 and 192 m long, respectively (see Figure 2). At these measurement stations, breakthrough curves of fluorescein, resazurin, and the reaction product resorufin were recorded in 10 s intervals with the help of an online fluorometer (GGUN-FL30, see *Lemke et al*. [2012], for details). Concentrations were validated by a number of grab samples that were collected over the course of the breakthrough curve and analyzed on a high-precision laboratory fluorometer. The breakthrough curves were smoothed before further processing by means of a moving median with window size 7 to remove potential outliers.

The temporal resolution of the concentration breakthrough curves was adjusted for the fitting procedure. A high resolution was chosen for the start, peak, and first part of the tailing of the breakthrough curves, and a coarser temporal resolution for the remaining part of the breakthrough curves. This approach was chosen to limit the number of measurements and speed up calculations, but still account for the increased spreading of breakthrough curves with greater distances from the injection point. The supporting information contain both the original breakthrough curves (full resolution with outliers), and the time series used for parameter estimation (cleaned with adaptive time resolution).

Even more important for the computation time is the length of the hyporheic travel time vector τ. Since small travel times were expected to play a greater role than large ones, a pseudologarithmic scaling was applied to the travel time vector τ with a high resolution of 5 s for the first 100 s, a 10 s resolution for the following 300 s, and a logarithmically increasing scaling thereafter (80 and 100 time intervals between 400 s and 1×10^5 s for the last and the other stream sections, respectively).

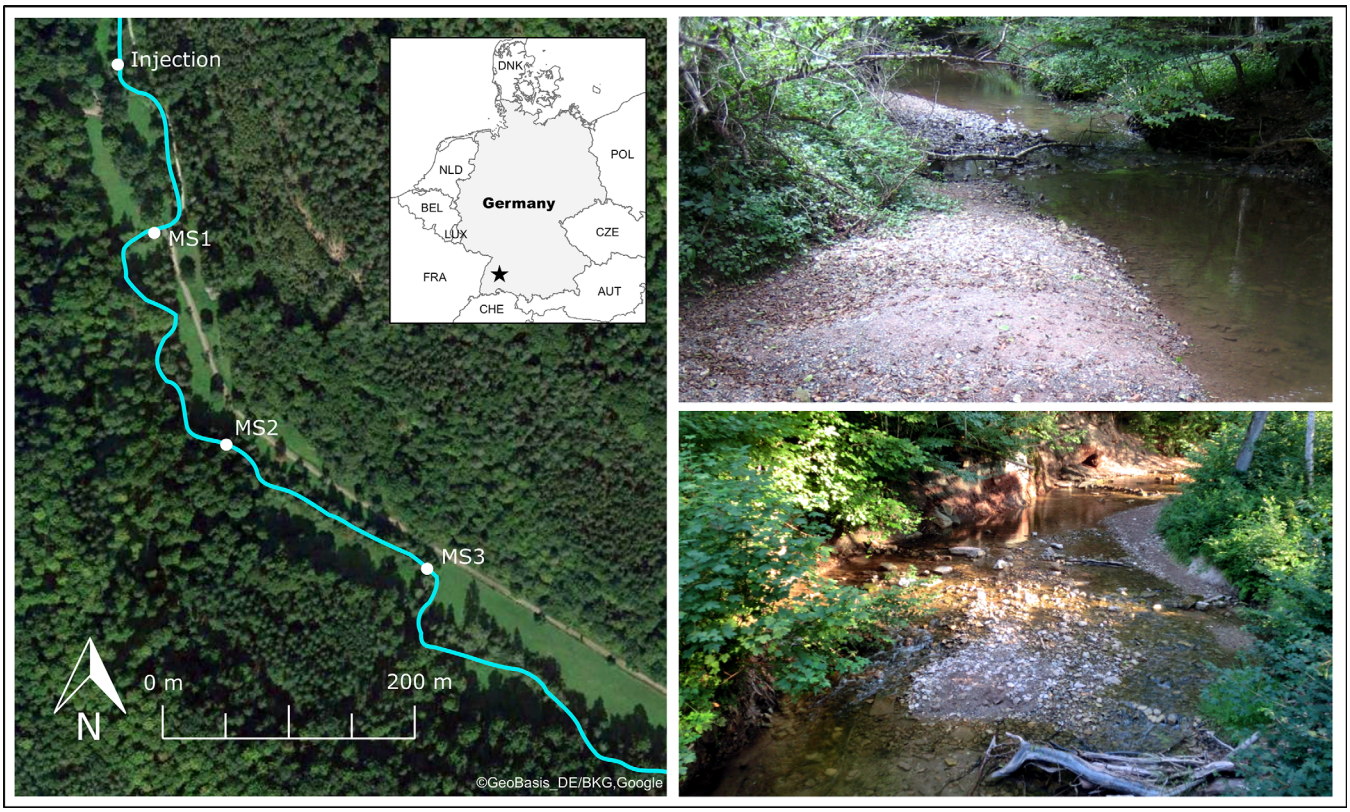

Figure 2. Map of the study sections at River Goldersbach, showing the location of the injection site and the different measurement stations. The photographs on the right illustrate the general setting of River Goldersbach.

The quantification limits of the GGUN-Fl 30 fluorometers for the different compounds were chosen as absolute error ε_{abs} (fluorescein: 0.266 μmol/m^3, resazurin: 3.981 μmol/m^3, resorufin: 2.345 μmol/m^3) and the relative error ε_{rel} was set to 1%.

4.2. Optimization Procedure

For each stream section, we first ran eight communicating chains with 8000 generations each (thus, 64,000 function evaluations per stream section) with measured concentrations of fluorescein and resazurin to jointly estimate all parameters related to these two tracers (eight in total, marked with an asterisk in Table 1). Wide initial parameter ranges were chosen with uniform sampling distribution (i.e. diffuse prior). After completion, function evaluations from the burn-in period (at least the first 70%) were discarded and only the best 10% (6,400 function evaluations) of all function evaluations were used to determine the posterior distributions of the estimated parameters.

After the successful estimation of parameters related to fluorescein and resazurin, the remaining five parameters associated with the production and decay of resorufin were estimated in a separate optimization run with five communicating chains with 50,000 generations each (thus, 250,000 function evaluations per stream section for resorufin-related parameters). For this, parameter sets of the eight jointly estimated parameters and the associated conservative transfer function $g_0(\tau)$ were drawn from the accepted ensemble members of the joint fit; the transfer function $g_1(\tau)$ of resazurin was evaluated for each ensemble member in a forward run, and then the resorufin parameters were fitted. A new parameter set was used for every function evaluation. Afterward, the first 90% of all function evaluations were discarded and the posterior parameter distributions and the hyporheic transfer functions $g_2(\tau)$ and $g_{12}(\tau)$ determined from the remaining 25,000 runs.

This approach was chosen to optimize computation time. Estimating the resorufin-related parameters requires accessing the transfer function of fluorescein, and is therefore very time consuming when it is incorporated into the updating of $g_0(\tau)$. In the chosen approach, $g_0(\tau)$ was only sensitive to parameters of

fluorescein and resazurin, but assumed fixed for the fitting of the resorufin curves. For the reaction product, only the global optimization step was therefore necessary, whereas the local optimization step was skipped. This facilitated parallelization of optimization steps (that is, the estimation of the resorufin-related parameters of stream section k can be performed while the fluorescein and resazurin optimization for stream section $k+1$ is already running), thus speeding up the whole process. This approach is valid because all parameters related to fluorescein and resazurin are independent of those related to resorufin (but not vice versa).

Due to the different time increments used for the different sections, an updating of the Laplace transformed input concentrations (see equation (10)) was necessary before the parameter estimation could commence for the following stream section. This is necessary because the tracer concentrations in Laplace space are calculated recursively, which requires concentration vectors of the previous section to be called and incorporated into the computation for all but the first stream section.

4.3. Results

The measured and fitted breakthrough curves are depicted in Figure 3. Measured concentration curves are shown as black dots, while colored lines indicate simulated breakthrough curves of fluorescein (green), resazurin (blue), and resorufin (red). The absolute peak concentrations (right) for fluorescein are much lower than those of resazurin due to the lower injected mass of the conservative tracer. However, we normalized the concentrations by the injected tracer masses so that differences between fluorescein and resazurin in the linearly scaled left subplot of Figure 3 mainly illustrate the loss of resazurin along the reach. The fit between measured and modeled concentrations is generally good for all stream sections with tracer concentrations above the limit of quantification of the applied instruments (goodness of fit quantified by the root mean square error normalized by the peak concentration of the curve, $nRMSE_{fluo}=2.1\times10^{-3}$, 4.4×10^{-3}, 1.1×10^{-2} for fluorescein, $nRMSE_{raz}=2.2\times10^{-3}$, 4.7×10^{-3}, 9.6×10^{-3} for resazurin, and $nRMSE_{rru}=9.7\times10^{-3}$, 7.8×10^{-2}, 8.5×10^{-2} for resorufin, see Table 2). The relative residuals increase once the tracer concentrations fall below the limit of quantification (shown in the right subplot of Figure 3 as horizontal dashed lines). Furthermore, the normalized error is of similar magnitude for fluorescein and resazurin, indicating that both curves were fitted equally well during the joint estimation, but larger for resorufin. For all three tracers, the error increases slightly with each consecutive stream section as would be expected, because uncertainties from previous sections carry over to the next. This means that errors from previous sections are likely not overcompensated by the fitting of the data in the following sections. That the global optimum was obtained during the joint estimation procedure for fluorescein and resazurin is also corroborated by the convergence statistics illustrated in supporting information Figure S1, showing the evolution of the $\hat{R}$-statistics of *Gelman and Rubin* [1992] of each parameter over the course of the optimization

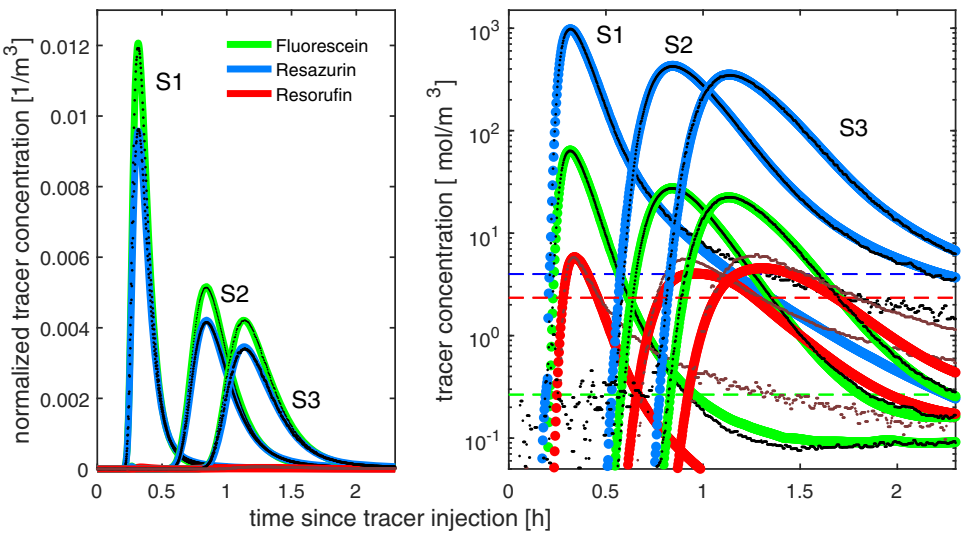

Figure 3. Measured (black dots for fluorescein and resazurin, and brown dots for resorufin) and simulated breakthrough curves with (left) linear and (right) logarithmic concentration scaling. Left concentrations are normalized by injected tracer masses. Dashed horizontal lines on the right indicate limits of tracer quantification.

Table 2. Estimated Parameters for the Different Stream Sections[a]

Symbol	Unit	Section 1	Section 2	Section 3
L	m	165	219	192
v	m/s	$1.7\times10^{-1} \pm 3.5\times10^{-4}$	$1.2\times10^{-1} \pm 1.2\times10^{-4}$	$2.0\times10^{-1} \pm 2.0\times10^{-4}$
D	m^2/s	$9.7\times10^{-2} \pm 1.5\times10^{-3}$	$3.7\times10^{-1} \pm 2.1\times10^{-3}$	$2.1\times10^{-1} \pm 3.2\times10^{-3}$
q^{he}	1/s	$3.3\times10^{-3} \pm 5.6\times10^{-5}$	$3.2\times10^{-4} \pm 3.7\times10^{-6}$	$3.4\times10^{-4} \pm 3.3\times10^{-6}$
λ_1	1/s	$4.0\times10^{-4} \pm 6.5\times10^{-6}$	$3.2\times10^{-5} \pm 1.8\times10^{-6}$	$2.6\times10^{-5} \pm 2.6\times10^{-6}$
R_1		$1.17 \pm 2.4\times10^{-3}$	$1.02 \pm 2.6\times10^{-3}$	$1.00 \pm 2.5\times10^{-3}$
K_1		$1.9\times10^{-1} \pm 1.3\times10^{-2}$	$1.7\times10^{-2} \pm 2.3\times10^{-3}$	$1.7\times10^{-3} \pm 2.0\times10^{-3}$
k_1	1/s	$1.3\times10^{-3} \pm 5.7\times10^{-5}$	$6.4\times10^{-1} \pm 3.6\times10^{-2}$	$9.4\times10^{-1} \pm 6.7\times10^{-2}$
$\log_{10}(\Theta)$	Θ in $1/s^3$	$-8.80 \pm 1.2\times10^{-2}$	$-11.25 \pm 1.0\times10^{-2}$	$-11.39 \pm 1.3\times10^{-2}$
λ_2	1/s	$5.6\times10^{-2} \pm 2.8\times10^{-3}$	$2.1\times10^{-5} \pm 4.7\times10^{-5}$	$1.6\times10^{-5} \pm 3.6\times10^{-5}$
λ_{12}	1/s	$4.1\times10^{-4} \pm 2.0\times10^{-5}$	$3.0\times10^{-5} \pm 7.8\times10^{-7}$	$2.7\times10^{-5} \pm 8.5\times10^{-7}$
R_2		$1.39 \pm 1.5\times10^{-1}$	$1.04 \pm 8.6\times10^{-2}$	$1.07 \pm 1.5\times10^{-1}$
K_2		$7.6\times10^{-1} \pm 1.8\times10^{-1}$	$3.1\times10^{-2} \pm 7.0\times10^{-2}$	$8.5\times10^{-2} \pm 1.3\times10^{-1}$
k_2	1/s	$3.4\times10^{-1} \pm 3.2\times10^{-2}$	$7.6\times10^{-2} \pm 4.8\times10^{-2}$	$2.4 \pm 1.7\times10^{-1}$
$nRMSE_{fluo}$		2.1×10^{-3}	4.4×10^{-3}	1.1×10^{-2}
$nRMSE_{raz}$		2.2×10^{-3}	4.7×10^{-3}	9.6×10^{-3}
$nRMES_{rru}$		9.7×10^{-3}	7.8×10^{-2}	8.5×10^{-2}
$\bar{\tau}$	min	2.4 ± 0.2	9.3 ± 0.4	9.8 ± 0.4
λ_d^a	1/s	0 by construction	$1.6\times10^{-6} \pm 2.4\times10^{-6}$	$1.3\times10^{-5} \pm 4.2\times10^{-6}$
λ_1^a	1/s	$1.6\times10^{-4} \pm 8.5\times10^{-6}$	$5.6\times10^{-6} \pm 1.5\times10^{-6}$	$4.2\times10^{-6} \pm 2.6\times10^{-6}$
λ_2^a	1/s	$2.9\times10^{-3} \pm 2.9\times10^{-4}$	$1.5\times10^{-5} \pm 1.1\times10^{-5}$	$1.7\times10^{-5} \pm 1.3\times10^{-5}$
λ_{12}^a	1/s	$2.0\times10^{-5} \pm 7.7\times10^{-6}$	$4.7\times10^{-6} \pm 3.7\times10^{-7}$	$4.6\times10^{-6} \pm 4.3\times10^{-7}$
$x_{c,raz}$	km	1.03	22.03	48.54
$x_{c,rru}$	km	0.06	8.34	12.06

[a]The section length L was not estimated, but determined from a site survey.

process. If a value of 1.2 or smaller is obtained for all parameters during the given number of function evaluations, convergence to a limiting distribution can be considered successful. This is the case for all stream sections here.

The modeled curves represent the median concentrations obtained from a forward run with an ensemble of the estimated parameters based on the 6400 function evaluations (or 25,000 function evaluations in case of resorufin) remaining after the evaluations of the burn-in period had been discarded. The simulations shown therefore represent samples drawn from the full posterior parameter distributions, instead of only a single best fit. Metrics of these distributions are given in Table 2 (best fit parameters and standard deviations), whereas plots of the full parameter distributions are included in the supporting information (Figures S3–S5). The distributions are very narrow—especially for the joint fit of fluorescein and resazurin, with parameter distributions generally encompassing a spread of only 10% or less of the most likely value. This indicates a high reliability of the fitted parameters.

The five parameters related to the reaction product resorufin could be determined with much less confidence. To a small extent, the large uncertainty of these parameters is caused by estimating the resorufin-related parameters using realizations of the other eight parameters drawn from the posterior ensemble of the joint fluorescein and resazurin fit, leading to a propagation of the uncertainty to the resorufin estimation. However, the small posterior variability of the eight parameters fitted first is only responsible for a very small part of the uncertainty of the resorufin-related parameters. A second reason for the relatively poor identifiability of the resorufin-related parameters is that the measured resorufin concentrations are quite low, falling below the level of quantification over practically the entire plume tails. [*Lemke et al*., 2012, Figure7] observed a systematic bias of the on-line fluorometer used in this study toward higher values for concentrations below the level of quantification, which would deem the heavy tails of resorufin artifacts. A third potential reason for large parameter uncertainty and mediocre fit of the resorufin tails could be conceptual uncertainty of the processes affecting resorufin concentrations. In our model, we assume that resorufin undergoes two-site sorption and first-order decay, whereas it is known that resorufin can reversibly be reduced to the nonfluorescent compound dihydroresorufin. Nothing is known regarding the sorption behavior of dihydroresorufin, thus, we cannot exclude that the elevated concentrations of resorufin in the tails are caused by delayed emergence of dihydroresorufin from the subsurface and subsequent reoxidation of dihydroresorufin to resorufin. In our study, the resorufin-related parameters regarding production and decay are strongly correlated, implying that the data are not informative enough to separate the effects of

the different processes affecting resorufin. An insufficient number of function evaluations and therefore incomplete convergence can be excluded as reason for broad parameter ranges, as the convergence statistics in the supporting information (Figure S2) show.

The obtained parameters generally lie in the expected ranges. Both the advective velocity v and the dispersion coefficient D do not differ greatly between the individual stream sections, which can be explained by the similarity of flow and morphology among the individual stream sections. The exchange parameters, by contrast, differ between the stream sections: the exchange rate q^{he} in the first section is about one order of magnitude higher than in the following two sections, and so is the transformation rate for resazurin, λ_1. Interestingly, nearly all resazurin is transformed to resorufin in all stream sections ($\lambda_{12} \approx \lambda_1$), but while the degradation of resorufin is negligible in the later stream sections, it is relatively high in the first section.

Our coefficients were obtained from instantaneous tracer injections, whereas the majority of studies inject the tracer compounds continuously over a longer time period. A continuous injection has the advantage that stationarity is achieved, facilitating the analysis of the resazurin-to-resorufin turnover, but is more expensive due to the high cost of resazurin. Ensuring comparability between our parameters and those determined in other studies with constant injection requires a conversion of our coefficients to apparent coefficients comparable to those obtained during continuous injections. The approach is explained in Appendix A and the values of the recoveries $\int_0^\infty g_i(\tau)\, d\tau$ and $\int_0^\infty g_{12}(\tau) d\tau$ for the different sections required for this calculated are listed in the supporting information (data set S7). The calculated apparent parameters that are adjusted for changes in discharge along the reach are given in Table 2. These decay and transformation rate coefficients are somewhat smaller than those observed by *Haggerty et al*. [2008, 2009], and this difference is most notable for stream sections 2 and 3, where our rate constants are up to one order of magnitude smaller. This difference probably reflects differences in site-specific properties of the sediment. That these constants may vary quite significantly between different streams and different reach sections was shown by *González-Pinzón et al*. [2014, 2015] and is the whole idea of using resazurin as a proxy tracer for aerobic respiration. *González-Pinzón et al*. [2014, 2015] assumes that the apparent decay constants of resazurin are proportional to respiration rates, which would hint at lower metabolic rates in our stream compared to those observed by studies conducted in the H.J. Andrews Experimental Forest [e.g., *González-Pinzón et al*., 2014, 2015; *Argerich et al*., 2011] (please note that the scaling factors of molar processing ratio of dissolved oxygen to resazurin K_{DO}^{Raz} suggested by *González-Pinzón et al*. [2012] were not determined, so absolute respiration rates cannot be computed). Our transformation rates, however, are in agreement with other reactive tracer studies conducted in lowland streams of temperate regions [e.g., *Liao et al*., 2013; *González-Pinzón et al*., 2014, 2015].

Figure 4 illustrates the estimated hyporheic transfer functions of the conservative tracer, $g_0(\tau)$, the reactive tracer, $g_1(\tau)$, and the reaction product, $g_2(\tau)$, as well as the cross-compound transfer function $g_{12}(\tau)$ quantifying the resorufin leaving the hyporheic zone for resazurin entering it. Figure 4 shows the median transfer functions as black solid lines and the probability range within the ensemble between 16% and 84% as gray shaded area, which would cover $\pm$ one standard deviation if the underlying distribution was Gaussian.

As mentioned above, the hyporheic transfer function $g_0(\tau)$ of the conservative tracer equals the recovery of the conservative tracer times the distribution of hyporheic travel times. The detected recoveries of the conservative tracer are 1.0 by construction in the first stream section, and 0.995 ± 0.008, respectively, 0.963 ± 0.011, in stream sections 2 and 3, indicating that dilution with water not originating from the stream was small. This is in agreement with a good fit of the measured curves to the grab samples and a low uncertainty of these grab samples (not shown here). The detected mean travel times in the hyporheic zone are generally short ($\bar{\tau} = 2.4 \pm 0.2$ min, $\bar{\tau} = 9.3 \pm 0.4$ min, and $\bar{\tau} = 9.8 \pm 0.4$ min for stream sections 1–3). This is smaller, but still in agreement with results of *Liao et al*. [2013], who found average travel times of 16 min for a downstream study section of the same stream. Differences to our study may be explained by lower discharge and finer bed sediments in the upper section, leading to smaller penetration depths and thus shorter overall hyporheic travel times, pointing toward small riffle-like features as the most important features for hyporheic exchange in the study reach.

The shape of the median hyporheic travel time distribution ($g_0(\tau)/\int_0^\infty g_0(\tau) d\tau$) resembles a truncated Gaussian distribution, whereas shapes of individual ensemble members range between two different extremes. While one end of the continuum of transfer functions may be described by a rapid decay that resembles the decay of an exponential distribution, the other extreme features a clearly distinct secondary

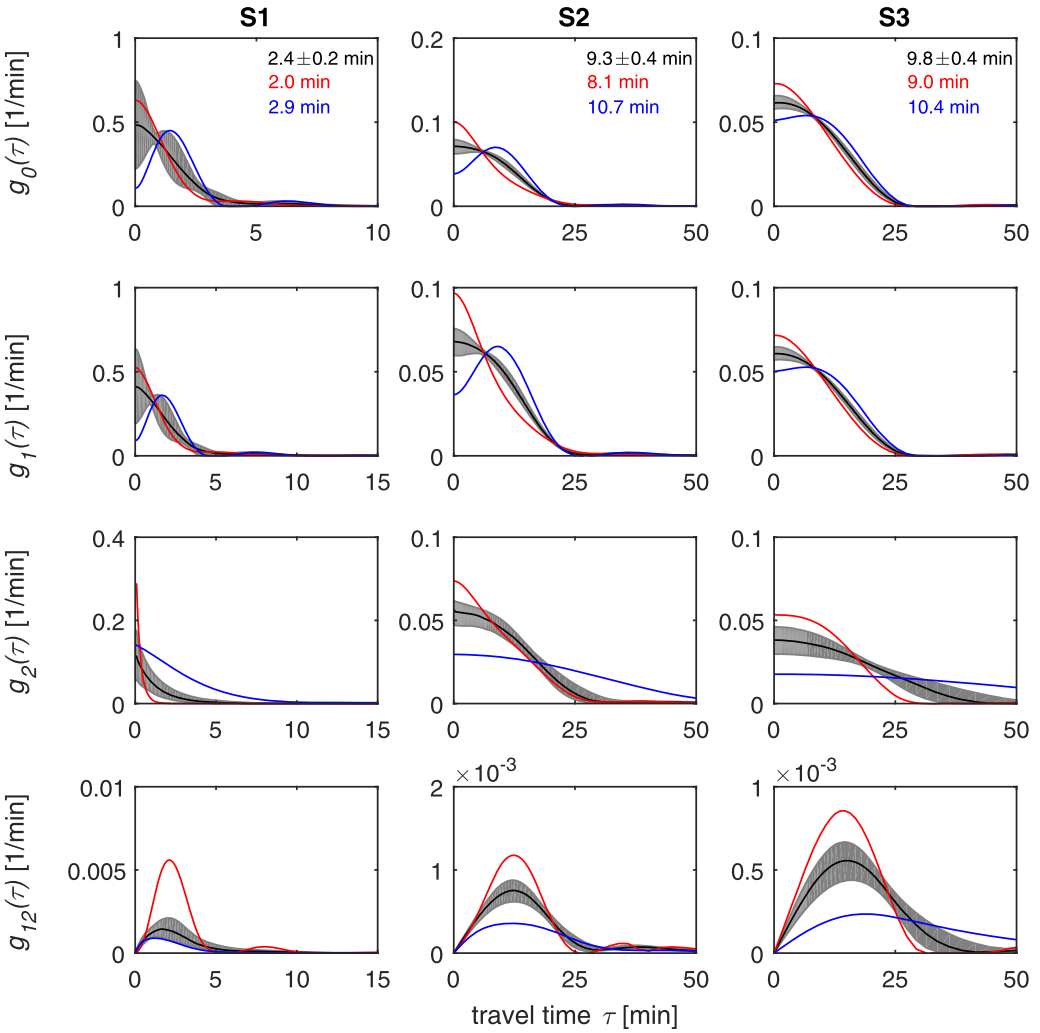

Figure 4. Hyporheic transfer functions $g_0(\tau)$, $g_1(\tau)$, $g_2(\tau)$, and $g_{12}(\tau)$ for all three stream sections. Solid black lines indicate median transfer functions of the ensemble, whereas the shaded areas depict the probability range between 16% and 84%. The blue and red lines illustrate two examples of extreme transfer functions. Panels for $g_0(\tau)$ also display mean travel times of the ensemble (black) and of the two extreme cases of travel time shapes displayed in the figure.

peak. Individual examples of extreme cases (outside the range of one standard deviation from the median) are shown in Figure 4 as blue and red lines. The different shapes of the hyporheic travel time distributions go along with different hydraulic parameters, with the combination of slightly lower dispersion coefficients D and higher hyporheic exchange rates q^{he} causing secondary or even tertiary peaks in the hyporheic travel time distribution, while higher dispersion coefficients in combination with lower hyporheic exchange rates favor exponential-like decay. In combination with the appropriate set of hydraulic parameters, both shapes of the hyporheic travel time distributions are able to fit the measured concentration breakthrough curves equally well. While both extreme shapes of the travel time distribution feature very similar recovery rates, the mean hyporheic travel times differ significantly, with much lower ones for those distributions with exponential decay than those featuring secondary peaks (see Figure 4).

The shape of the hyporheic travel time distribution carries over to the hyporheic transfer function $g_1(\tau)$ of resazurin. The delay of $g_1(\tau)$ in comparison to $g_0(\tau)$ is negligible, which is in accordance to small sorption coefficients (R_1 is close to unity, and K_1 close to zero). The decay of resazurin, already indicated by the loss of normalized concentration in the breakthrough curves shown in Figure 3, leads to a decrease in tracer recovery of resazurin in comparison to the conservative tracer. By contrast, the resazurin decay was relatively small, as is indicated by the recovery rates of 0.952 ± 0.005, 0.977 ± 0.007, and 0.951 ± 0.011 in the stream sections 1–3. These values are only slightly lower than the recoveries of the conservative tracer

stated above and are furthermore in agreement with by the already discusses small decay rates of the reactive tracer, revealing total resazurin decay of only a few percent. Consequently, the characteristic distances, after which only $1/e$ of the tracer mass remained, are very long for resazurin, ranging from approximately 1 km for the first section to 48 km for the last section, illustrating the low amount of tracer decay.

The hyporheic transfer functions $g_2(\tau)$ of resorufin are more strongly modified than those of resazurin, which can be explained by the interplay of stronger sorption ($R_2 > 1$, and $K_2 > 0$) at least for stream section S1, facilitating a time delay in comparison to the hyporheic travel time distributions $g_0(\tau)$, and stronger decay, which attenuates the tails. The wide parameter distributions explain why the importance of late travel times differs greatly between different shapes of the transfer function, and why some are marked by rapid decay, while others feature pronounced tailing.

The cross-compound transfer function $g_{12}(\tau)$ has a significantly different shape than the hyporheic travel time distribution or the single-compound transfer functions, $g_0(\tau)$, $g_1(\tau)$, and $g_2(\tau)$. In particular, it can be seen that the build-up of resorufin in the hyporheic zone takes time. In water parcels, returning after only a very short hyporheic passage, hardly any resazurin has been transformed to resorufin. That is, $g_{12}(\tau)$ starts at a value of zero for $\tau = 0$ by construction. The cross-compound transfer function $g_{12}(\tau)$ drops again at later hyporheic travel times because most water parcel have already left the hyporheic zone. Like for $g_2(\tau)$, the importance of late travel times differs greatly between some of the extreme shapes. This effect becomes more pronounced with greater distances from the injection site.

Liao et al. [2013] determined the 12 physical and reactive parameters listed in Table 1, and chose a value of $1\times10^{-12}/s^3$ for the smoothness parameter Θ based on visual inspection of the simulated breakthrough curves. In contrast, the smoothness parameter for the first stream section obtained in this study was approximately three orders of magnitude larger than those of the other two stream sections as result of our extensive optimization procedure, illustrating that a selection of the smoothness parameter based on visual inspection may not be an ideal procedure.

5. Conclusions

We have presented an efficient, reliable method of estimating a set of hydraulic and reactive parameters for solute transport in streams undergoing hyporheic exchange, together with a shape-free representation of the hyporheic travel time distribution. The optimization framework builds on nesting the local estimation of the hyporheic travel time distribution, keeping the other parameters fixed, into a global estimation of the hydraulic and reactive parameters together with the requested smoothness parameter of the hyporheic travel time distribution. This scheme yielded the posterior distribution of parameter sets for each stream section without relying on linearization and quantifying the parameter uncertainty in a reliable way. The nested approach also facilitated inferring the hyporheic travel time distribution without predetermining its smoothness parameter in a relatively efficient way.

The presented predictive model is an advancement of that introduced by *Liao et al.* [2013]. Instead of obtaining parameters for increasingly longer stream sections reaching from the injection point to the various measurement locations, we changed the boundary conditions to subdivide the stream reach into several distinct sections, where the output of one section is the input to the next. Estimating the parameters of distinct, subsequent stream sections improves the ability to identify differences in hyporheic exchange, in-stream transport, and reactivity among the different sections. It comes at the cost of reevaluating solute concentrations in preceding stream sections when estimating parameters related to sections further downstream.

The ambiguity of the obtained hyporheic travel time distributions reveals the clear advantage of the shape-free over parametric approaches. Since the whole continuum of shapes is able to recreate the measured concentration breakthrough curves equally well, the data cannot point to a single "correct" parametric shape. Preconstraining the hyporheic travel time distribution to a specific shape is therefore not advantageous. Specifically, choosing the exponential distribution as simplest parametric choice leads to a bias in the estimated mean hyporheic travel times, since these are much shorter for transfer functions with exponential decay than for transfer functions with several later peaks. An accurate estimation of the hyporheic

residence time, however, is of great importance in practice, e.g., when the effect of stream restoration efforts are to be evaluated with respect to nutrient transformation in the hyporheic zone. The advantages of the shape-free approach therefore clearly outweigh the increased complexity and computational efforts required for its estimation.

Improving the analysis of reactive stream-tracer tests, as done in this study, does of course not overcome well-known principal limitations of such tests. From our tracer data, we could only determine effects of hyporheic travel paths of very short duration, essentially representing ripples. By construction, artificial-tracer tests cannot determine travel times on the order or longer than the duration of the experiment itself. If hyporheic paths of such travel times existed in the stream-system investigated, however, they did not carry a significant fraction of the discharge, as they would otherwise have caused a substantial reduction in the measured recovery of the conservative tracer.

While we have streamlined the method for the interpretation of reactive stream-tracer tests, the local-in-global optimization approach could be helpful for a much broader range of applications, in which a set of parameters must be estimated in addition to a continuous function. Examples could be source-identification problems of reactive compounds, in which either the release history or the initial spatial distribution of the reactants would be the continuous function to be estimated, and the reactive-transport parameters would be assumed a set of scalar values. Without any doubt, our application, in which the measured quantities (i.e., the concentration time series) depend on the continuous function (i.e., the hyporheic travel time distribution) in a nonlinear way, is computationally particularly challenging so that turning from an all-global optimization scheme to the nested local-in-global method appears especially advantageous.

Appendix A

Under stationary conditions ($\frac{\partial c}{\partial t}=0$), the transport equations read as:

$$v_k \frac{\partial c_{0,k}}{\partial x_k} - D_k \frac{\partial^2 c_{0,k}}{\partial x_k^2} = -\lambda^a_{d,k} c_{0,k} \tag{A1}$$

$$v_k \frac{\partial c_{1,k}}{\partial x_k} - D_k \frac{\partial^2 c_{1,k}}{\partial x_k^2} = \left(\lambda^a_{d,k} + \lambda^a_{1,k}\right) c_{1,k} \tag{A2}$$

$$v_k \frac{\partial c_{2,k}}{\partial x_k} - D_k \frac{\partial^2 c_{2,k}}{\partial x_k^2} = \left(\lambda^a_{d,k} + \lambda^a_{2,k}\right) c_{2,k} + \lambda^a_{12,k} c_{1,k} \tag{A3}$$

with the apparent dilution rate constant $\lambda^a_{d,k}$ [T^{-1}], the apparent decay rate constants of resazurin and resorufin, $\lambda^a_{1,k}$ [T^{-1}] and $\lambda^a_{2,k}$ [T^{-1}], respectively, and the apparent transformation rate constant $\lambda^a_{12,k}$ [T^{-1}] of stream section k.

Assuming constant concentrations c_i over time, comparison of coefficients with equations (1) and (2) leads to:

$$\lambda^a_{d,k} = q^{he}_k \left(1 - \int_0^\infty g_{0,k}(\tau) d\tau\right) \tag{A4}$$

$$\lambda^a_{1,k} = q^{he}_k \left(1 - \int_0^\infty g_{1,k}(\tau) d\tau\right) - \lambda^a_{d,k} \tag{A5}$$

$$\lambda^a_{2,k} = q^{he}_k \left(1 - \int_0^\infty g_{2,k}(\tau) d\tau\right) - \lambda^a_{d,k} \tag{A6}$$

$$\lambda^a_{12,k} = q^{he}_k \left(\int_0^\infty g_{12,k}(\tau) d\tau + \int_0^\infty g_{2,k}(\tau) d\tau - 1\right) + \lambda^a_{d,k} + \lambda^a_{2,k} = q^{he}_k \int_0^\infty g_{12,k}(\tau) d\tau \tag{A7}$$

These apparent decay and transformation rate coefficients allow a comparison to decay and transformation rate coefficients obtained from constant tracer injections [e.g., *Haggerty et al.*, 2009; *González-Pinzón et al.*, 2014, 2015], since they are corrected for the effect of dilution. Thus, the coefficients obtained from equations (A4–A7) allows relating resazurin transformation and decay to aerobic respiration.

Furthermore, characteristic lengths of disappearance $x_{c,i}$ can be calculated for the tracer compound i, which quantifies the theoretical travel distance after which only $1/e$ of the tracer mass present at the start of the section remains:

$$c_{out} = c_{in} \exp\left(-\lambda_{i,k} t\right) = c_{in} \exp\left(-\lambda_{i,k} \frac{x_c}{v_k}\right) = \frac{1}{e} c_{in}$$

$$x_{c,i} = \frac{v_k}{\lambda_{i,k}}$$

Acknowledgments
The first author of this manuscript was funded through a doctoral scholarship of the Carl-Zeiss Stiftung (Carl-Zeiss Foundation). We thank Marc Schwientek for providing the photographs of River Goldersbach in Figure 2. Data sets of measured concentrations can be found in the supporting information together with a MATLAB Code of the predictive model.

References

Argerich, A., R. Haggerty, E. Martí, F. Sabater, and J. Zarnetske (2011), Quantification of metabolically active transient storage (mats) in two reaches with contrasting transient storage and ecosystem respiration, *J. Geophys. Res.*, *116*, G03034, doi:10.1029/2010JG001379.

Bäck, T., and H.-P. Schwefel (1993), An overview of evolutionary algorithms for parameter optimization, *Evol. Comput.*, *1*(1), 1–23.

Bencala, K., and R. Walters (1983), Simulation of solute transport in a mountain pool and-riffle stream: A transient storage model, *Water Resour. Res.*, *19*(3), 718–724.

Cirpka, O., M. Fienen, M. Hofer, E. Hoehn, A. Tessarini, R. Kipfer, and P. Kitanidis (2007), Analyzing bank filtration by deconvoluting time series of electric conductivity, *Ground Water*, *45*(3), 318–328.

Gelman, A., and D. B. Rubin (1992), Inference from iterative simulation using multiple sequences, *Stat. Sci.*, *7*, 457–472.

González-Pinzón, R., R. Haggerty, and D. Myrold (2012), Measuring aerobic respiration in stream ecosystems using the resazurin-resorufin system, *J. Geophys. Res.*, *117*, G00N06, doi:10.1029/2012JG001965.

González-Pinzón, R., R. Haggerty, and A. Argerich (2014), Quantifying spatial differences in metabolism in headwater streams, *Freshwater Sci.*, *33*(3), 798–811.

González-Pinzón, R., A. S. Ward, C. E. Hatch, A. N. Wlostowski, K. Singha, M. N. Gooseff, R. Haggerty, J. W. Harvey, O. A. Cirpka, and J. T. Brock (2015), A field comparison of multiple techniques to quantify surface water – groundwater interactions, *Freshwater Sci.*, *34*(1), 139–160, doi:10.1086/679738.

Gooseff, M. N., S. M. Wondzell, R. Haggerty, and J. Anderson (2003), Comparing transient storage modeling and residence time distribution (rtd) analysis in geomorphically varied reaches in the lookout creek basin, Oregon, USA, *Adv. Water Resour.*, *26*(9), 925–937.

Grathwohl, P., et al. (2013), Catchments as reactors: A comprehensive approach for water fluxes and solute turnover, *Environ. Earth Sci.*, *69*(2), 317–333.

Haggerty, R., and S. M. Gorelick (1995), Multiple-rate mass transfer for modeling diffusion and surface reactions in media with pore-scale heterogeneity, *Water Resour. Res.*, *31*(10), 2383–2400.

Haggerty, R., A. Argerich, and E. Martí (2008), Development of a "smart" tracer for the assessment of microbiological activity and sediment-water interaction in natural waters: The resazurin-resorufin system, *Water Resour. Res.*, *44*, W00D01, doi:10.1029/2007WR006670.

Haggerty, R., E. Martí, A. Argerich, D. Von Schiller, and N. B. Grimm (2009), Resazurin as a "smart" tracer for quantifying metabolically active transient storage in stream ecosystems, *J. Geophys. Res.*, *114*, G03014, doi:10.1029/2008JG000942.

Harvey, J. W., B. J. Wagner, and K. E. Bencala (1996), Evaluating the reliability of the stream tracer approach to characterize stream-subsurface water exchange, *Water Resour. Res.*, *32*(8), 2441–2451.

He, M., T. S. Hogue, K. J. Franz, S. A. Margulis, and J. A. Vrugt (2011), Characterizing parameter sensitivity and uncertainty for a snow model across hydroclimatic regimes, *Adv. Water Resour.*, *34*(1), 114–127.

Joseph, J., and J. H. Guillaume (2013), Using a parallelized mcmc algorithm in r to identify appropriate likelihood functions for swat, *Environ. Modell. Software*, *46*, 292–298.

Kitanidis, P. K. (1997), The minimum structure solution to the inverse problem, *Water Resour. Res.*, *33*(10), 2263–2272.

Laloy, E., and J. A. Vrugt (2012), High-dimensional posterior exploration of hydrologic models using multiple-try dream (zs) and high-performance computing, *Water Resour. Res.*, *48*, W01526, doi:10.1029/2011WR010608.

Lemke, D., P.-A. Schnegg, M. Schwientek, K. Osenbrück, and O. A. Cirpka (2012), On-line fluorometry of multiple reactive and conservative tracers in streams, *Environ. Earth Sci.*, *69*, 349–358.

Lemke, D., Z. Liao, T. Wöhling, K. Osenbrück, and O. A. Cirpka (2013), Concurrent conservative and reactive tracer tests in a stream undergoing hyporheic exchange, *Water Resour. Res.*, *49*, 3024–3037, doi:10.1002/wrcr.20277.

Liao, Z., and O. A. Cirpka (2011), Shape-free inference of hyporheic traveltime distributions from synthetic conservative and "smart" tracer tests in streams, *Water Resour. Res.*, *47*, W07510, doi:10.1029/2010WR009927.

Liao, Z., D. Lemke, K. Osenbrück, and O. A. Cirpka (2013), Modeling and inverting reactive stream tracers undergoing two-site sorption and decay in the hyporheic zone, *Water Resour. Res.*, *49*, 3406–3422, doi:10.1002/wrcr.20276.

O'Brien, J., I. Wilson, T. Orton, and F. Pognan (2000), Investigation of the alamar blue (resazurin) fluorescent dye for the assessment of mammalian cell cytotoxicity, *Eur. J. Biochem.*, *267*, 5421–5426.

Press, W. H., S. A. Teukolsky, W. T. Vetterling, and B. P. Flannery (1992), *Numerical Recipes in FORTRAN 77: The Art of Scientific Computation*, 2nd ed., Cambridge Univ. Press, New York.

Runkel, R. (1998), One-dimensional transport with inflow and storage (otis): A solute transport model for streams and rivers, *U.S. Geol. Surv. Water Resour. Invest. Rep.*, *98*, 73 p., U.S. Geological Survey, Denver, Colo.

Ter Braak, C. J. F. (2004), *Genetic Algorithms and Markov Chain Monte Carlo: Differential Evolution Markov Chain Makes Bayesian Computing Easy*, 010404, Biometris, Wageningen University and Research Center, Wageningen, Netherlands.

Vrugt, J. A., C. J. Ter Braak, M. P. Clark, J. M. Hyman, and B. A. Robinson (2008), Treatment of input uncertainty in hydrologic modeling: Doing hydrology backward with Markov chain Monte Carlo simulation, *Water Resour. Res.*, *44*, W00B09, doi:10.1029/2007WR006720.

Vrugt, J. A., C. Ter Braak, C. Diks, B. A. Robinson, J. M. Hyman, and D. Higdon (2009), Accelerating Markov chain Monte Carlo simulation by differential evolution with self-adaptive randomized subspace sampling, *Int. J. Nonlinear Sci. Numer. Simul.*, *10*(3), 273–290.

Wagener, T., L. A. Camacho, and H. S. Wheater (2002), Dynamic identifiability analysis of the transient storage model for solute transport in rivers, *J. Hydroinf.*, *4*(3), 199–211.

Wörman, A., A. I. Packman, H. Johansson, and K. Jonsson (2002), Effect of flow-induced exchange in hyporheic zones on longitudinal transport of solutes in streams and rivers, *Water Resour. Res.*, *38*(1), doi:10.1029/2001WR000769.